REPUBLIC OF TÜRKİYE

KIRŞEHİR AHİ EVRAN UNIVERSITY

INSTITUTE OF NATURAL AND APPLIED SCIENCES

DEPARTMENT OF MECHANICAL ENGINEERING

THEORETICAL AND EXPERIMENTAL INVESTIGATION OF POTABLE WATER PRODUCTION FROM ATMOSPHERIC AIR WITH AN ALTERNATIVE DEVICE DESIGN WITH A SOLAR TRACKING SYSTEM

MOHAMMED ORAL HASHIM AL-HURMUZI

MSc THESIS

KIRŞEHİR

2023

REPUBLIC OF TÜRKİYE

KIRŞEHİR AHİ EVRAN UNIVERSITY

INSTITUTE OF NATURAL AND APPLIED SCIENCES

DEPARTMENT OF MECHANICAL ENGINEERING

THEORETICAL AND EXPERIMENTAL INVESTIGATION OF POTABLE WATER PRODUCTION FROM ATMOSPHERIC AIR WITH AN ALTERNATIVE DEVICE DESIGN WITH A SOLAR TRACKING SYSTEM

MOHAMMED ORAL HASHIM AL-HURMUZI

MSc THESIS

SUPERVISOR

Asst. Prof. Dr. Merdin DANIŞMAZ

II. SUPERVISOR

Asst. Prof. Dr. Omer Adil ZAINAL

KIRŞEHİR

2023

KIRŞEHİR AHİ EVRAN UNIVERSITY INSTITUTE OF NATURAL AND APPLIED SCIENCE
MASTER'S THESIS STATEMENT OF ETHICS

In this thesis, I have read and understood Kırşehir Ahi Evran University Scientific Research and Publication Ethics Directive and prepared under Kırşehir Ahi Evran University Institute Of Natural And Applied Sciences Thesis Writing Rules;

- That I obtained the data, information and documents I presented in the thesis within the framework of academic and ethical rules.,
- I present all information, documents, evaluations and results according to scientific and ethical rules,
- That I have cited all the works I have benefited from in the thesis by making appropriate references,
- That I have not made any changes to the data used and the resulting results,
- This work, which I have presented as a thesis, is original,

Otherwise, I declare that I accept all legal actions to be taken against me and all loss of rights that may arise against me. 08/09/2023

SIGNATURE

Mohammed Oral Hashim AL-HURMUZI

LIST OF CONTENTS

ACKNOWLEDGEMENT

ÖZET

YÜKSEK LİSANS TEZİ

GÜNEŞ TAKİP SİSTEMLİ ALTERNATİF BİR CİHAZ TASARIMI İLE ATMOSFERİK HAVADAN İÇME SUYU ÜRETİMİNİN TEORİK VE DENEYSEL İNCELENMESİ

Mohammed Oral Hashim AL-HURMUZI

KIRŞEHİR AHİ EVRAN ÜNİVERSİTESİ
FEN BİLİMLER ENSTİTÜSÜ
MAKİNE MÜHENDİSLİĞİ ANABİLİM DALI

Danışman:	**Dr. Öğr. Üyesi Merdin DANIŞMAZ**
	Yıl: 2023, Sayfa: 133
Jüri:	**Prof. Dr. Ali Osman KURBAN**
	Dr. Öğr. Üyesi Cemalettin AYGÜN
	Dr. Öğr. Üyesi Merdin DANIŞMAZ
	Asst. Prof. Dr. Omer Adil ZAINAL
	Asst. Prof. Abbas Mohammed ISMAIL
İkinci Danışman	**Asst. Prof. Dr. Omer Adil ZAINAL**

Bu çalışma, Irak'ın Kerkük şehrinin iklim koşullarında atmosferik havadan temiz su üretiminin teorik ve deneysel olarak araştırılması amacıyla yapıldı. Kurutucu malzeme olarak mavi silika jel ve kompozit malzeme kullanıldı ve her biri 56 x 68 x 82.5 cm^3 boyutlarında birbirinden izole edilmiş iki özdeş kesitten oluşan tek eğimli aparat kullanıldı. Yoğuşma yüzeyi olarak akrilik levha ve kurutucu sıcaklığını artırmak için dahili reflektör kullanıldı. Ayrıca gün boyu güneşi takip etmek için güneş takip sistemi ve cihazı güneşin hareketi ile döndürmek için DC motor kullanıldı. Prosedür, gece boyunca nem adsorpsiyonunu ve gün boyunca su damlacıkları üretmek için nem desorpsiyonunu ve buhar yoğuşmasını içerir. Rejenerasyon işleminin sonuçları MATLAB programında 4. dereceden Runge-Kutta yöntemi kullanılarak teorik olarak tahmin edilmiş ve maliyet analizi kullanarak su üretim maliyeti hesaplanmıştır. Deneyler beş ay boyunca yapıldı ve her iki kurutucu için ayların sonuçları arasında, silika jel ile kompozit malzeme sonuçları arasında ve silika jel için teorik ve deneysel sonuçlar arasında bir karşılaştırma yapıldı. Sonuçlar, teorik birikmiş üretkenliğin toplanandan önemli ölçüde daha yüksek olduğunu, silika jelin üretkenliğinin kompozit malzemeden daha yüksek olduğunu ve yıllık su üretme maliyetinin 2.54 \$/L olduğunu gösterdi. Ayrıca, silika jel ve kompozit malzeme için sırasıyla %19 ve %10'luk bir sistem termal verimliliği ile en yüksek üretkenlik 160 g/m^2 ve 83 g/m^2 olarak bulunmuştur.

Anahtar Kelimeler: Adsorpsiyon/desorpsiyon, Temiz su, Kurutucu, Güneş enerjisi, Güneş takip sistemi

ABSTRACT

MSc THESIS

THEORETICAL AND EXPERIMENTAL INVESTIGATION OF POTABLE WATER PRODUCTION FROM ATMOSPHERIC AIR WITH AN ALTERNATIVE DEVICE DESIGN WITH A SOLAR TRACKING SYSTEM

Mohammed Oral Hashim AL-HURMUZI

KIRŞEHİR AHİ EVRAN UNIVERSITY
INSTITUTE OF NATURAL AND APPLIED SCIENCES
DEPARTMENT OF MECHANICAL ENGINEERING

Supervisor:	**Asst. Prof. Dr. Merdin DANIŞMAZ**
	Year: 2023, Pages: 133
Juries:	**Prof. Dr. Ali Osman KURBAN**
	Asst. Prof. Dr. Cemalettin AYGÜN
	Asst. Prof. Dr. Merdin DANIŞMAZ
	Asst. Prof. Dr. Omer Adil ZAINAL
	Asst. Prof. Abbas Mohammed ISMAIL
Co-Supervisor	**Asst. Prof. Dr. Omer Adil ZAINAL**

This study was conducted to investigate clean water generation from atmospheric air theoretically and experimentally in the climatic conditions of Kirkuk City, Iraq. Blue Silica gel and a composite material were used as desiccant materials, and a single-slope apparatus composed of two identical sections isolated from each other, having dimensions of 56 x 68 x 82.5 cm^3 for each, was employed. An acrylic sheet was used as a condensation surface, and an internal reflector was used to increase the desiccant temperature. Also, a solar tracking system was used to track the sunlight throughout the day, and a DC motor was employed to rotate the device with the sun's movement. The procedure involves humidity adsorption during the night and humidity desorption and vapour condensation to produce water droplets during the day. The results of the regeneration process were predicted theoretically using the fourth-order Rung-Kutta method in the MATLAB program, and the cost of water production was calculated using a cost analysis. The experiments were done for five months, and a comparison was made among the results of the months for both desiccants, between the results of Silica gel and the composite material, and between the theoretical and experimental results of Silica gel. The results showed that the theoretical accumulated productivity was notably higher than the collected one, the productivity of Silica gel was higher than the composite material, and the yearly cost of producing water was 2.54 \$/L. Also, the highest productivity was found to be 160 g/m^2 and 83 g/m^2, with a system thermal efficiency of 19 % and 10 % for Silica gel and composite material, respectively.

Key Words: Adsorption/desorption, Clean water, Desiccant, Solar energy, Solar tracking system

GENİŞLETİLMİŞ ÖZET

İçme suyuna erişim zorluğu geçtiğimiz yüzyılda ciddi bir küresel sorun haline geldi. Dünyadaki su kaynakları, değişen iklim ve diğer birçok sorun nedeniyle büyük bir baskı altındadır. Atmosferik havadan su üretmek te dahil olmak üzere içme suyu sağlamanın farklı yollarını geliştirmek için önemli araştırmalar yapıldı. Bu alanda birkaç araştırma olmasına rağmen, su toplama sürecini iyileştirmek için daha fazla ilerlemeye ihtiyaç vardır. Bu nedenle, içilebilir suyun atmosferden toplanmasını incelemek için tek eğimli bir cihaz tasarlandı ve inşa edildi. Deneyler Irak'ın Kerkük şehrinde (35.4666° K ve 44.3799° D) gerçekleştirildi. Birinci nem giderici malzeme olarak mavi silika jel tanecikleri ve atmosferik havadan nemi toplamak için ikinci bir nem giderici malzeme olarak kalsiyum klorür ve silika jelden oluşan bir kompozit malzeme kullanıldı. Proses, gece nem adsorpsiyonunu ve gün boyunca su damlacıkları oluşturmak için nem desorpsiyonunu ve buhar yoğuşmasını içerir. Aparat, her biri 56 x 68 x 82.5 cm^3 boyutlarında birbirinden izole iki özdeş bölümden oluşmaktadır. Her iki bölüm de silika jelin ve kompozit malzemenin su adsorpsiyonundaki performansını test etmek için aynı anda kullanıldı. Yüksek geçirgenliği (% 92) ve düşük emiciliği (% 4) nedeniyle yoğuşma yüzeyi olarak standart cam yerine 2.4 mm kalınlığında akrilik levha kullanıldı. Güneşin hareketi ile cihazı döndürmek için DC motor kullanılarak gün boyunca güneş ışığını takip etmek için güneş takip sistemi kullanıldı. Cihazdan çevreye olan ısı kaybını azaltmak için izolasyon olarak 2.5 cm kalınlığında ArmaFlex lastik levha kullanılarak taban ve duvar içlerindeki boşluğa yerleştirildi. Kurutucu sıcaklığını yükseltmek için tüm aparat duvarlarına dahili alüminyum reflektör monte edildi. Dahili reflektörlü ve reflektörsüz ekipmanın eş zamanlı incelenmesi, bunların eklenmesinin kurutucunun sıcaklığını yaklaşık 30°C yükseltebileceğini gösterdi. Gündüz güneş radyasyonu ve adsorpsiyon sürecindeki kütle transfer katsayısı için bir takım denklemler kullanılarak teorik bir hesaplama yapıldı. Ayrıca, silika jel ve örtü sıcaklıklarını, su üretkenliğini ve sistemin rejenerasyon sürecindeki etkinliğini teorik olarak tahmin etmek ve sonuçları deneysel bulgularla karşılaştırmak için MATLAB programında 4. dereceden Runge-Kutta yöntemi kullanıldı. Tüm bağımlı ve bağımsız değişkenlerdeki hata yüzdesini tahmin etmek için Root Sum Square yöntemi kullanılarak bir belirsizlik analizi yapıldı. Su üretim maliyetini belirlemek için bir dizi denklem kullanılarak maliyet analizi yapıldı. Deneysel testler, her ay birkaç gün seçerek Temmuz'dan Kasım'a kadar beş ay boyunca gerçekleştirildi. Her iki kurutucu için ayların sonuçları arasında, silika jel ile kompozit malzeme sonuçları arasında ve silika jel için teorik ve deneysel sonuçlar arasında bir karşılaştırma yapıldı. Ayrıca, her iki kurutucu için farklı değişkenlerin diğerleri ile değişimi

incelendi. Sonuçlar, teorik güneş radyasyonunun ölçülenden çok daha yüksek olduğunu gösterdi çünkü Kerkük Şehri'ndeki atmosfer, güneş radyasyonunu emen ve saptıran petrol rafinerileri nedeniyle kirlenmiş, bu nedenle cihaza daha az güneş radyasyonu ulaşıyor. Beş aylık sonuçlarının karşılaştırılması, biriken su miktarının Aylar ilerledikçe kademeli arttığını gösretdi bunun nedeni ise, bağıl nemin artması ve dolayısıyla adsorbe edilen nem miktarının artmasıdır. İki Kasım'da, su üretkenliği en yüksek seviyedeydi ve silika jel ile kompozit malzeme için sırasıyla sistem termal verimliliği %19 ve %10 olmak üzere ve su üretkenliği 160 g/m^2 ve 83 g/m^2 olarak bulundu. Teorik birikmiş üretkenlik, toplanandan önemli ölçüde daha yüksekti çünkü rejenerasyon sürecinde sızan buharın miktarı ve toplanmayan üretilen su damlacıklarının miktarı teorik hesaplamada dikkate alınmadı. Silika jel ile kompozit malzeme arasındaki karşılaştırma sonuçlarına göre, nemi daha iyi emme kabiliyeti nedeniyle silika jelin üretkenliğinin daha yüksek olduğu bulundu. Hem adsorpsiyon oranının hem de kütle transfer katsayısının orantılı olarak bağıl neme bağlı olduğu bulundu. Bunun nedeni, bağıl nemin adsorbe edilen nem miktarı üzerindeki en önemli etken olmasıdır. Ayrıca, her iki kurutucu malzemenin su verimliliğinin, güneş radyasyonu ve kurutucu sıcaklığının artmasıyla arttığı bulundu. Bunun nedeni, güneş radyasyonun, adsorbe edilmiş nemin buharlaşması için gerekli kurutucu sıcaklığını yükselten ısıtma kaynağı olmasıdır. Maliyet analizi sonucunda yıllık su üretme maliyeti 2.54 $/L olarak bulundu. Kerkük'ün bağıl nemi düşük olmasına rağmen 160 g/m^2 toplandı. Bu prosedür yüksek bağıl neme sahip farklı bir ortamda uygulanırsa daha önemli su üretim seviyeleri elde edilebilir. Ek olarak, bu cihaz sadece test amaçlı yapılmış bir prototip olduğundan, aparatın boyutları büyütülürse daha fazla kurutucu kullanılabilir ve daha fazla su üretilebilir. Her iki senaryoda da su üretme maliyeti önemli ölçüde daha düşük olacaktır.

LIST OF TABLES

LIST OF FIGURES

X

XI

LIST OF SYMBOLS AND ABBREVIATIONS

Symbols		Clarification
A	:	Apparent direct normal solar flux at the outside of the atmosphere of the earth, W/m^2
A_b	:	Area of the bed, m^2
A_{cov}	:	Area of the cover, m^2
A_s	:	Internal surface area of the apparatus, m^2
a, b, n	:	Mc Adams relation coefficients, dimensionless
B	:	Bias error
C_b	:	Heat capacity of the bed, J/m^2. K
C_{cov}	:	Heat capacity of the cover, J/m^2. K
c_c	:	Specific heat of the carrier material, J/Kg. K
c_{cov}	:	Specific heat of the cover, J/Kg. K
c_d	:	Specific heat of desiccant, J/Kg. K
c_w	:	Specific heat of water, J/Kg. K
D	:	Factor of diffused radiation, dimensionless
E	:	Coefficient of apparent atmospheric extinction, dimensionless
$F_{cov\text{-}sky}$	:	Shape factor between the cover and the sky, dimensionless
$\overline{F}_{cov\text{-}sky}$	:	View factor between the cover and the sky, dimensionless
$F_{d\text{-}cover}$	:	Shape factor between the desiccant and the cover, dimensionless
F_{ss}	:	Angle factor between sky and surface, dimensionless
h	:	Hour angle, degree
H	:	Theoretically calculated global solar radiation, W/m^2
H_E	:	Experimentally measured global solar radiation, W/m^2
H_b	:	Beam radiation, W/m^2
H_{bn}	:	Normal beam radiation, W/m^2
H_d	:	Diffuse radiation, W/m^2
$h_{cov\text{-}sky}$	:	Convection heat transfer coefficient between the cover and the sky, W/m^2. ^oC
h_{fg}	:	Latent heat of evaporation, J/Kg

I	:	Interest per year, dimensionless
K_a	:	Thermal conductivity of air, W/m. $^{\circ}$C
L	:	Latitude angle, degree
M	:	Total amount of produced water over the year, Kg
m_c	:	Mass of the carrier, Kg
$\dot{m}$	:	Rate of adsorped moisture, g/hr
m_{cov}	:	Mass of the cover, Kg
m_d	:	Mass of the desiccant, Kg
m_w	:	Mass of the adsorbed water, Kg
N	:	Day number of the year, dimensionless
N_r	:	Number of readings, dimensionless
P	:	Water productivity, Kg/s
P_{cov}	:	Vapor pressure on the cover surface, MPa
P_d	:	Vapor pressure on desiccant surface, MPa
P_{∞}	:	Vapor pressure of the ambient air, mbar
$P_{sat@cov}$	:	Saturated pressure of water vapour at cover temperature, mbar
$P_{sat@Ta}$	:	Saturated vapour pressure at ambient temperature, mbar
Ps	:	Precision error
q_c	:	Heat transfer by conduction, W/ m^2
$q_{cov\text{-}sky}$	:	Heat transfer between the cover and the sky, W/ m^2
q_e	:	Heat transfer by evaporation, W/ m^2
q_r	:	Heat transfer by radiation, W/ m^2
S	:	Salvage value, $
T	:	Conversion factor, dimensionless
T_a	:	Ambient temperature, $^{\circ}$C
T_{cov}	:	Theoretically calculated cover temperature, $^{\circ}$C
T_{covE}	:	Experimentally measured cover temperature, $^{\circ}$C
T_d	:	Theoretically calculated desiccant temperature, $^{\circ}$C
T_{dE}	:	Experimentally measured desiccant temperature, $^{\circ}$C
T_{sky}	:	Sky temperature, $^{\circ}$C

t	:	Time, hr
Y	:	Number of the years, dimensionless
θ	:	Altitude angle, degree
α_b	:	Absorptivity of the bed, dimensionless
ΔP	:	Vapor pressure difference, KPa
Δy	:	Air gap thickness, m
σ	:	Constant of Stefan Boltzmann, W/ m^2. K^4
δ	:	Declination angle, degree
η	:	System efficiency, dimensionless
ε_{cov}	:	Emissivity of the cover, dimensionless
ε_d	:	Emissivity of the desiccant, dimensionless
γ	:	Inclination angle of the adsorption surface, degree
ξ	:	Inclination angle of the transparent cover, degree
β	:	Mass transfer coefficient, g/m^2. KPa. hr
$\emptyset$	:	Relative humidity, %
τ_{cov}	:	Transmissivity of the cover, dimensionless
v	:	Wind speed, m/s
Abbreviation		**Clarification**
AC	:	Annual Cost, $
AMC	:	Annual Maintenance Cost, $
AST	:	Apparent Solar Time, hr
ASV	:	Annual Salvage Value, $
CPK	:	Cost of a Produced Kilogram of water, $/Kg
CRF	:	Capital Recovery Factor, dimensionless
ET	:	Equation of Time, min
FAC	:	Fixed Annual Cost, $
LL	:	Local Longitude, degree
LST	:	Local Solar Time, hr
PC	:	Capital Cost, $
SFF	:	Sinking Fund Factor, dimensionless
SL	:	Standard Longitude, degree

1. INTRODUCTION

One of the most severe dilemmas that the globe is facing nowadays is the shortage of potable water, especially in distant areas and deserts. Like nourishment and energy, drinkable water is a basic need for retaining life on earth (Yousef et al., 2019). The apportionment of water on the planet's surface is very unequal, with just 3% of it being fresh. The Arctic and Antarctic contain the bulk of freshwater (69%), and under the earth's surface, there is about 30% of clean water and the rest 1% forms the lakes and rivers. Ninety-seven per cent of the water on earth is saline, creating oceans and seas unfit for human consumption or industrial use (Kabeel et al., 2020; Arunkumar et al., 2012).

Lack of potable water happened due to many reasons, like rapid industrial growth and increment in inhabitants (Velmurugan & Srithar, 2007), contamination of rivers and lakes because of industrial effluents and wastewater discharge (Omara et al., 2011), an incommensurate apportionment of potable water for the needs of each area (Kumar & Kurmaji, 2013), inefficient usage of water in industry and farming (Wang et al., 2022), and the climate change (Kanae, 2009).

According to a recent study, the world's two-thirds of the population faces water scarcity for at least one month each year due to seasonal fluctuations in water demand and accessibility. Even worse, half a billion individuals worldwide confront acute water shortages for the whole year (Tu et al., 2018), like water shortages in portions of Africa, the Middle East, Asia, and South America. As a result of the struggle for fresh water supplies, a water deficit could cause future global dangers, disputes, and warfare (Salehi et al., 2020).

Diseases like diarrhoea and cholera, which are the fundamental reasons for the deaths of millions of people, including children, are caused by drinking polluted water. According to estimates, contaminated water, a lack of water, and poor hygiene cause a high percentage (85-90%) of diarrheal disease in impoverished countries (Modi & Modi, 2019).

As a result, it became imperative to solve this problem effectively, so researchers always strive to develop practical solutions for obtaining drinkable water through various methods (Danışmaz & Alhurmuzi, 2022). Some ways to deal with the problem are (Hamed et al., 2010):

  I.   Transporting of water for long distances from other locations.

 II.   Desalination process for salty water.

III.   Potable water harvesting from the atmospheric air.

The first solution, which includes water transmission to the arid regions, is not economical since it costs a lot (Gad et al., 2001). The second solution cannot be used in areas that do not have an ample salty or brackish water supply. Furthermore, substantial financial expenditures are required for desalination facilities and large pipes. As a result, desalination is not a logical choice in impoverished and non-coastal areas, where many people face persistent water shortages (Inbar et al., 2020).

Water harvesting from the ambient atmosphere is a new approach to addressing the clean water shortage (Srivastava & Yadav, 2018a). The atmosphere contains around 3100 cubic miles of water; the most significant portion (98 per cent) is vapour, while the rest (2 per cent) is clouds. According to the estimations, nearly 280 cubic miles of H_2O vaporise or leak into the atmosphere daily. Furthermore, one cubic mile of water holds about 1 trillion gallons (Alahmer et al., 2018). This approach has several benefits: (a) Air is a sustainable and safe potable water supply. (b) atmospheric Water volume is estimated to be 14000 cubic kilometres. In contrast, clean water in all lakes, as well as rivers all around the world, is estimated to be approximately 1200 cubic kilometres (Hamed et al., 2011). (c) This method uses Solar power as a clean and sustainable energy source; plenty of space exists to capture solar energy and air (William et al., 2015). As a result, extracting water from the atmosphere is valuable for collecting water in remote regions and rural villages, not dependent on water availability (ground or underground). So, atmospheric water generation is a suitable alternative for isolated communities that cannot bear the high capital costs (Mohamed et al., 2017). The techniques mentioned below would be used to harvest water from ambient air (Talaat et al., 2018):

I. Moisture condensation via subjecting the humid air to a surface colder as compared with the air's dew point.

II. Fog-related wet collecting.

III. Sorption of the humidity using desiccants, desorption process, and condensation on a surface.

Fog collection is one of the earliest techniques for gathering water droplets in the environment. Furthermore, because it requires a constant high relative humidity (RH), this method could only be used in a limited number of locations (Danışmaz & Alhurmuzi, 2022).

The refrigeration technique could be accomplished by condensing the moist air by subjecting it to a surface colder than the air's dew point to produce water droplets. Refrigeration is considered an inefficient method in areas where the relative humidity is regularly below 40 per cent or when there is no electrical power (Li et al., 2018a).

2

Adsorption and regeneration techniques include adsorbing or absorbing the humidity from atmospheric air during the nighttime, followed by vaporising the adsorbed humidity during the daytime. Choosing an appropriate absorber with water-holding capability is one of the most challenging aspects of designing an absorption or regeneration device. In the meantime, the absorber should be able to regenerate a significant volume of vapour at a lower regeneration temperature, which is critical for solar energy consumption (Wang et al., 2017b).

1.1. Solar Energy

Solar energy is dependable, cost-efficient, and eternally renewable for future energy needs. It is suitable for long-term energy concerns since it is promising and readily accessible (Kannan & Vakeesan, 2016). Various elements like latitude, climatic conditions, diurnal fluctuation, and regional variance substantially determine the strength of solar radiation across the atmosphere (Kabir et al., 2018). Statistics show that the quantity of solar radiation that the globe gets is 4200 times larger than the quantity of energy that the world will need in 2035. The world's energy needs could be met by developing efficient solar energy collection capacity to eliminate the need for additional energy sources (Guangul & Chala, 2019). In this study, we used solar radiation to heat the desiccant material during the daytime operation to cause the moisture that the desiccant has absorbed to evaporate and condense on the condensing surface.

There are some essential terms that it is used in solar energy calculations as can be clarified as follows:

I. **Beam radiation** is solar radiation that has not been dispersed by the atmosphere as it comes from the sun. Direct solar radiation is a term used to describe beam radiation (Duffie & Beckman, 2006).

II. **Diffuse Radiation** is the solar energy received by the earth after being redirected by the atmosphere (Duffie & Beckman, 2006).

III. **Total solar radiation** is the solar radiation incident on a horizontal surface, including both direct and diffuse solar radiation. Most people use to figure out how much radiation comes from the sun (Duffie & Beckman, 2006).

IV. **Declination angle, δ** is the inclination at which solar radiation strikes the earth's centre and equator as it travels from the sun's centre (Figure 1.1). Positive declinations are north of the equator, whereas negative declinations are south. It ranges from (23.45º) to (-23.45º); this angle's value varies with the year's seasons (Kalogirou, 2013).
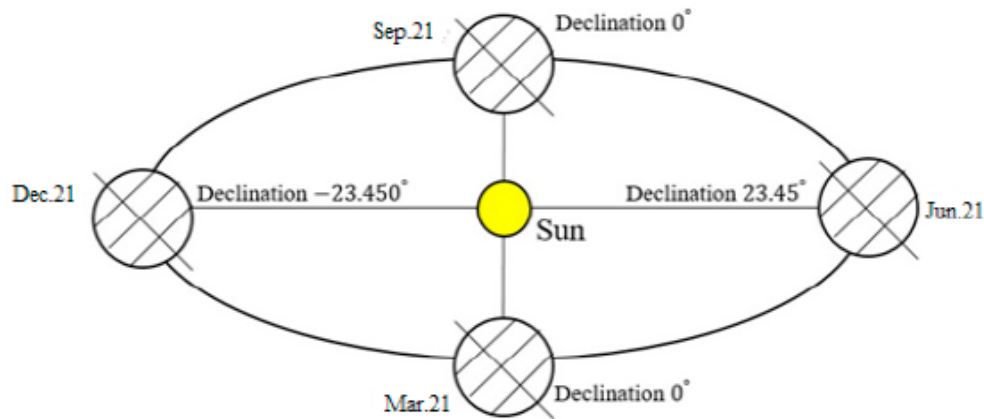
Figure 1.1. Values of declination angle (Kalogirou, 2013)

V. **Hour angle, h** It is the angle that describes the earth's rotation around its axis (Figure 1.2). It is equivalent to 15 degrees for every hour in the morning (before noon) and equivalent to -15 degrees for every hour in the evening (afternoon). It equals zero at noon, considered a reference time (Mousavi Maleki et al., 2017).

VI. **Altitude angle, Θ** is an angle generated by solar rays with the horizontal level (Kalogirou, 2013).

VII. **Zenith angle, Φ** is an angle created by solar rays with the vertical level (Kalogirou, 2013).

VIII. **Latitude, L** is the angle that determines the location of the body concerning the south or north of the equator. It is confined between (+90°) in the northern hemisphere and (-90°) in the southern hemisphere, and it is equal to (0°) at the equator (Mousavi Maleki et al., 2017).
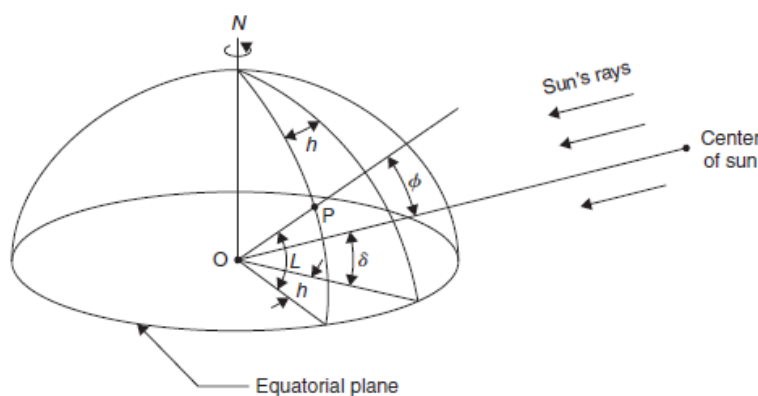
Figure 1.2. The hour angle (Kalogirou, 2013)

1.2. Desiccant

Many things can absorb water from the environment with diverse physical or chemical methods. Besides salts, wood, polymers, paper, and fibres are all examples of

widespread materials with a strong affinity for water. Some substances are classified as drying agents or desiccants because they exhibit enough water absorption capacity, drying effectiveness, and the necessary physical and chemical characteristics (Cohen, 2003). Lowering the moisture content of the surrounding air can be done by drawing the moisture out of the air using desiccants (hygroscopic materials) (Ramli et al., 2021). Desiccants may either absorb or adsorb the water vapour due to the change in water vapour pressure between the surface of the desiccant and the atmospheric air. The desiccant's temperature increases in desorption, and the absorbed moisture evaporates. The water vapour then moves toward a colder surface, where the transported moisture condenses (Daou et al., 2006). They may be used once or repeatedly by regenerating the desiccant after each usage to restore it to its active condition.

Desiccants may be divided into two categories: liquid and solid. Solid desiccants can physically or chemically adsorb moisture without undergoing any chemical change. Contrarily, liquid desiccants collect moisture via absorption and chemically change while removing the moisture (Gandhidasan & Abualhamayel, 2009). Types of solid desiccants include Silica gel (SiO_2), artificial polymers, natural zeolite (alumino silicate), activated alumina (Al_2O_3), as well as molecular sieves. In contrast, liquid desiccant examples include lithium chloride, Calcium chloride, and lithium bromide (Ramli et al., 2021). The optimum desiccant material is the one that regenerates at low temperatures and possesses a high adsorption capability at various ranges of relative humidity. Depending on the desired use, a specific desiccant type can be chosen (Misha et al., 2012).

1.2.1. Calcium chloride ($CaCl_2$)

At room temperature and in an aqueous solution, $CaCl_2$ acts as an ionic halide for Calcium ions. It is often created via a direct reaction between limestone and hydrochloric acid, a significant by-product of the Solvay operation (Singh et al., 2018). It is considered one of nature's most effective humidity-absorbing substances, and it comes in second place behind salt as the most frequent constituent of the sea. Calcium chloride (Figure 1.3) might be a liquid or a solid dehumidifier. It is non-toxic, ecologically friendly, and one of the most cost-effective liquid moisture absorbers. It can be used in various ways to reduce the latent heat content of air (Badrakia, 2015). The main benefit of this product is that it is inexpensive enough to be thrown away after usage in small quantities. The compositions of commercially available anhydrous $CaCl_2$ vary between $CaCl_2$. 0.05 H_2O and $CaCl_2$. 0.25 H_2O (Cohen, 2003).

Figure 1.3. Calcium chloride $CaCl_2$ (2005, Source: Wikipedia)

1.2.2. Silica gel (SiO_2)

Silica gel is a solid organic material and an amorphous form of silicon dioxide synthesised artificially from sodium Silicate. Because of its large surface area, Silica gel has the maximum humidity adsorption power (Das et al., 2021). Silica gel with microporous and macroporous grain sizes are the two types of SiO_2. Microporous SiO_2 takes longer to adsorb water than macroporous SiO_2, which quickly saturates with the environment. To eliminate the humidity from Silica gel (Figure 1.4), it typically has to be heated to a dehumidification temperature of 90–150 °C (Singh et al., 2018).

Figure 1.4. Silica gel SiO_2 (2006, Source: Wikipedia)

Essentially, Silica gel does not react chemically when it adsorbs moisture, and the humidity is adsorbed until the microcavities are filled or until balance occurs between the water vapour pressure of the surroundings and the microcavities (Amarakoon & Navaratne,

2017). Pure Silica makes Silica gel ($SiO_2 \cdot xH_2O$), which preserves chemically bound water residues (nearly 5 per cent). It is frequently used at temperatures below 200 °C because it loses its adsorption ability when it loses water due to overheating (Srivastava & Eames, 1998).

1.2.2.1. Blue silica gel (indicator)

It is hard to determine whether SiO_2 needs to be changed or regenerated because it is often white or colourless and does not change colour while used. Therefore, a visual indicator must determine whether the desiccant is saturated with humidity (Nayak & Bera, 2011). Through its colour change, the coloured SiO_2 can be utilised to detect its humidity adsorption condition. Indicating Silica gels can be in various colours, like blue and orange (Kumar et al., 2021). In blue Silica gel, Cobalt chloride is responsible for this colour characteristic (Kumar & Yadav, 2015c). The Silica gel's blue colour indicates that it is in its dehumidified form. In contrast, the pink demonstrates that it is saturated (Figure 1.5).
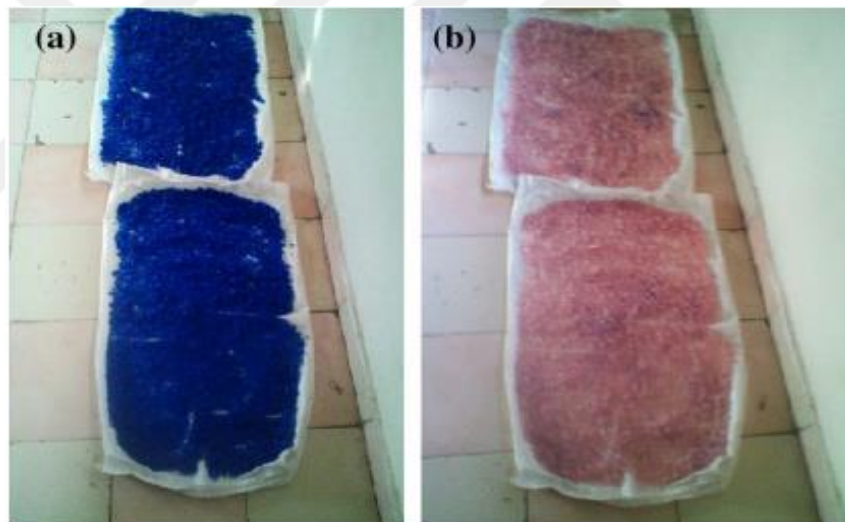
Figure 1.5. Blue Silica gel (Das et al., 2021)

1.2.3. Composite desiccants (selective water sorbents)

Composite desiccants are prepared by impregnating a hygroscopic salt inside the cavities of the host material to form a two-phase substance. Because of their superior sorption capabilities, those substances are anticipated to hold great promise for being used in various fields, including the extraction of potable water from the atmosphere (Aristov et al., 1996). Hygroscopic salts such as lithium chloride, Calcium chloride, magnesium sulfate, sodium sulfate, lithium nitrate, and lithium bromide are often impregnated inside the pores of host matrices, including SiO_2, vermiculite, floral foam, and chitosan to manufacture a composite material (Rajamani & Maliyekkal, 2018). It is possible to control the composite's

sorption capabilities at the nanoscale by adjusting the chemical composition of the hygroscopic substance, the host matrix's pore size, and the synthesis circumstances (Simonova et al., 2009). The composite material is prepared by drying the host material to eliminate any water it has adsorbed, impregnating the pores with a salt solution, filtering, and then drying the wet composite (Gordeeva & Aristov, 2012).

Composite material's sorption characteristics may be affected by different factors, including (Aristov, 2007):

      a. The salt's chemical composition.

      b. Hygroscopic salt content.

      c. The host matrix's chemical composition.

      d. The host matrix's porous structure.

      e. The circumstances of the synthesis.

1.3. Objective of The Thesis

This study aims to investigate potable water collection from atmospheric air in a single-day process over several months using Silica gel as the first desiccant and a composite material consisting of Silica gel and Calcium chloride as the second desiccant material. It also aims to compare the experimental results of both materials, the experimental results of each material over several months, and the experimental results of Silica gel with the theoretical one.

1.4. Importance of The Thesis

The apparatus used in the experimental study is rotatable. It rotates from sunrise to sunset with the sun's movement using a solar tracking system consisting of light sensors and an Arduino system. To rotate the apparatus, a DC motor was used with an endless gearbox that reduces the motor's speed and increases its torque. Also, internal reflectors were used to improve the device's desiccant temperature and reduce the regeneration period. Two types of desiccant materials were used to investigate water generation from the atmospheric air, and a comparison between their results was made.

2. LITERATURE REVIEW

Over the years, many attempts have been made to collect potable water from the atmosphere. For this purpose, numerous theoretical, simulation, or experimental studies were carried out by researchers, and various types of desiccant materials were used to extract water vapour in the nighttime, vaporise the moisture in the daytime, and then condense it on a condenser and collect the generated clean water. The studies were categorised according to the utilised desiccant type as follows:

2.1. Calcium Chloride ($CaCl_2$)

Calcium chloride is a liquid-type desiccant since it is prepared by dissolving the white crystalline solid $CaCl_2$ in water to obtain a liquid solution. Liquid desiccant requires the use of a bed to carry the solution, and different types of bed material were used in the studies, so the studies that were done using $CaCl_2$ were categorised according to the used bed material as follows:

2.1.1. Sandy bed

An atmospheric moisture collection using desiccant like Calcium chloride and bed material like sand was examined. Seven strata were used with $CaCl_2$/sand proportions varying from 0.1 to 0.4. The effects of several factors were studied, including how the mass transfer coefficient is affected by desiccant concentration and the Grashof number and the impact of mixing a percentage of sand with desiccant on the absorption rate. The results demonstrated that when concentration rises, the mass transfer also increases and that the mass transfer may decrease quickly as the mixing ratio is reduced (Hamed, 2003). Kabeel (2006) employed sand impregnated with $CaCl_2$ in a solar/ collector system to harvest moisture from the surrounding air. The device was tested utilising three different inclination angles (15, 20, and 25°), and a mathematical paradigm was used to examine the impacts of various variables on productivity. According to the findings, the amount of gathered water was 1.2 L/m^2/day, and a 25° tilt angle provided optimal results. An experimental study was conducted to investigate the water generation from atmospheric air and evaluate the impact of various parameters on the system's productivity. For this purpose, an apparatus with a surface area of 0.5 m^2 was designed and constructed, and a sandy bed impregnated with Calcium chloride was used. The results showed that this system produced 1 L/m^2 of clean water (Hamed et al., 2011).

2.1.2. Black cotton cloth

Potable water generation from atmospheric air was investigated experimentally using a box-shaped device and a layer of corrugated fabric soaked in Calcium chloride as moisture-absorbing material. The process involved absorbing moisture at night, desiccant regeneration and vapour condensation during the day. A fan circulated the air at nighttime to extract moisture, while a condenser was used as a condensing surface during the daytime. The experiments were conducted with and without the condenser, and the results revealed that using a condenser reduces the system's efficiency by 5% and 1.5 litres per square meter per day of clean water was collected (Gad et al., 2001). This study examined how mass is transferred between a fabric's parallel layers impregnated with Calcium chloride, having a concentration ranging between 0.2-0.5 in absorption/ desorption. Experimental observations were utilised to calculate the mass transfer coefficient and Sherwood number. Also, an effort has been made to match the Sherwood number to the Reynolds number's function for the Schmidt number's available range (Hamed & Sultan, 2002). A research was conducted theoretically and experimentally to identify different variables that affect the efficiency of a "finned double-faced conical shaped" apparatus with fins constructed to be utilised in humidity harvesting from the air by using $CaCl_2$ as a desiccant and black cloth as a bed material. According to the findings, the system generated potable water between 0.3295 and 0.6310 kg/m^2/day, costing only 0.062 dollars per kilogram (Talaat et al., 2018). Experiments for potable water harvesting from the atmosphere using a tubular solar still were carried out by Elashmawy (2020). A black cotton rag soaked in Calcium chloride was employed to absorb moisture, a small air blower was used to circulate the ambient air during the nighttime procedure, and the absorption process was studied under five air velocity conditions (natural, 1/2, 1, 2, and 3 m/s). The findings revealed that for natural convection, the water productivity, efficiency, and cost were 230 mL/m^2/day, 12.2 %, and 0.4 $/L, respectively. In contrast, the results for forced convection with air velocity of 4 m/s were 467 mL/m^2/day, 25 %, and 0.2 $/L, respectively. This work presented a novel method for gathering humidity from the surrounding air in shallow relative humidity areas using a tubular solar still. The proposed approach aimed to increase the desiccant's temperature during desorption using a solar radiation concentrator to enhance the apparatus's ability to remove moisture from a strong $CaCl_2$ desiccant at very low humidity. The results revealed that the proposed procedure generated 0.51 litres of fresh water per kilogram of Calcium chloride with a system thermal efficiency of 24.61 per cent, costing $0.15. While water production cost decreased by 25%, the water generation rate increased by 292.4 per cent, and the system's efficiency rose by 82.3 per cent (Elashmawy & Alshammari, 2020). Fathy et al. (2020)

conducted a theoretical and practical investigation on using a foldable device with an accordion shape to collect atmospheric moisture. The desiccant chosen for this experiment was Calcium chloride, and a black cotton cloth was used as a bed for the liquid desiccant. The operation was mathematically modelled, and the overall cost was determined using cost estimation. The results showed that producing one kilogram of water costs around 0.086 dollars.

2.1.3. More than one bed

Kabeel (2007) constructed and used two similar multi-shelved pyramidal-shaped solar systems to collect moisture from the surrounding air. The systems were identical in terms of dimensions but had distinct bed materials. In contrast to the second pyramid's usage of a cloth layer soaked in Calcium chloride, the first one's absorbing material was saw wood impregnated with Calcium chloride. Experiments were conducted in various environmental situations to determine how the device's shape may affect the absorption/desorption process, and the findings showed that a cloth bed had a higher absorptivity than saw wood, and the highest productivity was 2.5 Liter/m^2/ day. A trapezoidal prism-shaped device with four fibreglass surfaces was built and used by William et al. (2015). The collector has a multi-shelf bed designed to maximise the bed surface area. Sand and cloth layers served as the test beds, while $CaCl_2$ with a 30 per cent concentration was utilised as the desiccant. Results showed that at a 30 per cent Calcium chloride concentration, the total quantity of desorbed vapour from a cloth bed was 2.32 slit/day.m^2, compared to 1.23 slit/day.m^2 on a sandy bed and the system efficiency using cloth was 29.3 per cent, whereas the efficiency using sand was 17.76 per cent.

2.1.4. Without bed

In research, an analytical technique was devised to compute the amount of absorbed moisture. Calcium chloride was used as a desiccant and an air-exposed, sloping surface as an absorptivity surface. It was found that the increment of the desiccant's flow rate, air relative humidity, and wind speed enhance the quantity of the absorbed humidity (Gandhidasan & Abualhamayel, 1996). Gandhidasan & Abulhamayel (1997) recommended the usage of a suitable liquid desiccant to collect moisture from the surrounding air. Their procedure included a diurnal phase in which the desiccant was regenerated at the same unit that absorbed moisture all night. The system consisted of a single glass covering an inclined flat surface painted black with an air gap of about 45 centimetres. At night, the desiccant flowed in a thin layer over the glazing, becoming diluted due to moisture absorption. While during the day, the sun's energy heated the diluted desiccant as it flowed downward on the

absorption surface. The water productivity was found to be 1.92 Kg/m. In a study, an appropriate apparatus was constructed for clean water generation from atmospheric air using Calcium chloride as a desiccant. The study employed four different flow rates of $CaCl_2$ and desiccant concentrations (32.5 per cent–33.5 per cent). The findings showed that increasing the ambient temperature, wind velocity, solution concentration, and absorbent flow rate boosted the regeneration rate while increasing the temperature of the ambient air and sun radiation and reducing the desiccant flow rate improved absorption efficiency. According to the absorbent flow rate, absorbed humidity was 2.11 $L/m^2/day$, whereas vaporised moisture was 1.15 $L/m^2/day$ (Gandhidasan & Abualhamayel, 2009).

2.2. Silica Gel (SiO_2)

An experimental study was conducted to generate clean water from ambient air using solar radiation as a heat source, Silica gel as a desiccant, and an open, inverted book-shaped enclosure breather dehumidifier. It was discovered that the Silica gel might be activated by applying it in granular form in a thin layer on a dark, heat-absorbing surface and then exposing that surface to sunlight (Dunkak, 1949). A study was conducted to collect potable water from the surrounding air using Silica gel as a desiccant material in a water recovery apparatus with multiple heat reservoirs. The best placement for an adsorbent layer is directly over a heat reservoir. This method involves passing daytime air for desorption of moisture first via the adsorbent layer and then via the heat reservoir, and this is done after passing nighttime air for water adsorption first via the heat reservoir and then through the adsorbent layer. Also, solar radiation could warm the daytime air (Hussmann, 1982).

The elevation of the air gap, the tilt angle, the optimum glass thickness, and the optimum number of glasses were all studied to determine the optimum design criteria for drinking water collection from the atmosphere. Silica gel was used as a desiccant material in three identical box-shaped apparatuses. The findings showed that the design conditions for maximal production include adequate glass thickness of 3 mm, air gap height of 0.22 m, inclination angle of 30°, and single glazing. Also, the quantity of freshwater produced at the most effective rate throughout the experiment was 200 mL/Kg/day (Kumar & Yadav, 2015c). In an experimental study, activated alumina, molecular sieve 13X, and Silica gel were all used to remove humidity from the atmospheric air, and a fixed-focus Scheffler reflector with 1.54 m^2 was employed to increase the desiccants' temperature in the regeneration process. According to the results, the maximum water productivity was found to be 155 ml per day using Silica gel, while the productivity using a molecular sieve and activated alumina was 43 ml per day and 38 ml per day, respectively (Srivastava & Yadav,

2018b). Essa et al. (2020) studied experimentally the performance of an apparatus with a novel design that uses SiO_2 to harvest moisture from the surrounding air. Using gravel in the basin and adding longitudinal fins were two enhancements considered. Also, the regeneration operation was speeded by employing a parabolic solar concentrator that raises the desiccant temperature. A mathematical model was used to anticipate productivity under different input parameters. According to the findings, utilising longitudinal fins alone enhanced productivity and efficiency by 72 per cent and 15 per cent, while employing longitudinal fins in conjunction with gravel raised productivity and efficiency by 166 per cent and 35 per cent. A 400 mL/m^2 water production was determined to be the greatest. A prototype was manufactured to experimentally generate clean water from the atmosphere in a controlled indoor environment. The prototype comprised the desiccant material, a water sorbent unit, a condenser, and a reflector. An orange Silica gel has been used as a desiccant material. The findings showed that raising relative humidity accelerates the adsorption cycle and increases the moisture adsorption, desorption, and collection rates. When exposed to a radiant intensity of 556 W/m^2, the prototype could produce 159 grams of water / 1 kilogram of desiccant in a half-day operation. At a desiccant layer thickness of 25 mm, the device generated 800 mL of water in 24 hours, with a system efficiency of 50% (Sleiti et al., 2021). Water production from atmospheric air was studied using an orange Silica gel in a solar recovery system. The device's absorptivity was enhanced by painting the device's rear with black paint. According to the findings, the water productivity was 0.98 L daily (Kumar et al., 2021).

2.3. Metal-Organic Framework (MOF)

Atmospheric water collection was done experimentally using a box-shaped device. Porous metal-organic framework-801 (MOF-801) was used as an absorbing material, and solar radiation was used as the heat source required for the regeneration process. At a relative humidity of 20 per cent, the prototype gathered 2.8 litres of water per kilogram of MOF per day with no further energy input (Kim, 2017). Fathieh et al. (2018) conducted a laboratory-to-desert experiment investigating water harvesting from arid air using MOF-801 and MOF-303 as absorbers. Two essential parts comprised the prototype used in the test: the moisture sorption unit, which retains the MOF, and the case that houses it. A reflector is fastened to the cover to ensure the MOF is only exposed to solar radiation on its surface. The findings showed that a kilogram of MOF-801 generated 100 grams of water, whereas 1 kg of MOF-303 produced twice as much water in a single day's work. Kim et al. (2018) proposed a moisture collection system that utilised MOF-801" as an absorbing material for arid

environments, and they painted the rear of the MOF black to serve as a solar radiation absorber. They estimated that 0.25 litre of water might be generated per kilogram of MOF daily. When they utilised MOF-801 to check its ability to produce water, they found that the MOF structure was stable in water and that neither metal ions nor organic linkers were contaminating the water. An adsorption/desorption method was used in a study to harvest moisture from the atmospheric air using various types of metal-organic frameworks (MOFs) under the climatic conditions of Central Australia, the Sahara desert, and Saudi Arabia. According to the results, the three MOFs: Co_2Cl_2 (BTDD), MIL-101 (Cr)-SO_3H, and MIL-101 (Cr), were found to be the most promising for Australia. At the same time, CAU-10 (PyDC) and MIL-160 were appropriate in both Saudi Arabia and the Sahara (Gordeeva et al., 2020).

2.4. Hydrogels

Zhao et al. (2019) used an atmospheric water harvester (AWH) to produce high-efficiency water using super moisture absorbent gel in various relative humidity conditions. Since the design was a successful technique for controlling water molecule mobility, it offered a novel approach to improve AWH. Nandakumar et al. (2019) studied water harvesting from the atmosphere above sea level. Solar radiation as the heat source in the regeneration and a hygroscopic nanoporous hydrogel as a desiccant in a floating prototype with a Styrofoam base were used. The results revealed that in excessively humid environments, the hydrogel could absorb moisture more than 420 per cent of its weight, and even after 1000 cycles of absorption and regeneration, the hydrogel displayed exceptional stability. Also, it was found that it is possible to get more than 10 litres of drinkable water per kilogram of hydrogel daily by absorbing and releasing it several times.

2.5. Composite Desiccant

Alayli et al. (1987) used an s-shaped composite material to harvest humidity from atmospheric air by soaking it in a physicochemical liquid. The findings showed that the absorptivity of the surface diminishes as temperature increases and that the surface should be slanted at a 50-degree angle to absorb humidity. Selective water sorbents (SWSs) developed by Aristov et al. (1999) were used to remove humidity from the ambient air. The SWSs included hygroscopic salts such as lithium bromide (LiBr), Calcium chloride, and host materials like Silica gel (SiO_2), alumina (IK 02 200), and porous carbon (subunit). The lab experiment results demonstrated that a litre of water might be produced for every square meter of composite material. Also, it was found that it is possible to have three to five tones of clean water using ten tons of SWSs. A novel composite adsorbent with excellent

efficiency was developed to capture moisture from the surrounding air. The composite material MCM-41 comprised $CaCl_2$ as a desiccant and a large-pore crystalline substance as a host material. The results showed that the composite material has an intriguing adsorption rate and the potential to adsorb 1.75 kg of moisture/kg of composite material, and it does not require a high temperature to commence the desorption operation. Also, the amount of water generated was 1.2 kg/m^2 (Ji et al., 2007). A novel composite material was employed in a study to harvest moisture from atmospheric air. Three solar systems were used, each with a 0.36 m^2 collecting area, and six distinct $CaCl_2$ patterns generated at various concentrations were employed. The findings showed that the quantity of moisture harvested in the nighttime and the collected water amount in the daytime increased when $CaCl_2$ concentration increased. Also, the optimum productivity was 180 mL of water per kilogram of desiccant daily at a 60% concentration (Kumar & Yadav, 2015b). In another study, tests were done to check the performance of a newly developed composite desiccant material ($CaCl_2$/flower foam) in moisture harvesting from the surrounding air. Three identical box-shaped apparatuses were used, and different concentrations of Calcium chloride were prepared and employed in six patterns. The amount of water collected grew in proportion to the concentration of $CaCl_2$, where the highest adsorption percentage was 0.043992 kilogram per hour, and water generation was 0.35 millilitre per cubic centimetre per day at a Calcium chloride concentration of 37 per cent (Kumar & Yadav, 2015a). To optimise mass transfer area and improve the adsorption efficiency for air-to-water systems, a new composite material consisting of Activated Carbon Fibre felts (ACF felts) as a host matrix and Calcium chloride as a salt was produced. According to the results, ACF30 has the highest sorption capacity of water absorption at 1.7 g/g, which is almost three times greater than SiO_2-$CaCl_2$. This makes ACF more suited as a host material for composite adsorbents (Wang et al., 2016). A novel composite adsorbent was used to absorb environmental moisture. Hygroscopic salt such as Calcium chloride was combined with host materials such as vermiculite and saw wood to create a composite material. A box-shaped apparatus having an inclination angle of 30° was used, and six patterns of $CaCl_2$ with different concentrations were prepared. The total amount of water collected by utilising 2.5 kilograms of the adsorbent was found to be 195 mL/Kg/day (Kumar & Yadav, 2016). Open and semi-open devices were constructed to use the sorption technique to gather drinkable water from the surrounding air. Collecting 0.32 kg of pure water was accomplished using a roll-up concept device and 2.25 kg of ACF-$CaCl_2$ as a composite material. The upgraded semi-open device used a solar collector with a 4 m^2 surface area to capture 9 kilos of potable water and corrugated and flat adsorbents were constructed to load 40.8 kg of the composite material with a 0.4 x 0.4 x 0.6 m dimensioned

15

bed (Wang et al., 2017a). A very effective semi-open system was developed to remove drinking water from the atmosphere. A composite material consisting of active carbon felt, lithium chloride and nano-Silica particles were used, and forming the composite material into mass-transmission channels was simple because of its corrugated structure. According to the results, the increment in relative humidity, absorbed moisture amount, and the desiccant temperature increased the generated water quantity. Also, after using 40.8 kilogrammes of the composite material, 14.7 kilogrammes of water were produced (Wang et al., 2017b). Li produced a hybrid absorbing material consisting of a flexible PAM-CNT hydrogel and Calcium chloride. They used a simple-to-assemble prototype and 35 g of dry PAM-CNT-$CaCl_2$ to generate potable water under field conditions. The amount of water produced by the absorbing material was calculated to be 20 g in 2.5 hours, and the materials required to create such a device, which would provide a person with his 3 kg daily water requirement, were estimated to cost only 3.2 dollars (Li et al., 2018a). A theoretical model was created in a study, and a prototype was constructed. For the research, a desiccant that works in a wide range of RH and is temperature-insensitive was used to achieve a high water collection capability in various climates. The prototype gathered 38.5 kg/ day of potable water using 7.2 MJ of heat / Kg of clean water (Wang et al., 2018). A composite desiccant consisting of an alginate-derived matrix, such as sodium alginic acid as a host material and Calcium chloride as a desiccant, was produced to harvest atmospheric moisture. The composite material was made as spherical beads because the spherical structure encourages high gas permeability in packed beds. According to the results, at a water vapour pressure of 10 mbar, the composite desiccant could absorb atmospheric moisture as much as its weight, and according to estimates based on the material's bulk density and water absorption, 660 kg of water/ m^3 of desiccant could be collected (Kallenberger & Fröba, 2018). The performance of three composite materials consisting of Calcium chloride with vermiculite-saw wood, jute, and burnt clay was experimentally studied using a box-shaped device. According to the results, the highest productivity was 130 mL/Kg/day using $CaCl_2$-vermiculite-sawed wood as a composite material (Kumar et al., 2017). In a study, three active carbon felt composites were manufactured, their performance was examined, and both theoretically and experimentally evaluated. Also, a 3-phase sorption model was suggested after the thermodynamics of various phases were examined. The comprehensive investigation showed that a combined adsorption-absorption process might significantly increase the sorption capacity, and the results showed that at 70% RH without any leakage, the most significant ability was 2.9 g of water per g of composite. Also, this prototype collected 1.51 g of potable water each cycle per g of the composite at an RH of 70 %

(Entezari et al., 2019b). Compounding composite materials were produced by mixing Silica gel, salt, and polymers. Adding Polyvinylpyrrolidone (PVP) to the Silica gel-Lithium chloride composite boosted sorption capacity while reducing the moisture hold-up in the desorption process by 35 to 55%. These materials' increased water extraction capacity allowed them to be used as adsorbers in sorption-based systems. A small prototype was utilised to assess the viability of using Silica gel-LiCl-PVP in the existing system. According to the results, the produced water amount was 0.43 g for every g of sorbent (Entezari et al., 2019a). A novel Nano-sized vapour sorbent made of a hollow nano-carbon capsule with a lithium chloride solution within the void core was prepared in research. The sorbent absorbed the equivalent of its weight in water vapour from the atmosphere within three hours when the relative humidity was 60 %, and it swiftly desorbed the collected moisture within 30 minutes under 1 kW/m^2 solar irradiation. During a single-day experiment outdoors, the unit could complete three absorption/regeneration cycles in less than 10 hours, yielding 1.6 kg of water per kilogram of sorbent (Li et al., 2020). In a study, gold cubes (AuNC) and rods (AuNR), and carbon black (CB) were attached as a heat source to enhance the surface temperature of the adsorber, boost the regeneration of the water vapour, and enable more atmospheric water capture (AWC) cycles each day. In the regeneration process, simulated solar energy (1-Sun) was used, and the desiccants' adsorptive phases were examined at 40, 60, and 80 per cent relative humidity levels. According to the results, carbon black-coated Silica gel could be used in ten adsorption/ desorption cycles to generate 0.47 g of drinkable water/ g of adsorber in a half day (Mulchandani et al., 2020).

2.6. Extra Researches

Using straightforward methods, Ackerman (1968) manufactured an apparatus that can generate water from the atmospheric air at almost any location on the planet's surface. The water-generating device comprised a glass "greenhouse" container with a lid section, a receptacle portion, and a second container containing evenly distributed cone-shaped plates. As an absorber, a hydrophilic substance (MgSO$_4$.7H$_2$O) was used. The amount of collected water was found to be one litre in a single summer day. The disadvantage of lithium chloride is that it is expensive, while the drawback of Calcium chloride is that it is unstable. Hence, Ertas et al. (1992) mixed them in various weight ratios to stabilise CaCl$_2$ and lower the cost of LiCl. The research aimed to assess the physical characteristics of multiple parameters, like density and viscosity, as well as vapour pressure, which is essential for analysing the transfer of heat and mass in a hybrid desiccant cooling system. Under specific temperature and concentration conditions, the solubility of this novel liquid desiccant was also

investigated. Krumsvk's (1998) research goal was to develop a technique for extracting water from a moist environment that does not require an external power source using a pyramid-shaped device. A cellulose fibre, such as ground or shredded newspaper waste, was used due to its large surface area in a well-known process of atmospheric moisture adsorption followed by cooling-induced condensation. A study was conducted to develop applications for the solar trough concentration beyond heating and cooling, including obtaining clean water from the atmosphere. A solar concentrator and a double-effect ammonia chiller were used to achieve this, where solar energy was used to heat the air and a chiller to condense the atmospheric moisture. It was found that using a slant angle of 25° will get the highest results (Scrivani et al., 2007). Bardy discussed obtaining drinkable H_2O from atmospheric air via solar concentration. The AQUASOLIS project's results were used to assess the performance of a solar trough concentration system in various uses, like water production, besides heating and cooling (Bardi, 2008). Using anhydrous and hydrated salt couples, a study was done to extract water vapour from dry atmospheric air and supply potable water using solar radiation as the only energy source. A bi-layered composite disc was used for moisture collection while testing 14 common anhydrous and hydrated salts. Copper chloride ($CuCl_2$), copper sulfite ($CuSO_4$), and magnesium sulfate ($MgSO_4$) stand out among the salt couples studied because of their capacity to absorb and regenerate water, as well as their chemical and physical stability. According to the findings of this study, $CuCl_2$ performs better in locations with low relative humidity and high solar radiation, like deserts, whereas $CuSO_4$, as well as $MgSO_4$, are better suited for areas with high relative humidities and little solar radiation, such as islands or mountainous regions (Li et al., 2018b). A study was conducted for atmospheric water generation using three composite materials consisting of sand with lithium Chloride (CM 1), Calcium Chloride (CM 2), and Lithium Bromide (CM 3). The atmospheric air was utilised to extract moisture using absorption/desorption procedures. A Scheffler reflector with a 1.54 m^2 surface area was constructed for the regeneration procedure throughout the day. According to the results, the generated water quantity using CM 1, CM 2, and CM 3 were 90, 115, and 73 millilitres, respectively. It was found that water generation costs $0.71, $0.53, and $0.86 per year, respectively (Srivastava & Yadav, 2018a). A simultaneous adsorption-desorption procedure was used in an experimental study to gather drinkable water from the atmosphere using a floating glass box-shaped device. An "Interfacial Solar-Driven Atmospheric Water Generator (ISAWG)" was employed as an absorbing material that consists of a hydrophilic carbon membrane as an interfacial solar absorber and 1-ethyl-3-methyl-imidazolium acetate as a liquid absorbent.

According to the findings, the amount of water generated is 0.5 L/m^2/h and 2.8 L/m^2/day (Qi et al., 2019).

2.7. Simulation

Kabeel et al. (2014) examined a different method for obtaining drinking water from the environment. The studied technique was appropriate for nations in the Arabic Gulf or other comparable locations since it used solar-based thermoelectric generators. The simulation was carried out using Star-CCM+, and three different climatic zones (the Red Sea, the Arabic Gulf, and South Spain) were evaluated for various criteria. According to the findings, 3.9 litres of water were produced per square metre per hour using an air fan with a maximum pumping power of 9.1 watts. Mohammed et al. (2017) studied theoretically how various operating circumstances may impact the system's effectiveness. As a desiccant, Calcium chloride was employed with multiple initial concentrations, and two types of beds (sand and black cloth) were considered in a mathematical model that was developed to study how the system would operate throughout the desorption phase. The total amount of water that could be generated was 3.02 L per square meter daily.

From the studies listed above, various structured apparatuses were built for atmospheric water collection, including pyramidal, box-shaped, and accordion-shaped ones. Various types of absorbers like Silica gel, Calcium chloride, MOFs, and hydrogels were used to absorb moisture from the air. Various bed materials like sand and black cloth were employed as liquid desiccant holders inside the device. Researchers increased the number of used shelves or inserted fins within the device to expand its surface area, utilised gravels to enhance the desiccant's working temperature and employed concentrators to focus solar energy into a specific spot (Danışmaz & Alhurmuzi, 2022).

3. MATERIALS AND METHODS

3.1. Materials

In this section, all the materials used in the setup of the apparatus, the instruments used in the measurements, the selection of condensation surface material, the information about internal reflectors, and the preparation of the utilised desiccant materials were all explained in detail.

3.1.1. Experimental setup

As demonstrated in Figure 3.1, a single-slope apparatus comprises two identical sections isolated from each other by a wall and insulating material within the wall, and each section with dimensions of 56 x 68 x 82.5 cm^3 can be used as a small integrated apparatus. The device's frame was built from aluminium columns with a 4 cm thickness. The base, middle, and side walls were constructed of two sheets with a gap between them. An aluminium sheet of 0.7 mm thickness was used as an internal sheet, while an Alucobond sheet of 2.5 mm thickness was used as an external sheet. To lessen the heat loss from the device to the surroundings, an ArmaFlex rubber sheet with a 2.5 cm thickness was used for insulation and placed in the gap inside the base and the walls. The top inclined surface and the front surfaces were made of an acrylic sheet of 2.4 mm thickness. On the backside, doors were used that were constructed from polyvinyl chloride (PVC).
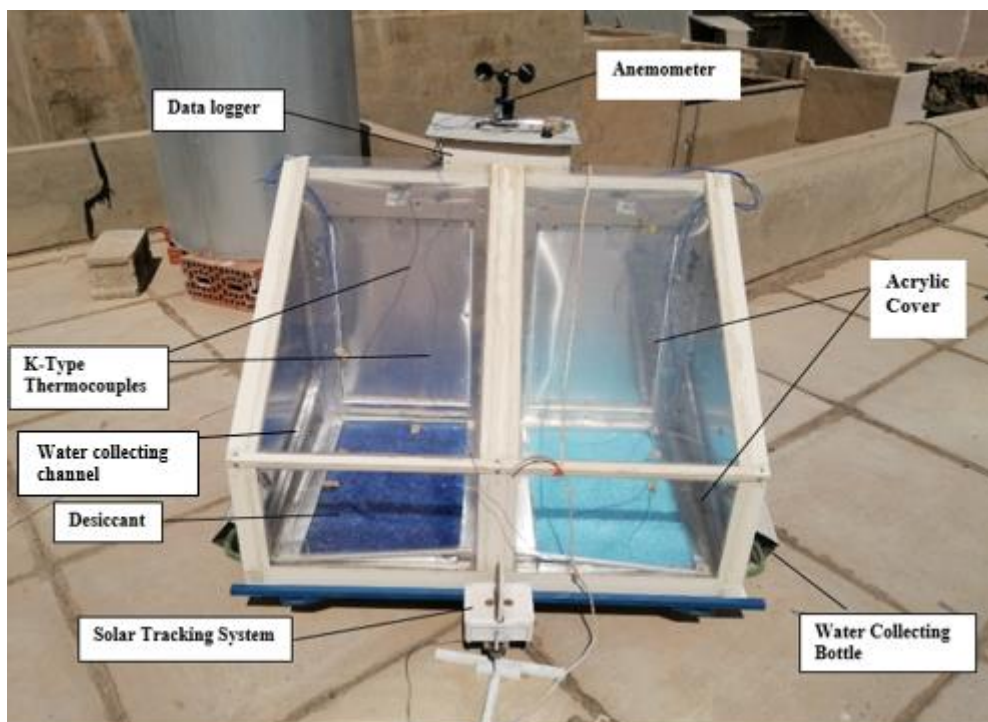
Figure 3.1. Actual image of the apparatus

Figure 3.2 depicts the setup's schematic. To increase the temperature inside the device, aluminium sheets were used on the internal surfaces of the base, the sides, and the middle walls to act as internal reflectors. Trays made of aluminium sheet with 0.7 mm thickness and 36 X 57 X 2 cm dimensions were used to hold the desiccant inside the device. To collect the condensed water droplets, channels made of aluminium sheets were placed on the side and the middle walls, as well as on the front glass surface. The droplets were transported from the channels to bottles placed outside the device via a water hose. A solar tracking system followed the sunlight throughout the day, and a DC motor was used to rotate the device with the sun's movement.
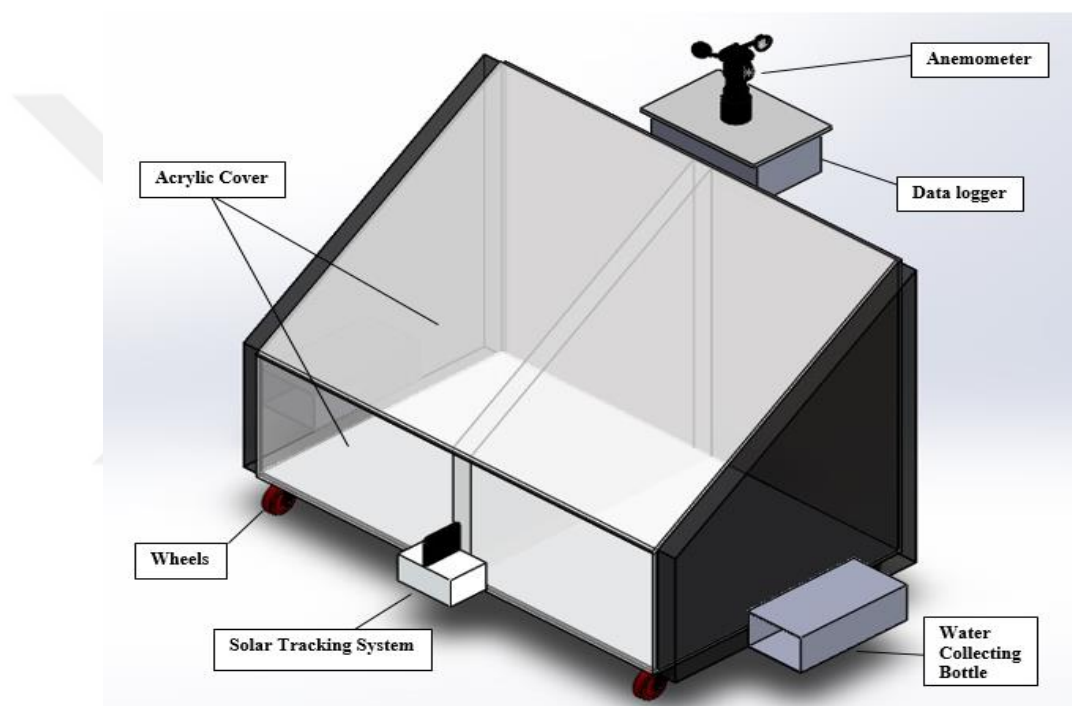
Figure 3.2. Schematic diagram of the apparatus

3.1.2. Devices used in the experiment

3.1.2.1. Solar power meter

A solar power meter type TES-132 (Figure 3.3) was used to measure the total (direct and diffused) solar radiation during regeneration. It receives solar radiation via the white part, with a resolution of 2000 W/m^2 and an accuracy of ± 10 W/m^2 ($\pm$ 5%).
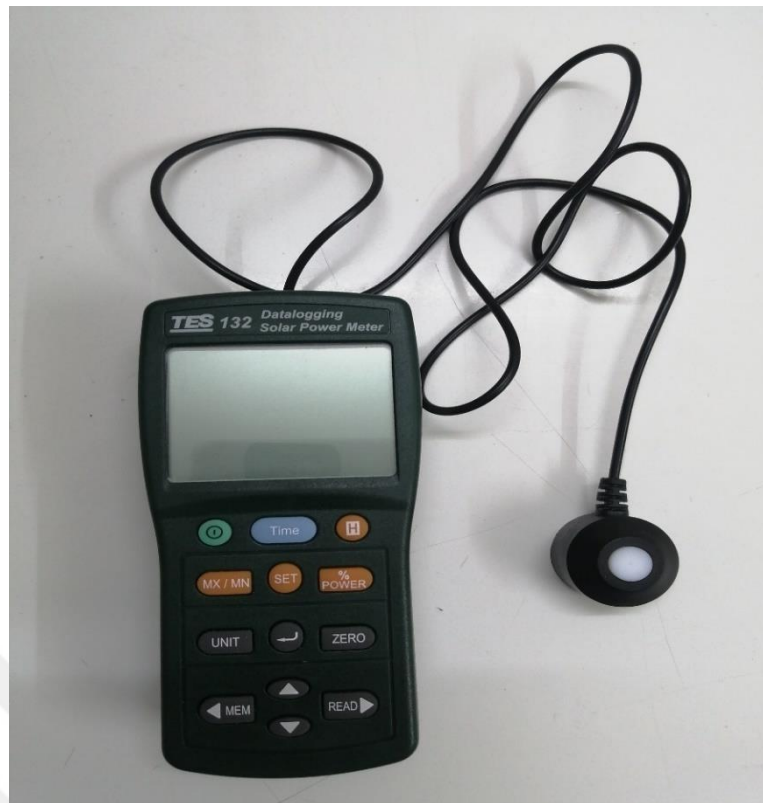
Figure 3.3. Solar power meter

3.1.2.2. Wind speed sensor

The wind speed was measured using a polycarbon wind speed sensor type RS-FSJT-V05 (Figure 3.4). It has a resolution of 0.1 m/s and works within a 0 – 60 m/s range.

Figure 3.4. Wind speed sensor

3.1.2.3. K-type thermocouples

Temperatures of the ambient air, the desiccant surface, the interior surface of the glass, and the temperature inside the apparatus were measured using thermocouples of type K (Figure 3.5). They can be used from −270 °C to 1.370 °C, with errors within 0.5 to 2 °C, and they have a sensitivity that is approximately 41 microvolts per °C.
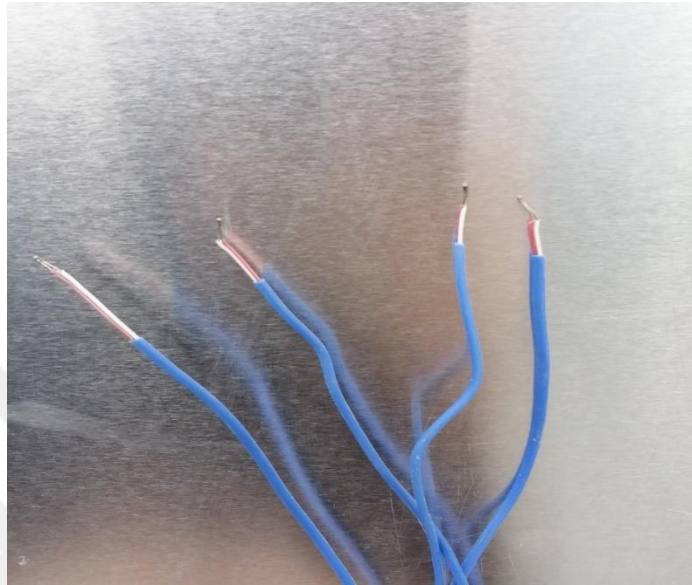
Figure 3.5. K-type thermocouple

3.1.2.4. Relative humidity sensor

The relative humidity was measured using AM2302 (wired DHT22) sensor, as shown in Figure 3.6. This sensor is suitable for 0-100% humidity readings with 2-5% accuracy.

Figure 3.6. AM2302 type sensor

The accuracy, resolution, and measuring range of these instruments and sensors are listed in Table 3.1.

Table 3.1. Measuring instruments' accuracy, resolution, and ranges

Sensor/Device	Type	Range	Accuracy	Resolution
Solar power meter	TES-132	0-2000 W/m^2	±10 W/m^2	0.1
Thermocouples	K	-270 to 1260 °C	±0.25 °C	0.5
Relative humidity sensor	AM2302 (wired DHT22)	0-100 %	± 2-5 %	0.1
Wind speed sensor	RS-FSJT-V05	0-60 m/s	± (0.2+0.03v) m/s	0.1

3.1.2.5. Weighing machine

To measure the mass of the desiccant bed before and after both the absorption and regeneration processes, a high-sensitivity weighing machine (Figure 3.7) was used. It has a capacity of 40 Kg with a division of 1 g.

Figure 3.7. Weighing machine

3.1.2.6. Hotplate and magnetic stirrer

A Hot plate and Magnetic stirrer (Figure 3.8) with a speed range of 60 – 1500 rpm were used to prepare the Calcium Chloride solution. The magnetic stirrer produces a rotational field using a spinning magnet rod. For stirring the liquid, the stir rod is submerged in it. Teflon coating makes the bar chemically inert, preventing it from contaminating or reacting with its reaction mixture.

Figure 3.8. Hotplate and Magnetic stirrer

3.1.2.7. Standard Oven

To dry Silica gel before using it alone as the first desiccant material or mixing it with Calcium Chloride to prepare a composite material as the second desiccant, a standard oven (Figure 3.9) of "WiseVen Won" company has been used. The oven has a temperature range of +5 ^{o}C up to 230 ^{o}C with an accuracy of ±0.3 ^{o}C. It also has a temperature uniformity of about ±1% of the reached temperature.

3.1.2.8. Desiccator

After drying, Silica gel was placed in a desiccator to prevent it from getting humidity from the air. Desiccators are devices that dry or prevent chemicals from getting "wet" due to ambient moisture. A glass bowl and cover make up the desiccator (Figure 3.10), and they both have thick glass edges that, once greased, may form a perfect sealer. Barium Chloride BaCl (Figure 3.11) was used within the desiccator to absorb possible excited humidity and keep the Silica gel dry. It was placed beneath the perforated ceramic disk, and Silica gel was positioned over it.

Figure 3.9. A standard oven

Figure 3.10. Desiccator

3.1.2.9. UPS power supply

A UPS power supply (Figure 3.12) of the "Power Max" company was used to ensure that the data logger continues working even when the electricity is cut out. The power supply has a capacity of 1500VA/900W.
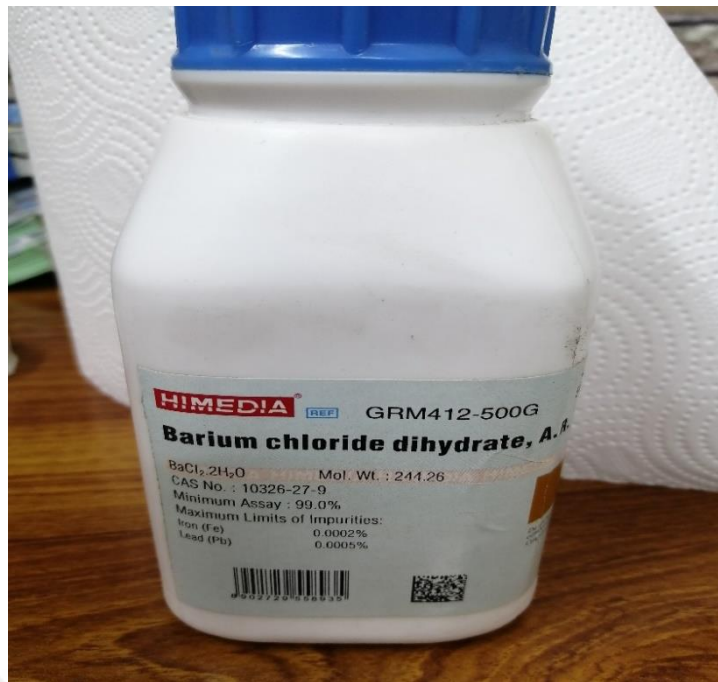
Figure 3.11. Barium Chloride

Figure 3.12. UPS power supply

3.1.2.10. Solar tracking system

The solar tracking system consists of a box containing two light sensors (LDR) on the surface, and a barrier separates them. The sensors are connected to a Nano-type Arduino placed inside the box that receives the signals from the sensors and sends commands to DC motors to rotate the apparatus. As the sun moves in the sky, the barrier's shadow falls on the sensor located in the opposite direction of the sun's movement, leading to an increment in

the sensor's resistance. As a result, the apparatus rotates in the same direction as the sun's movement until the sunlight strikes both sensors and the barrier's shadow disappears. At sunset, a magnetometer stops the sensors from working and rotates the apparatus to the south to be ready to work again the following day with the sunrise.
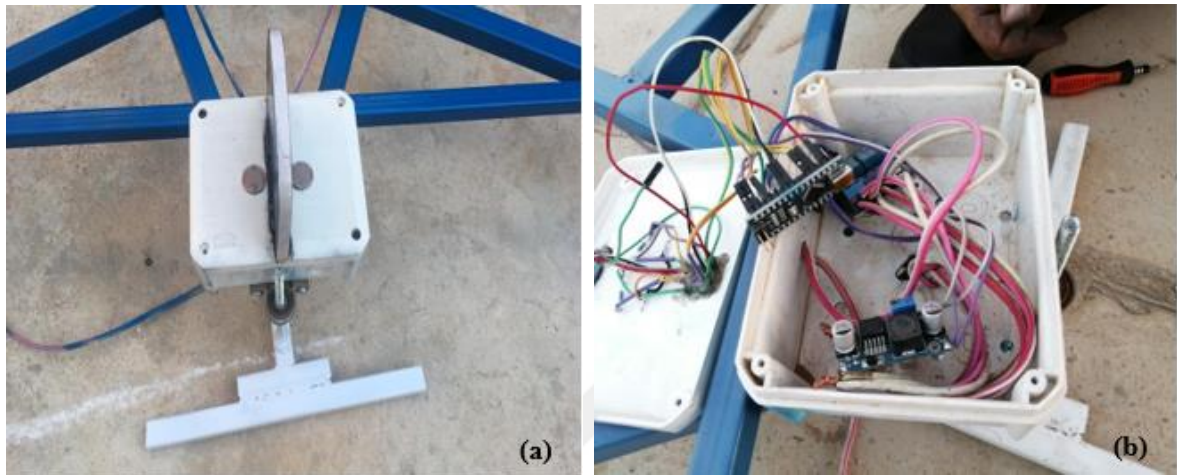
Figure 3.13. Solar tracking system: (a) from outside, (b) from inside

3.1.2.11. DC motor

To rotate the apparatus with the sun's movement throughout the day, two ZGY370-type DC motors (Figure 3.14) were used. The motor contains a worm gearbox that reduces its speed and increases its torque. The motors rotate the apparatus as they receive the command from the Nano-type Arduino.
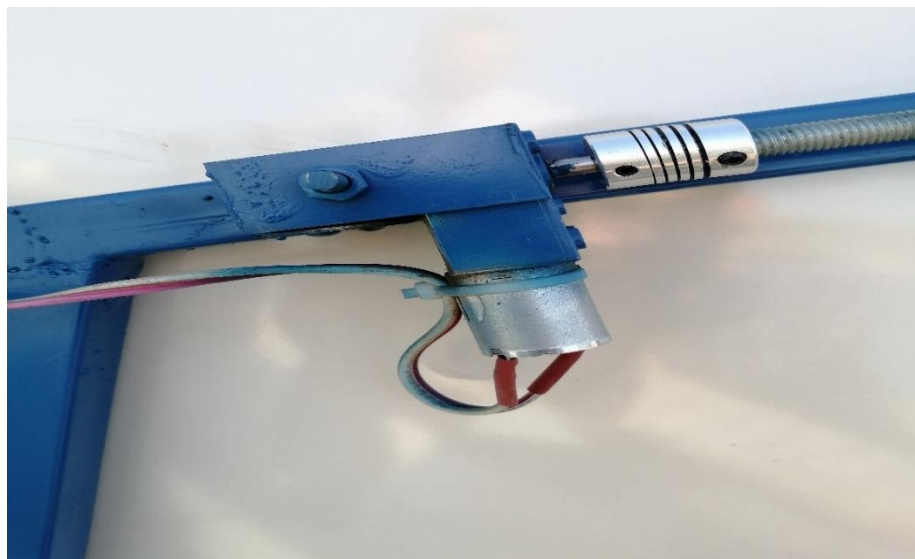
Figure 3.14. DC motor with a worm gearbox

3.1.2.12. Data logger

A data logger (Figure 3.15) was used to collect data like relative humidity, wind speed, solar intensity, and temperatures at different points 24 hours a day. The K-type thermocouples used for temperature measurement send the data to the MAX 6675 module, which transfers it to a microprocessor (Arduino). For solar intensity measurement, a resistor supplied with 5 volts was used; when the sunlight increases, the voltage in the resistor decreases, and the output voltage is transferred to the Arduino. The AM2302 (wired DHT22) sensor measures relative humidity, and polycarbon wind speed sensor type RS-FSJT-V05, which measures the wind speed, sent the data to the Arduino. The Arduino then saved all data to an SD card.
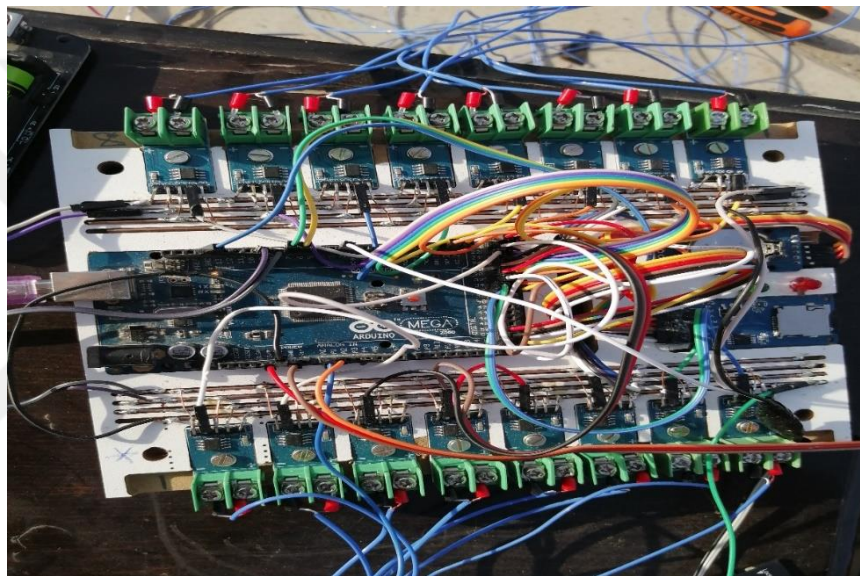
Figure 3.15. A data logger

3.1.3. Insulation material

To prevent vapour leakage from the device to the surroundings in the regeneration process, the side walls, middle wall, and the base of the device were insulated using an ArmaFlex rubber sheet with 25 mm thickness (Figure 3.16) manufactured by Armacell (Germany). Armaflex® class O sheet is manufactured from nitrile rubber foam that is chlorofluorocarbon (CFC) free. Armaflex was used in many experiments (Jerman, 2011; Yousef & Hassan, 2019; Meng et al., 2020) as an insulating material, and it was selected in this study due to its many advantages like its high level of protection towards water vapour dispersion, flexibility, hygienic properties, installation simplicity and many other features (Karpov et al., 2021). The service lifespan is 25 years and may be utilised in a temperature range of -50 to +105°C (+85°C when a sheet is glued to flat surfaces) and its thermal conductivity of 0.033 W/m).

Figure 3.16. ArmaFlex rubber sheet

3.1.4. Condensation surface

Experiments were conducted to select the appropriate type and thickness of transparent material to be used as a condensation surface:

3.1.4.1. Selecting material type

The transparent cover is one of the essential elements in our experiment since it is the surface on which the solar radiation transmits to heat the desiccant material in the regeneration process, and it is also used as the condensation surface to generate water droplets. So, we conducted a test to select the best material type for this purpose. A comparison was made among three types of materials. Regular and plastic glasses of 3 mm thickness and an Acrylic sheet of 2.4 mm thickness were used. The transmissivity of these materials was tested using a wood stand to hold the patterns and a solar power meter to measure the amount of the transmitted solar radiation through them (Figure 3.17). The test was done on three different days from 8:00 a.m. to 18:00 at the two-hour interval, and the test results are presented in Appendix B. According to the results, the Acrylic sheet has the highest radiation transmissivity and the lowest radiation reflectivity, which we need in this experiment.

3.1.4.2. Selecting material thickness

According to Kumar & Yadav (2015c), the thickness of the transparent cover used in the experiment device can affect solar radiation transmissivity. So, we conducted a test (Figure 3.18) to choose the most appropriate thickness. Regular and plastic glasses with 3 mm and 4 mm thicknesses for each were used in the test. A wood stand was used to hold the glass patterns, and a solar power meter was used to test the transmissivity in each case. The test was done on three different days from 9:00 a.m. to 17:00 at the two-hour interval, and

30

the test results are given in Appendix B. The findings revealed that less thickness means better transmissivity, which agrees with the results of Kumar & Yadav (2015c), who found that 3 mm thickness is better than 4 mm and 6 mm thickness.
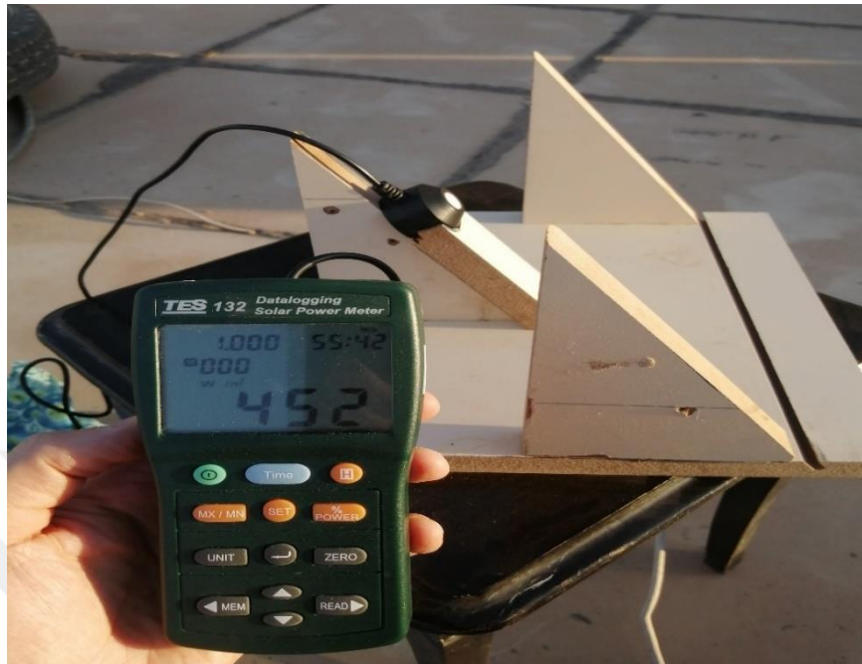
Figure 3.17. A wood stand and solar power meter

Figure 3.18. Material test

3.1.5. Internal reflector

To be able to speed up water generation and shorten the time needed for water collection by increasing the bed surface temperature, which is necessary for the vaporisation of moisture from the desiccant material, an internal reflector made of aluminium was

installed on all walls of the device (Figure 3.19). According to Karimi Estahbanati et al. (2016), as compared to a device without internal reflectors, installing internal reflectors on all walls may boost distillate output by 65%, 22%, and 34% over the winter, summer, and full year.

Figure 3.19. Internal reflectors

3.1.6. Preparation of desiccant material

The preparation of Silica gel, Calcium chloride, and the composite material were all done in the laboratory of the Chemistry department, Sciences College, Kirkuk University.

3.1.6.1. Silica gel preparation

A blue-coloured indicator Silica gel bead with a 4-6mm grain size was used. It is a solid desiccant, so it was used directly without a preparation process. Since it can adsorb moisture, it may adsorb a small quantity before using it in the experiments. Therefore, it must be dried before usage. To do so a standard oven was used for this purpose. One kilogram of Silica gel was placed in the oven (Figure 3.20) and closed the door. Firstly, the air inside the oven was drawn out using a discharge process via a motor (Figure 3.21) connected to the oven. The motor switched on and continued discharging until the pressure inside the oven became -0.6 bar, and then the motor switched off. Secondly, the oven was turned on, the temperature was set to 120 ºC (Aristov, 2007), and the drying continued for two hours. Silica gel was removed from the oven (Figure 3.22) and preserved in containers to keep it from humidity until the experiment day. Table A.1 of Appendix A presents the characteristics of the Silica gel employed in our studies.

Figure 3.20. Drying process of SiO_2

Figure 3.21. A motor used in discharging operation

Figure 3.22. Silica gel after the drying process

3.1.6.2. Preparation of calcium chloride

Calcium Chloride is in a powder-form salt; to use it in composite desiccant, it must first be prepared as a liquid solution. According to the study by Yu et al. (2014), a liquid solution with 30 wt% is the most appropriate for a composite desiccant preparation. So, 300 grams of $CaCl_2$ flakes were introduced into 700 ml of purified water and then dissolved using a "Hot plate and Magnetic stirrer" apparatus. The process continued until $CaCl_2$ was utterly dissolved in the water (Figure 3.23).
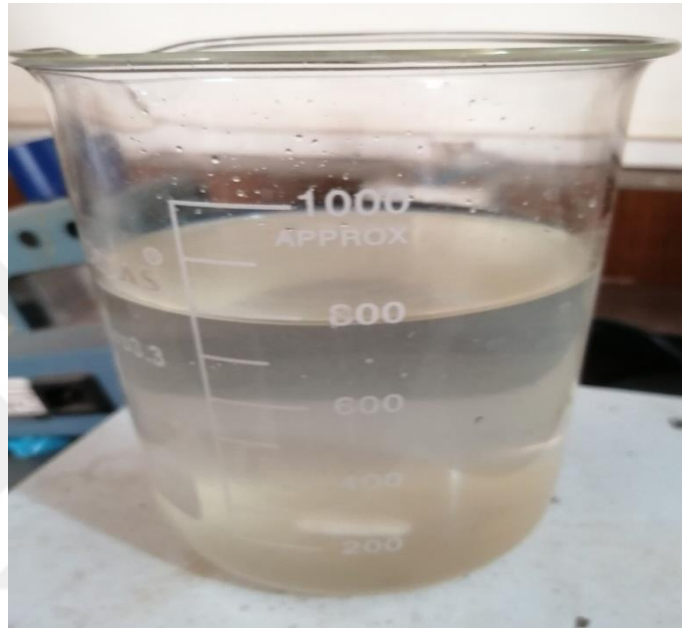
Figure 3.23. Calcium Chloride solution

3.1.6.3. Preparation of a composite desiccant

The composite desiccant (SiO_2-$CaCl_2$) was prepared by impregnation of the dried Silica gel with the aqueous solution of Calcium Chloride at 30 wt% (Aristov et al., 1996) at ambient temperature (T) for 20 hours (Figure 3.24). After that, the composite was filtered to remove the unadsorbed solution and then put in the oven for drying. The composite was dried in the oven at 120 °C for 4 hours (Zheng et al., 2014) and then preserved in containers to use on the test day (Figure 3.25).
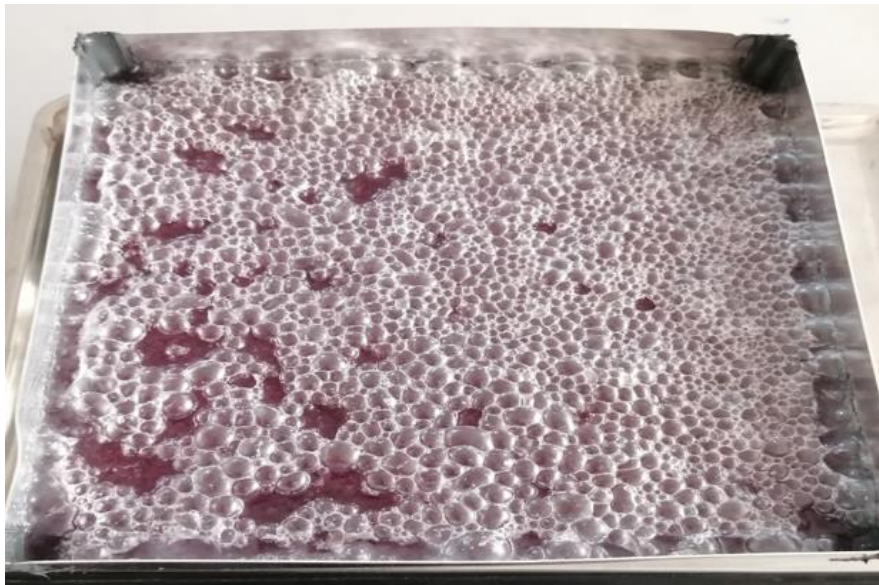
Figure 3.24. Silica gel impregnated with Calcium Chloride

Figure 3.25. Composite desiccant

3.2. Methods

In this section, the experimental procedure, the mathematical models, the uncertainty analysis, and the cost analysis were all explained in detail.

3.2.1. Experimental procedure

The experiments were conducted in the climatic conditions of Kirkuk, Iraq (latitude 35.4666° N and longitude 44.3799° E). The experiments were done in three steps: adsorption, regeneration, and condensation. At night, the adsorption process started with the sunset by exposing the desiccant material to the atmospheric air. As a result of the difference in vapour pressure between the absorber surface and the surrounding air, moisture began to

move from the air to the desiccant, and this process persisted until the difference in vapour pressure became zero. It was observed that the Silica gel's colour changed from dark blue to light purple (Figure 3.26), and the composite's colour changed from sky blue to light blue or white (Figure 3.27), indicating that moisture had been adsorbed.
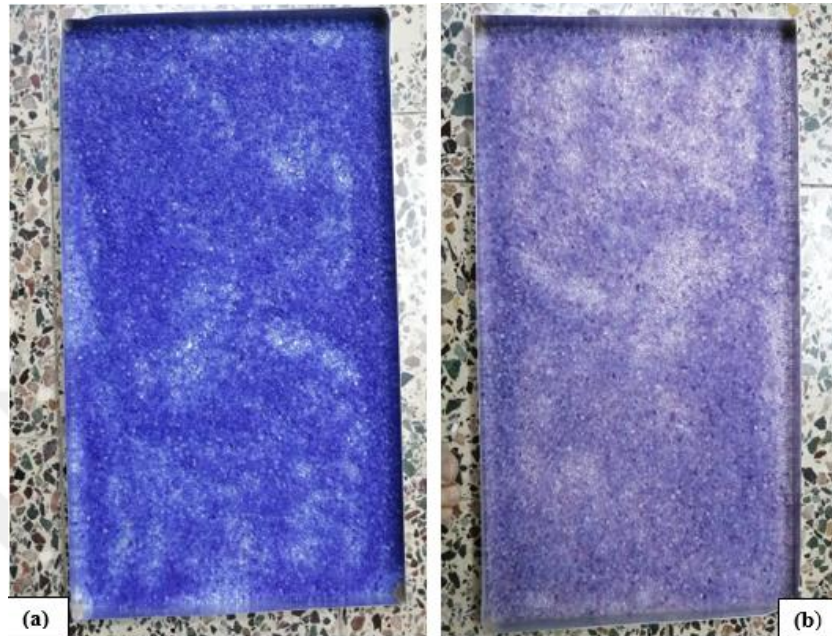
Figure 3.26. Silica gel: (a) before moisture adsorption, (b) after moisture adsorption
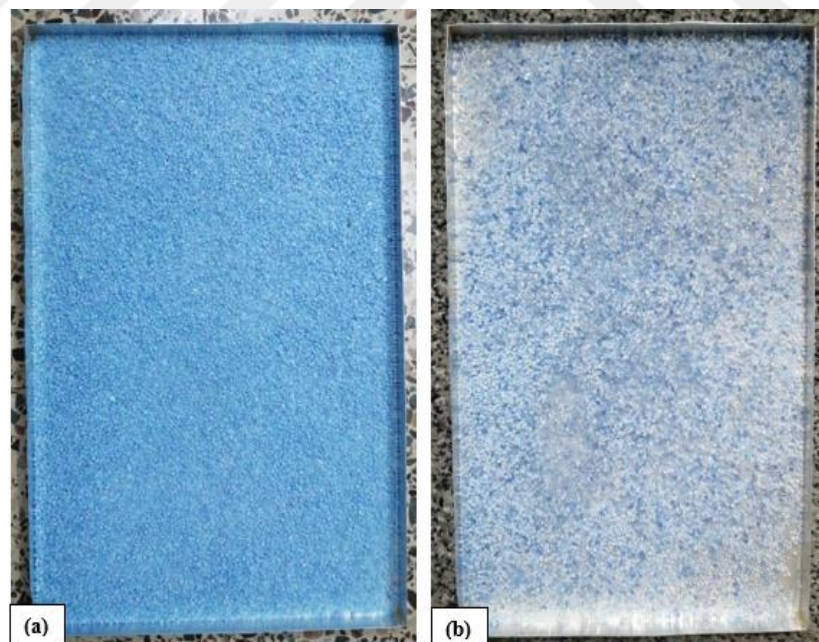
Figure 3.27. Composite: (a) before moisture adsorption, (b) after moisture adsorption

In the daytime, after putting the desiccant inside the device and closing the doors, the regeneration process started with the sun rising. The sun began to transmit energy to the desiccant material, raising the temperature and the vapour pressure on the adsorber's surface.

Consequently, the moisture evaporated and transferred toward the internal surface of the acrylic sheet due to the difference in the vapour pressure, and the evaporated water condensed on the acrylic cover (Figure 3.28). The evaporation and condensation processes ended when there was no pressure differential. The Silica gel's colour changed from light purple to dark blue again, and the composite changed from light blue to sky blue, showing that they lost all of their water during the regeneration process.

Figure 3.28. water droplets condensed on the cover surface

3.2.2. Mathematical models

An adsorption operation, a desorption mechanism, and a model of solar intensity comprise the mathematical model. During the device's daily operation, the solar intensity model was used to determine the power of the sun's rays. The adsorption process model was employed to compute the mass transfer coefficient and the volume of moisture adsorbed during the adsorption (nighttime process). Finally, various parameters were theoretically predicted in the regeneration process using the 4th-order Runge Kutta method in the MATLAB program due to its good results in the research conducted by Fathy et al. (2020).

3.2.2.1. Solar intensity model

Solar intensity is crucial for desorption since the sun is the heat origin in evaporating the adsorbed moisture. Solar radiation on a horizontal surface was employed since the desiccant surface is horizontal, and the following formulae were used to determine the theoretical total solar radiation (Kalogirou, 2013):

$$H = H_b + H_d \tag{3.1}$$

The direct beam radiation (H_b) can be expressed as (Mousavi Maleki et al., 2017):

$$H_b = H_{bN} \, Sin \, \Theta \tag{3.2}$$

Where H_{bn} is the normal beam radiation on a horizontal plane, and it may be found from (Talaat et al., 2018):

$$H_{bN} = A.exp\left[\frac{-E}{sin \, \Theta}\right] \tag{3.3}$$

The altitude angle ($sin \, \theta$) can be determined from (Kalogirou, 2013):

$$sin(\Theta) = sin(L)sin(\delta) + cos(L)cos(\delta)cos(h) \tag{3.4}$$

The declination angle (δ) can be calculated from the equation (Duffie & Beckman, 2006):

$$\delta = 23.45sin\left[\frac{360}{365}(284 + N)\right] \tag{3.5}$$

N: is the day number of the year; it can be selected from Table A.2 in Appendix A

The hour angle (h) may be calculated using the equation (Kalogirou, 2013):

$$h = (AST - 12)15 \tag{3.6}$$

AST: apparent solar time. It can be computed from (Mousavi Maleki et al., 2017):

$$AST = LST + \frac{ET}{60} + \frac{4}{60}[SL - LL] \tag{3.7}$$

SL and LL are the standard and local longitudes, respectively, of the studying location.

ET: equation of time, can be calculated from (Mousavi Maleki et al., 2017):

$$ET = 9.87sin\,2G - 7.53cos\,G - 1.5cos\,G \tag{3.8}$$

Where:

$$G = \frac{360(N - 81)}{365} \tag{3.9}$$

The diffused radiation on the horizontal plane (H_d) may be expressed as (Fathy et al., 2020):

$$H_d = DH_{bn}F_{ss} \qquad (3.10)$$

F_{ss}: angle factor between sky and surface, it can be found from (Talaat et al., 2018):

$$F_{ss} = 0.5(1 + cos\,\gamma) \qquad (3.11)$$

The values of A, E, and D are all constants and can be found in Table A.3 in Appendix A, and theoretical solar radiation calculations are detailed in Appendix C.

3.2.2.2. Adsorption process

The mass transfer of the water vapour between the desiccant's surface and the ambient air is primarily influenced by the amount of moisture adsorbed from the atmosphere during the adsorption phase and the difference in water partial pressure, which acts as a driving factor. The mass transfer was determined from (Fathy et al., 2020):

$$\beta = \frac{\dot{m}}{A_b \Delta p} \qquad (3.12)$$

Δp is the vapour pressure difference between the ambient air and desiccant surface, which can be expressed as (Gad et al., 2001):

$$\Delta p = p_\infty - p_d \qquad (3.13)$$

The vapour pressure of the ambient air (P_∞) may be found in (Talaat et al., 2018):

$$P_\infty = \emptyset P_{sat@T_a} \qquad (3.14)$$

$P_{sat@Ta}$ is the saturated vapour pressure at ambient temperature and may be computed from (Fathy et al., 2020):

$$P_{sat@T_a} = 6.11 \times 10^{\frac{7.5 \times T_a}{237.3 + T_a}} \qquad (3.15)$$

The desiccant's surface water vapour pressure can be expressed as (Gad et al., 2001):

$$log_{10}\,P_d = -3.21254 + 3.13619 \times 10^{-2}\,T_{dE} - 1.22512 \times 10^{-4}\,T_{dE}^2 \qquad (3.16)$$
$$+ 3.63841 \times 10^{-7}\,T_{dE}^3 - 5.67607 \times 10^{-10}\,T_{dE}^4$$

Detailed theoretical calculations of the mass transfer coefficient during the adsorption process are given in Appendix D.

3.2.2.3. Regeneration process

In the daytime, solar radiation fell on the surface of the cover, where a large portion was transmitted to the inside of the apparatus, the cover absorbed a small amount, and the rest was reflected. Heat transmission occurs from the desiccant surface towards the cover across the air gap by radiation, conduction, and evaporation, followed by heat loss from the cover towards the surrounding air. Heat balance equations for the Silica gel's surface and the transparent cover were used in the desorption model. These equations were numerically solved using the Runge-Kutta 4th order approach, and the system's behaviour was simulated using the MATLABTM programme. The software assessed the theoretically predicted system transient parameters and performance traits. The codes written in MATLAB for the theoretical calculations are given in Appendix G. For composite material, theoretical calculations were not conducted because the physical and chemical properties of the prepared composite material, which are a necessary prerequisite for performing theoretical calculations, are not available since various types of laboratory devices are needed to determine them. The heat balance for the cover and the desiccant can be calculated using the following equations (Mohamed et al., 2017):

$$C_b \left(\frac{dT_d}{dt} \right) = \tau_{cov} \alpha_b H_E - (q_e + q_c + q_r) \tag{3.17}$$

$$C_{cov} \left(\frac{dT_{cov}}{dt} \right) = (q_e + q_c + q_r + H_E) - (\tau_{cov} H_E + q_{cov-sky}) \tag{3.18}$$

The thermal capacity of the bed (C_b) is the product of the multiplication of the specific heat of desiccant, absorbed water, and the material of the desiccant carrier, c_d, c_w, c_c, respectively, with the mass of desiccant, absorbed water, and desiccant carrier material, m_d, m_w, m_c, respectively (Fathy et al., 2020):

$$C_b = (c_d \, m_d + c_w m_w + c_c \, m_c)/A_b \tag{3.19}$$

The thermal capacity of the cover (C_{cov}) is the multiplication of the specific heat of the cover with its mass (Talaat et al., 2018):

$$C_{cov} = (c_{cov} \, m_{cov})/A_{cov} \tag{3.20}$$

The heat transfer between the cover and the sky ($q_{cov-sky}$) can be determined by (Mohamed et al., 2017):

$$q_{cov-sky} = h_{cov-sky}(T_{cov} - T_a) + F_{cov-sky}\sigma\left[(T_{cov} + 273)^4 - (T_{sky} + 273)^4\right] \quad (3.21)$$

The convection heat transfer coefficient ($h_{cov-sky}$) may be calculated from the following equation (Kabeel, 2006):

$$h_{cov-sky} = a + bv^n \quad (3.22)$$

a, b, and n are Mc Adams relation coefficients and can be found in Table A.4 in Appendix A

The shape factor between the cover and the sky ($F_{cov-sky}$) may be estimated from (Fathy et al., 2020):

$$F_{cov-sky} = \cfrac{1}{\cfrac{1 - \varepsilon_{cov}}{\varepsilon_{cov}} + \cfrac{1}{\bar{F}_{cov\text{-}sky}}} \quad (3.23)$$

$\bar{F}_{cov\text{-}sky:}$ is the cover-sky view factor, and it can be expressed as (Talaat et al., 2018):

$$\bar{F}_{cov.sky} = 0.5(1 + \cos \xi) \quad (3.24)$$

The sky temperature can be calculated from (Fathy et al., 2020):

$$T_{sky} = T_a - 10 \quad (3.25)$$

Heat transfer from the desiccant to the cover by conduction (q_c) may be determined from (Gad et al., 2001):

$$q_c = K_a \frac{(T_d - T_{cov})}{\Delta y} \quad (3.26)$$

The heat transfers from the bed surface to the cover by radiation (q_r) can be calculated as (Kabeel, 2006):

$$q_r = F_{d-cov}\, \sigma\, [(T_d + 273)^4 - (T_{cov} + 273)^4] \quad (3.27)$$

$F_{d\text{-cover}}$: is the shape factor between the desiccant and the cover and can be found from (Fathy et al., 2020):

$$F_{d-cov} = \frac{1}{\dfrac{1}{\varepsilon_d} + \dfrac{1}{\varepsilon_{cov}} - 1} \tag{3.28}$$

Evaporation heat transfer due to evaporated water from the bed (q_e) may be estimated by (Mohamed et al., 2017):

$$q_e = 0.0061 \left[(T_d - T_{cov}) + \left(\frac{p_d - p_{cov}}{0.265 - p_d} \right) (T_d + 273) \right]^{1/3} (p_d - p_{cov}) h_{fg} \tag{3.29}$$

P_{cov}: is a vapour pressure on the cover surface that can be considered as a saturated pressure of water vapour at the cover's internal surface temperature ($P_{sat@Tcov}$), Mpa, and it can be computed from (Fathy et al., 2020):

$$P_{sat@Tcov} = 6.11 * 10^{\frac{7.5*T_{cov}}{237.3+T_{cov}}} \tag{3.30}$$

P_d: is the partial pressure of the water vapour at the desiccant surface and may be obtained from the following formula (Gad et al., 2001):

$$\begin{aligned} log_{10} P_d = &-3.21254 + 3.13619 \times 10^{-2} T_d - 1.22512 \times 10^{-4} T_d^2 + 3.63841 \\ &\times 10^{-7} T_d^3 - 5.67607 \times 10^{-10} T_d^4 \end{aligned} \tag{3.31}$$

h_{fg}: latent heat of the water and can be estimated from the following relation (Kabeel, 2006):

$$h_{fg} = (2501.67 - 2.389T_d)10^3 \tag{3.32}$$

The accumulated productivity of the system can be calculated as (Talaat et al., 2018):

$$P = \frac{\Sigma q_e}{\Sigma h_{fg}} \tag{3.33}$$

The predicted thermal efficiency of the system can be figured out by utilising the following formula (Fathy et al., 2020):

$$\eta = \frac{\Sigma q_e}{\Sigma H_E} \tag{3.34}$$

Table (3.2) provides all the constants utilised in the abovementioned equations.

Table 3.2. Constants used in the formulae of the regeneration process

Energy balance			
α_b	0.95	-	(Zheng et al., 2015)
τ_{cov}	0.92	-	(Rose, 2019)
c_d	765	J/Kg. K	(Faizal et al., 2014)
m_d	1	Kg	We chose
c_c	900	J/Kg. K	(Cengel & Boles, 2014)
m_c	0.365	Kg	By weighing
c_w	4180	J/Kg. °C	(Cengel & Boles, 2014)
A_b	0.2052	m^2	By calculating
c_{cov}	1470	J/Kg. K	(District & Ratchasima, 2010)
m_{cov}	1.13	Kg	By weighing
A_{cov}	0.3565	m^2	By calculating
Heat transfer from the cover to the ambient (q_{cov-a})			
σ	$5.67 * 10^{-8}$	W/m^2. K^4	(Fathy et al., 2020)
ε_{cov}	0.86	dimensionless	(Nascutiu et al., 2016)
ξ	35	degree	We selected
a	5.61	-	(Mohamed et al., 2017; Fathy et al., 2020)
b	1.09	-	(Mohamed et al., 2017; Fathy et al., 2020)
n	1	-	(Mohamed et al., 2017; Fathy et al., 2020)
Heat transfer by conduction (q_c)			
K_a	0.0288	W/m. °C	(Çengel & Ghajar, 2015)
Δy	0.57	m	By calculating
Heat transfer by radiation (q_r)			
ε_d	0.85	dimensionless	(Yuce et al., 2022)

3.2.2.4. Experimental calculations

The following relationship was used to determine the system efficiency using the experimental data (Srivastava & Yadav, 2018a):

$$\eta = \frac{m_w . h_{fg}}{H_E . A_s . T} * 100 \tag{3.35}$$

Where T = 3600/1000 (conversion factor), and A_s = 0.3808 m^2 (internal surface area of the apparatus).

3.2.3. Uncertainty analysis

The experiment's measured values are inaccurate, which are impacted by the variations brought on by different errors. Systematic error and random error are the two categories of errors. Random errors are brought about by arbitrary and unexpected changes in the experimental settings, while systematic errors are caused by instrument and environmental flaws. Also, personal mistakes might happen while the observer collects the

data (Kumar et al., 2017). The parameters experimentally measured in this study are solar intensity, relative humidity, wind speed, acrylic cover temperature, desiccant surface temperature, and ambient temperature. An experimental error analysis was carried out based on the content provided by Tahseen (2014). The percentage of uncertainty was determined using the Root Sum Square (RSS) approach as follows:

3.2.3.1. Uncertainty of independent parameters

I.   The uncertainty in solar intensity, wind speed, and relative humidity measurements can be calculated from the following equations:

The bias error can be expressed as:

$$B = \pm\left[(\frac{1}{2}Resolution)^2 + (accuracy)^2\right]^{0.5} \tag{3.36}$$

The average value of the readings may be found from:

$$\overline{X} = \frac{1}{N_r}\sum_{i=1}^{N_r} X_i \tag{3.37}$$

The standard deviation can be computed from the following:

$$\sigma_x = \left[\frac{1}{N_r - 1}\sum_{i=1}^{N_r}(X_i - \overline{X})^2\right]^{0.5} \tag{3.38}$$

The mean standard deviation may be expressed as:

$$\sigma_{\overline{X}} = \frac{\sigma_X}{\sqrt{N_r}} \tag{3.39}$$

The precision can be calculated from the following equation:

$$Ps_X = t_{(N_r-1),95\%} * \sigma_{\overline{X}} \tag{3.40}$$

Where $t_{(N_r-1),95\%}$ is the student-t distribution at a 95% confidence interval with the (N_r-1) degrees of freedom. Its value can be obtained from the t-table given in Appendix F.

The absolute uncertainty at 95% confidence may be found from the following:

$$U_X = \pm[B^2 + Ps^2]^{0.5} \tag{3.41}$$

The relative uncertainty can be expressed as:

$$\frac{U_X}{X}\% = \left(\frac{U_X}{X}\right) * 100 \tag{3.42}$$

II.   The uncertainty in acrylic cover temperature, desiccant surface temperature, and ambient temperature measurements can be determined from:

$$U_{Temp} = \pm \left[(U_{Std})^2 + \left(U_{Fitting\text{-}curve}\right)^2\right]^{0.5} \tag{3.43}$$

Where: U_{std} is the absolute uncertainty and can be calculated from the same equations used in the absolute uncertainty calculations of the solar intensity, wind speed, and relative humidity measurements.

The uncertainty of the fitting curve can be explained as follows:

$$U_{Fitting\text{-}curve} = \sigma_{\overline{\chi}} \times t_{(N_r-1),95\%} \tag{3.44}$$

Where $B_{fitting\text{-}curve} = 0$

The relative uncertainty can be calculated from the following equation:

$$\frac{U_T}{T}\% = \left(\frac{U_T}{T}\right) * 100 \tag{3.45}$$

3.2.3.2. Uncertainty of dependent parameters

I.   Uncertainty of saturated water pressure at desiccant temperature P_d:

$$\frac{U_{P_d}}{P_d} = [\left(\frac{U_{T_{dE}}}{T_{dE}}\right)^2]^{0.5} * 100 \tag{3.46}$$

II.   Uncertainty of saturated water pressure on cover temperature P_{cov}:

$$\frac{U_{P_{cov}}}{P_{covE}} = [\left(\frac{U_{T_{covE}}}{T_{covE}}\right)^2]^{0.5} * 100 \tag{3.47}$$

III.   Uncertainty of the latent heat h_{fg}:

$$\frac{U_{h_{fg}}}{h_{fg}} = [\left(\frac{U_{T_{dE}}}{T_{dE}}\right)^2]^{0.5} * 100 \tag{3.48}$$

IV.   Uncertainty of heat transfer by evaporation q_e:

45

$$U_{q_e} = \left[\left(\frac{U_{h_{fg}}}{h_{fg}} \right)^2 + \left(\frac{U_{T_{dE}}}{T_{dE}} \right)^2 + \left(\frac{U_{T_{covE}}}{T_{covE}} \right)^2 + \left(\frac{U_{P_d}}{P_d} \right)^2 + \left(\frac{U_{P_{covE}}}{P_{covE}} \right)^2 \right]^{0.5} * 100 \qquad (3.49)$$

V.   Uncertainty of the water productivity P:

$$\frac{U_P}{P} = \left[\left(\frac{U_{q_e}}{q_e} \right)^2 + \left(\frac{U_{h_{fg}}}{h_{fg}} \right)^2 \right]^{0.5} * 100 \qquad (3.50)$$

VI.   Uncertainty of the system efficiency η:

$$\frac{U_\eta}{\eta} = \left[\left(\frac{U_{qe}}{q_e} \right)^2 + \left(\frac{U_{H_E}}{H_E} \right)^2 \right]^{0.5} * 100 \qquad (3.51)$$

An example of the calculations is given in Appendix F; the resultant uncertainties of the different parameters are listed in Table 3.3

Table3.3. Resultant uncertainty of different parameters

Independent parameters	
Parameter	**Uncertainty (%)**
Solar intensity	±1.17
Wind speed	±3.3
Relative humidity	±5.23
Ambient temperature	±1.77
Desiccant temperature	±1.46
Cover temperature	±1.61
Dependent parameters	
Parameter	**Uncertainty (%)**
Water pressure at the desiccant surface	±1.46
Water pressure at the cover surface	±1.61
Latent heat	±1.46
Heat loss by evaporation	±3.41
Water productivity	±3.7
System efficiency	±3.6

3.2.4. Cost analysis

The total amount of adsorbed moisture in one night is nearly 70 g; a large portion of this is evaporated, a portion of the vapour is lost, while the rest is condensed and collected as potable water. The cost was calculated using the following equations:

Capital Recovery Factor, CRF: It can be expressed as (Talaat et al., 2018):

$$CRF = \frac{I(I+1)^Y}{(I+1)^Y - 1} \qquad (3.52)$$

Fixed Annual Cost, FAC: It can be estimated from the equation (Fathy et al., 2020):

$$FAC = PC^*CRF \qquad (3.53)$$

Annual Maintenance Cost, AMC: It is assumed as 15% of the FAC:

$$AMC = 0.15^*FAC \qquad (3.54)$$

Annual Salvage Value, ASV:

In order to calculate the ASV, the sinking fund factor, SFF must first calculate (Das et al., 2021):

$$SFF = \frac{I}{(I+1)^Y - 1} \qquad (3.55)$$

And the Salvage value, S, maybe calculate from the following equation (Fathy et al., 2020):

$$S = 0.2 * PC \qquad (3.56)$$

Now ASV can be determined from (Kumar & Yadav, 2015a):

$$ASV = SFF^*S \qquad (3.57)$$

Annual Cost, AC:

From the above equations, the annual cost can be computed from (Talaat et al., 2018):

$$AC = FAC + AMC - ASV \qquad (3.58)$$

The total volume of water generated annually, M: It can be expressed as (Das et al., 2021):

$$M = amount\ of\ collected\ water * 365 \qquad (3.59)$$

Cost of a Produced Kilogram of water, CPK:

$$CPK = \frac{AC}{M} \qquad (3.60)$$

The formulas above show that it costs 2.54 dollars per kilogramme to produce one kilogramme of water, which is not economically practical compared to humidity harvesting

in humid air conditions. However, this device would function better in usual humid settings, which might be acceptable in arid, remote, and isolated regions with insufficient humidity. The calculations of cost analysis are detailed in Appendix G. Table 3.4 shows the capital cost of the apparatus.

Table 3.4. The capital cost of the apparatus

| Items	Cost in ID/ $
Apparatus structure	150000/ 103.05
PVC door	50000/ 34.27
Acrylic sheet	14000/ 9.59
Insulating material	20000/ 13.71
Solar tracking system	25000/ 17.14
DC motor	25000/ 17.14
Silica gel	15000/ 10.28
Total	299000/ 205.18

4. RESULTS AND DISCUSSION

The experiments were conducted for various days over several months, and theoretical calculations were done in the MATLAB program using a fourth-order Rung-Kutta method. The change of each variable with time for several months, a comparison between the theoretical calculations and the experimental one using the data from September for several days, a comparison between Silica gel and the composite material using the average data of November, and the change of different variables with others for both desiccants using the average data from October were all plotted and presented below. Also, the change of each variable with time for Silica gel and composite material over several days was plotted using the average data of August and presented in Appendix H.

4.1. Variation of Surrounding Conditions

Figure 4.1. Presents a comparison between the average Solar radiation rate for several months. Solar radiation increases with time from sunrise until its maximum value at midday and gradually decreases until sunset. It can be noticed that July has the highest rate of Solar radiation, while November has the lowest one, where the Solar radiation rate of each month decreases from July to November.
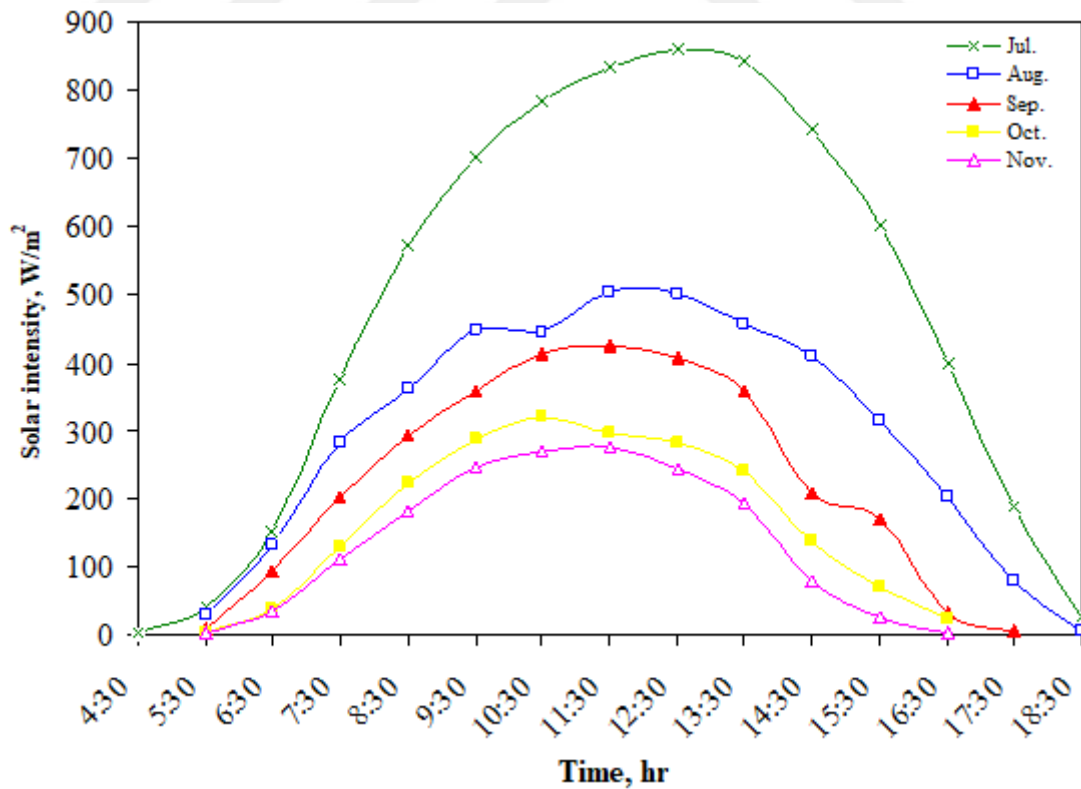

Figure 4.1. Change of solar radiation for several months

For several test days, the theoretical and recorded solar radiation are presented in Figure 4.2. The necessary details for additional days are given in Appendix I. The oil refinery in Kirkuk City impacts solar radiation because it releases multiple contaminants and greenhouse emissions into the atmosphere that may absorb and deflect solar radiation, so less solar radiation reaches the apparatus. This explains why the recorded solar radiation for the same day is considerably lesser than the theoretical one.
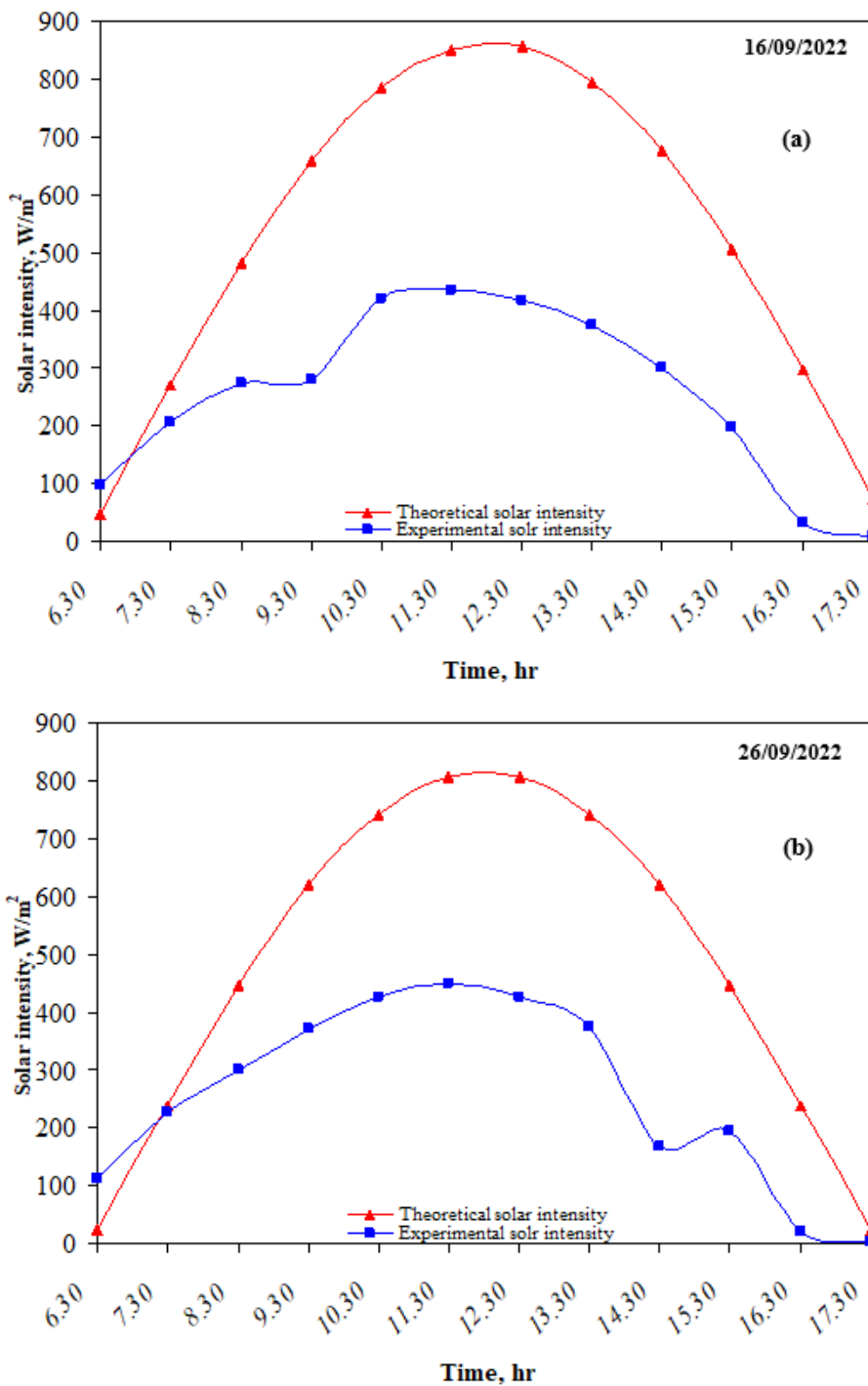
Figure 4.2. Comparison between the theoretical and measured solar radiation for two days

The variation of average wind velocity with time for various months is displayed in Figure 4.3. The wind speed value fluctuates for the whole night in all months. It can be noticed that wind speed value does not depend on the month order over the year, where its value in October is higher than in November and in August is higher than in July, September and November.
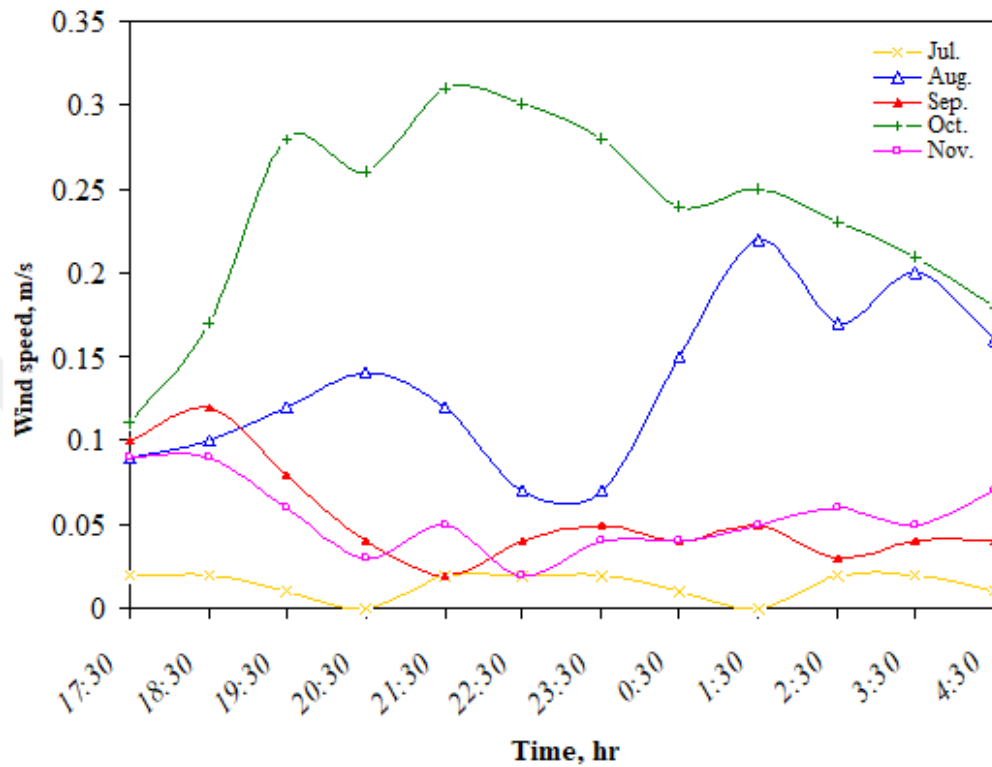
Figure 4.3. Variation of wind speed for various months

Figure 4.4. illustrates the change of average relative humidity with time for several months. For all months, relative humidity increased through the nighttime until it reached its maximum value at dawn, except for July, which increased until 1:30 a.m. and then decreased. The comparison between the average ambient temperature rate of several months is shown in Figure 4.5. Since solar radiation affects the ambient temperature, the latter also decreases as months pass, where the temperature in July is nearly 20 Celsius higher than in November.
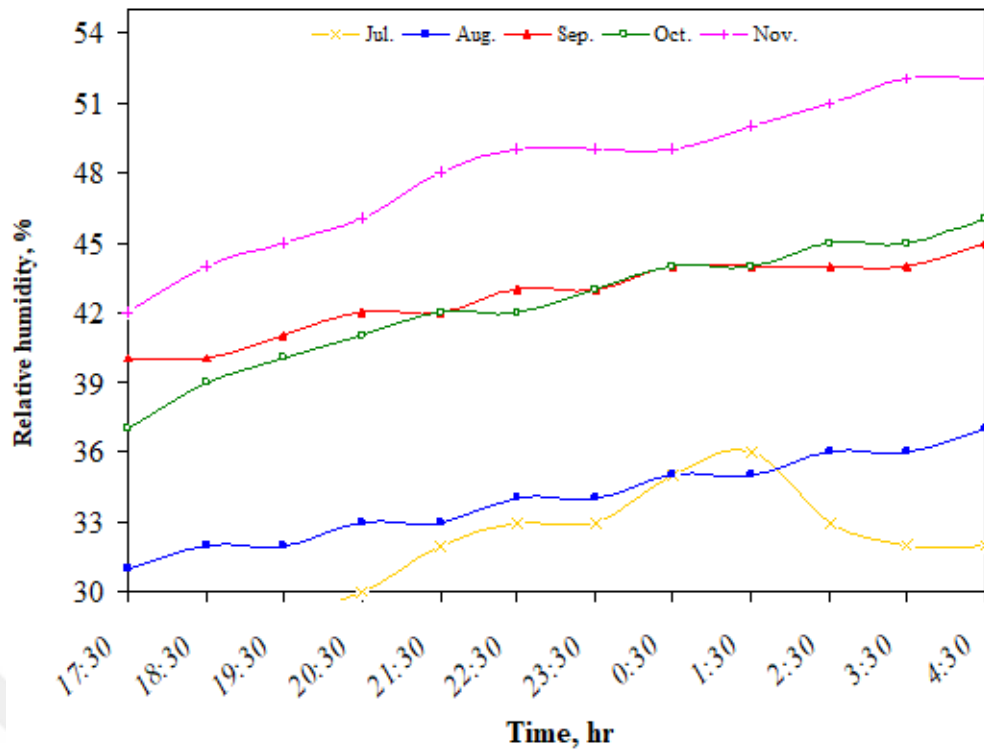
51

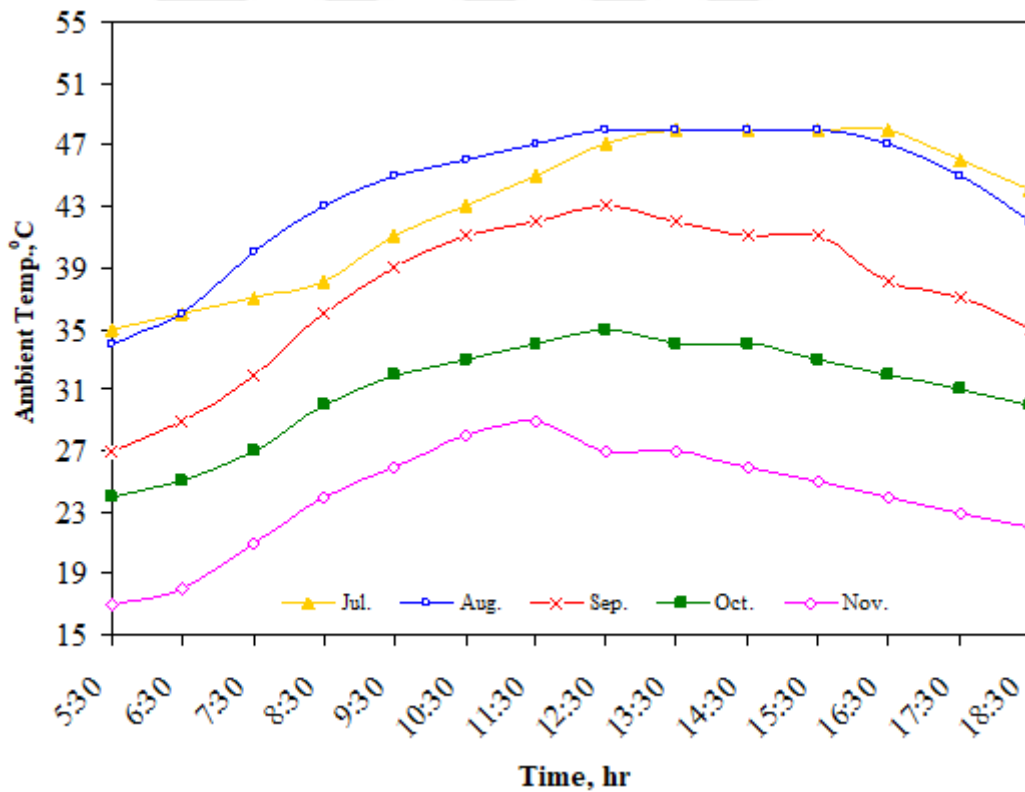**Figure 4.4.** Change of relative humidity for several months

Figure 4.5. Variation of ambient temperature for various months

4.2. Theoretical and Experimental Variation of Setup's Temperature

Figure 4.6. presents a change in the average temperature of the translucent cover over time for different months. The cover's temperature increases from sunrise, reaching its

maximum value at different hours from one month to another, then decreases gradually until sunset. The temperature of the cover in all months is notably less than the desiccant's temperature. This is due to the high transmissivity of the cover material (92%), which transmits the bulk of the received solar radiation and absorbs only 4% of it.
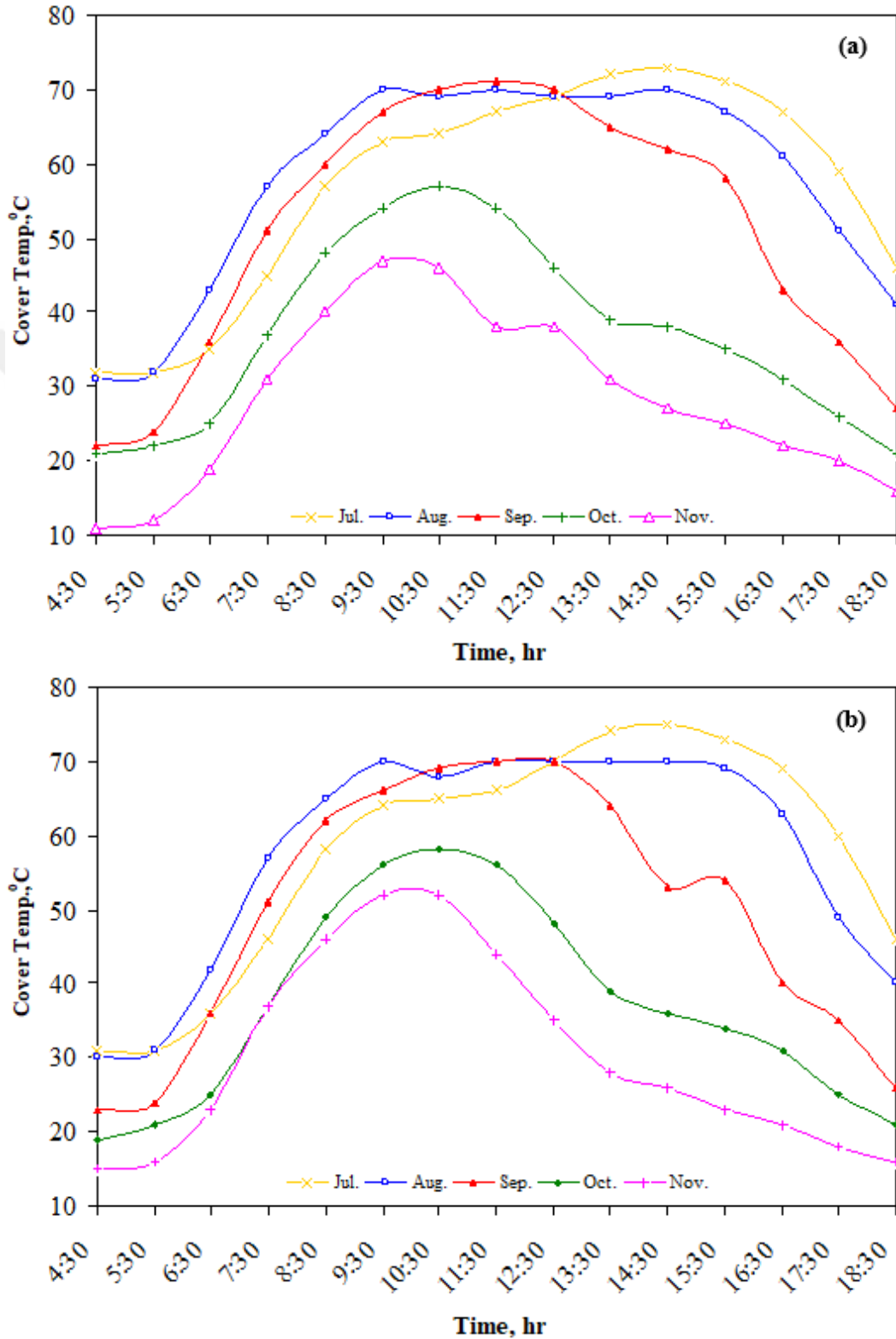

Figure 4.6. Cover temperature for (a) Silica gel, (b) Composite material

Figure 4.7. illustrates a comparison between the average desiccant temperature rate of several months. The temperature increases from sunrise, reaching its maximum at midday in July, August, and September, while it reaches its highest value at 10:30 a.m. in October and November and then decreases gradually.
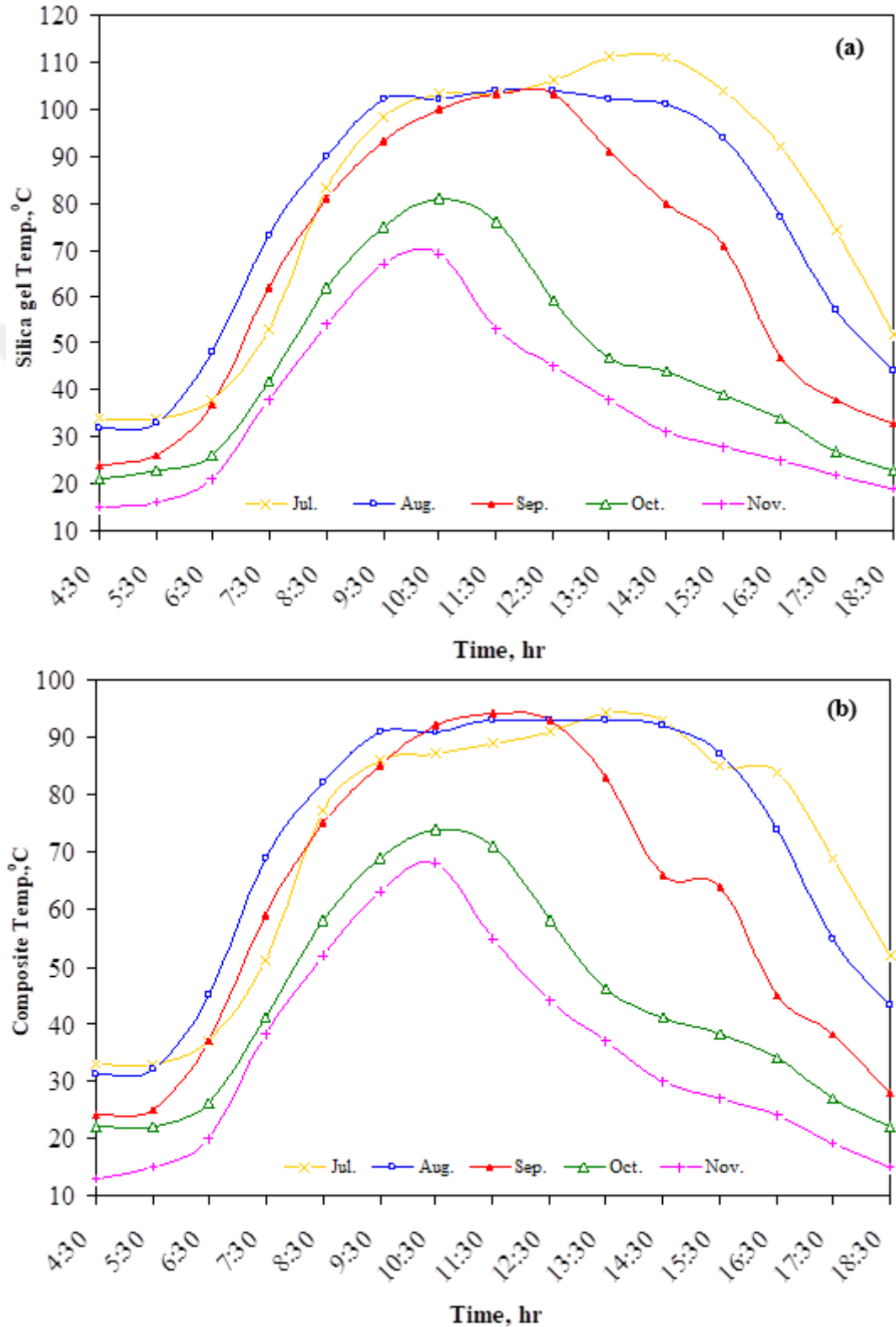

Figure 4.7. The desiccant temperature of (a) Silica gel, (b) Composite material

It can be noticed that the average temperature decreases as months pass from July to November. This is because desiccant temperature depends proportionally on solar radiation, which in turn decreases as months pass. Figure 4.8 shows a comparison between composite and Silica gel average temperatures and another comparison between the average cover temperature of the apparatus sections. The difference between Silica gel and composite temperatures and between the cover temperature of both apparatus sections is slight because both sections were constructed identically using the same materials and dimensions in all details.
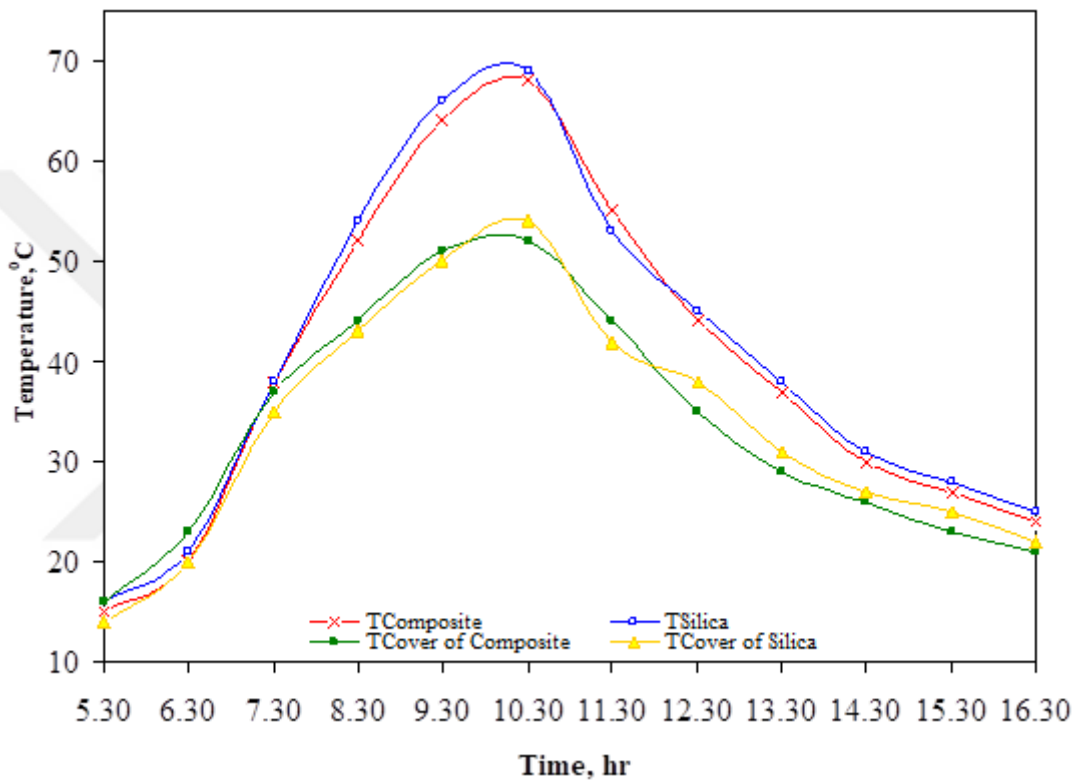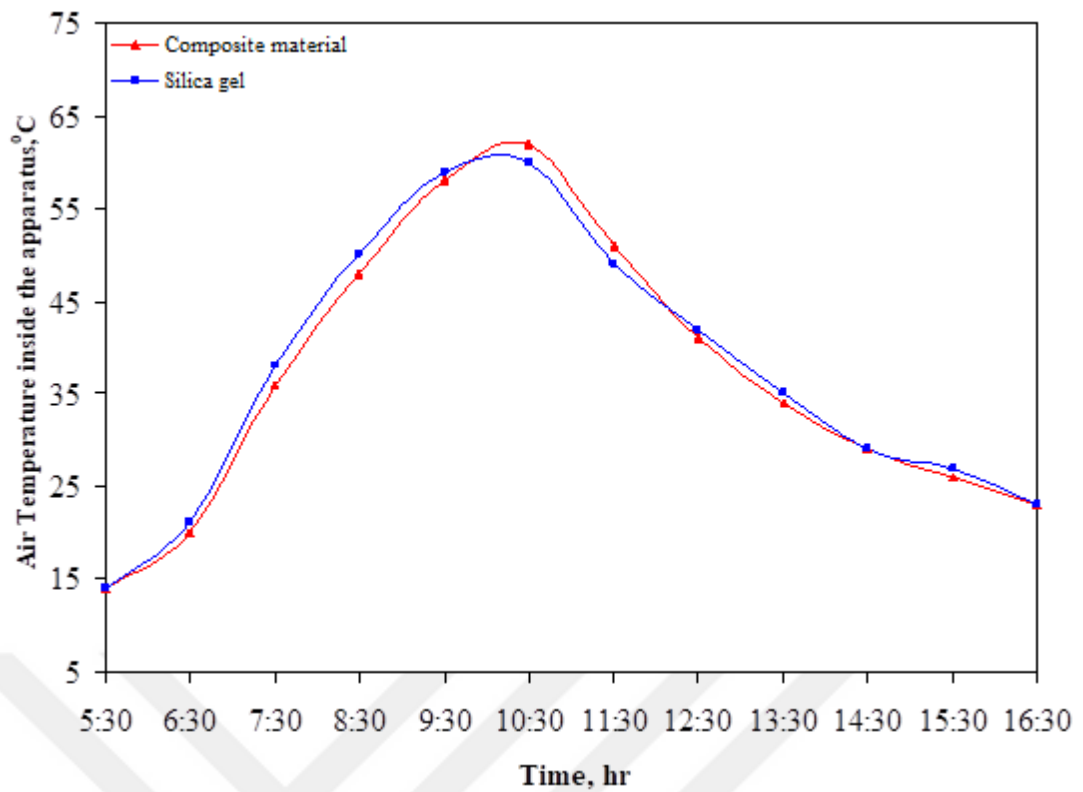

Figure 4.8. Comparison between Silica gel and composite material for desiccant and cover temperatures for November

Variation of average air temperature inside the apparatus for several months with time is demonstrated in Figure 4.9. There is an apparent difference in the air temperature inside the apparatus between July and November, where its maximum value in July is 86 ℃, while its maximum value in November is 62 ℃ because the air temperature inside the apparatus decreases with the decrement in solar radiation as months pass. A comparison between the average air temperature inside both sections of the apparatus is illustrated in Figure 4.10. Both temperatures increase as time passes within the day, reaching their maximum at 10:30 and then decreasing gradually. The difference between them is slight because both apparatus sections were identical and measured under the same surrounding conditions.
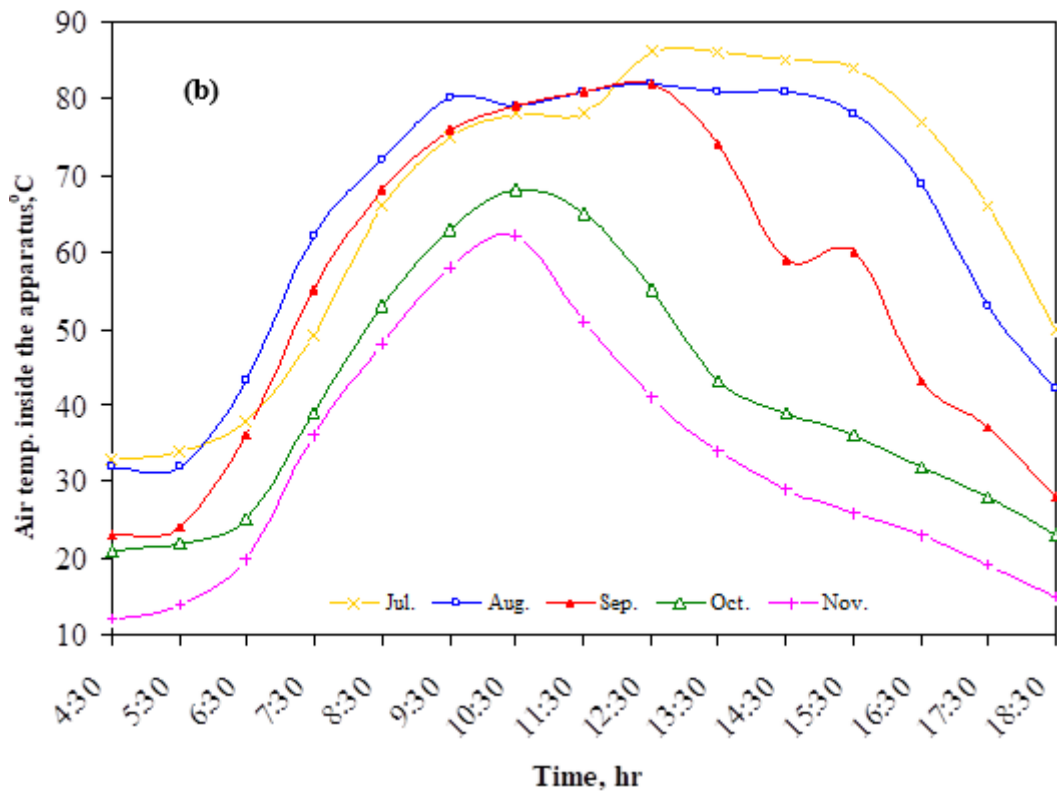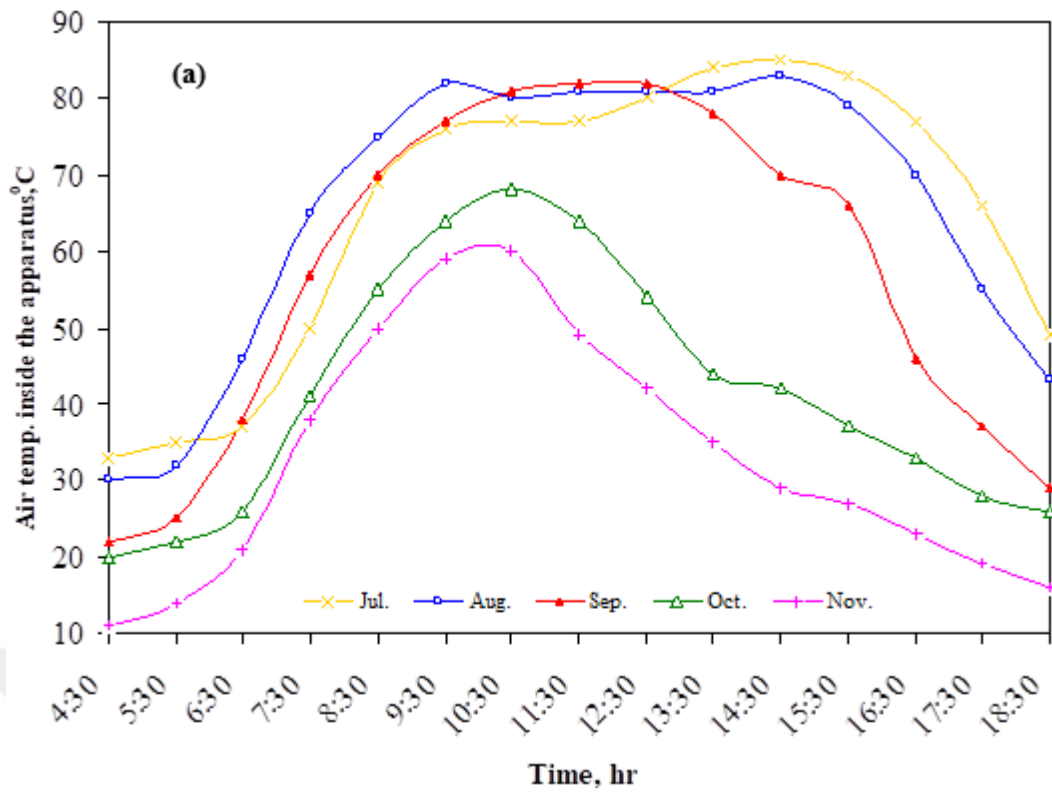
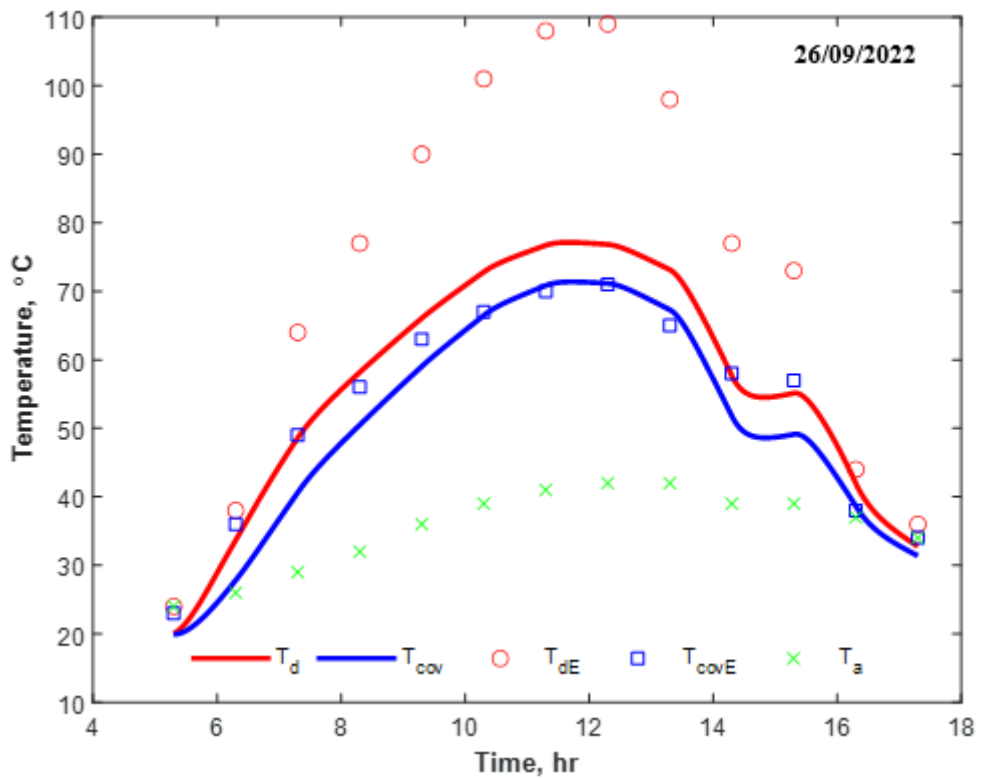**Figure 4.9.** Air temperature inside the apparatus for (a) Silica gel, (b) composite material
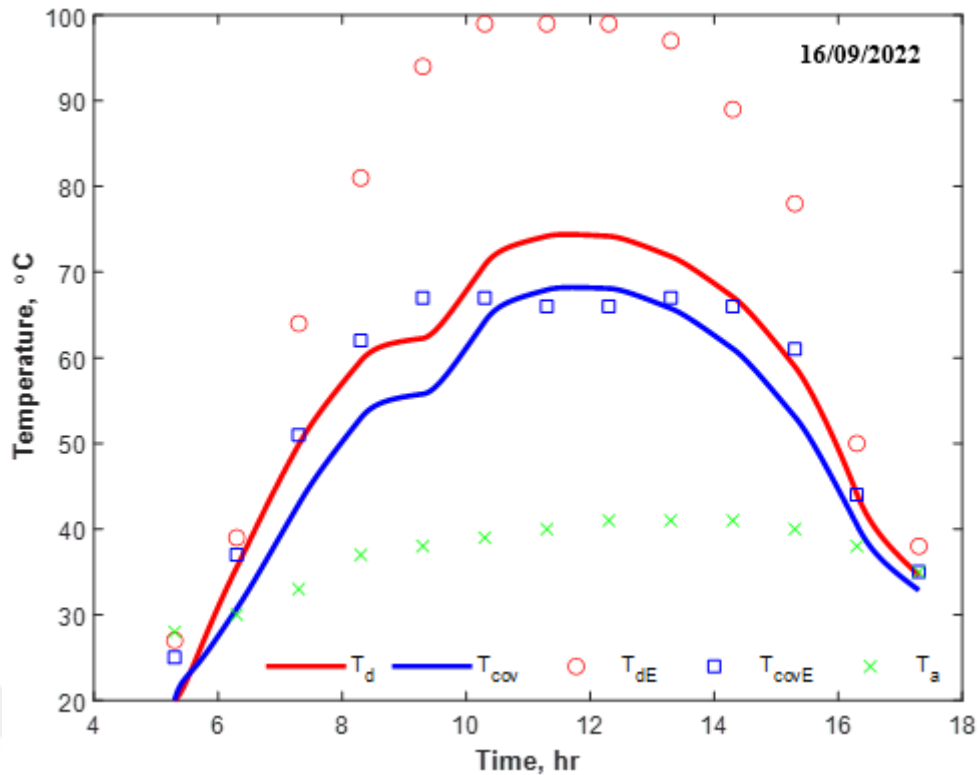
Figure 4.10. Comparison between the air temperature inside the apparatus of Silica gel and composite material for November

The change in temperature at various points over time for several days is shown in Figure 4.11.

Figure 4.11. Comparison between the theoretical and experimental setup temperatures for two days

Figure 4.11. (Continue)

The desiccant's temperature that was measured experimentally is higher than it was predicted theoretically. Because internal reflectors are employed, most of the sunlight that touches the desiccant and elevates its temperature is reflected, explaining why this is the case. The difference between the theoretically predicted and experimentally measured cover temperatures is slightly undersized, and this can be attributed to the cover's high transmissivity, which effectively eliminates the bulk of the reflected solar intensity, which reduces the effect of the internal reflectors on the cover.

4.3. Variation of Adsorption and Desorption

Figure 4.12. illustrates the variation of the average adsorption rate of the Silica gel and composite material for several months. It can be noticed that the adsorption rate in all months fluctuates in the nighttime process due to the change in several surrounding conditions like relative humidity, wind speed, and ambient temperature that influence moisture adsorption during the nighttime. The adsorbing process starts at different hours throughout the months because the sunset differs from one month to another. The maximum value of the adsorption rate was 6 g/hr and 5 g/hr for Silica gel and composite material, respectively, as seen in September and November.

58
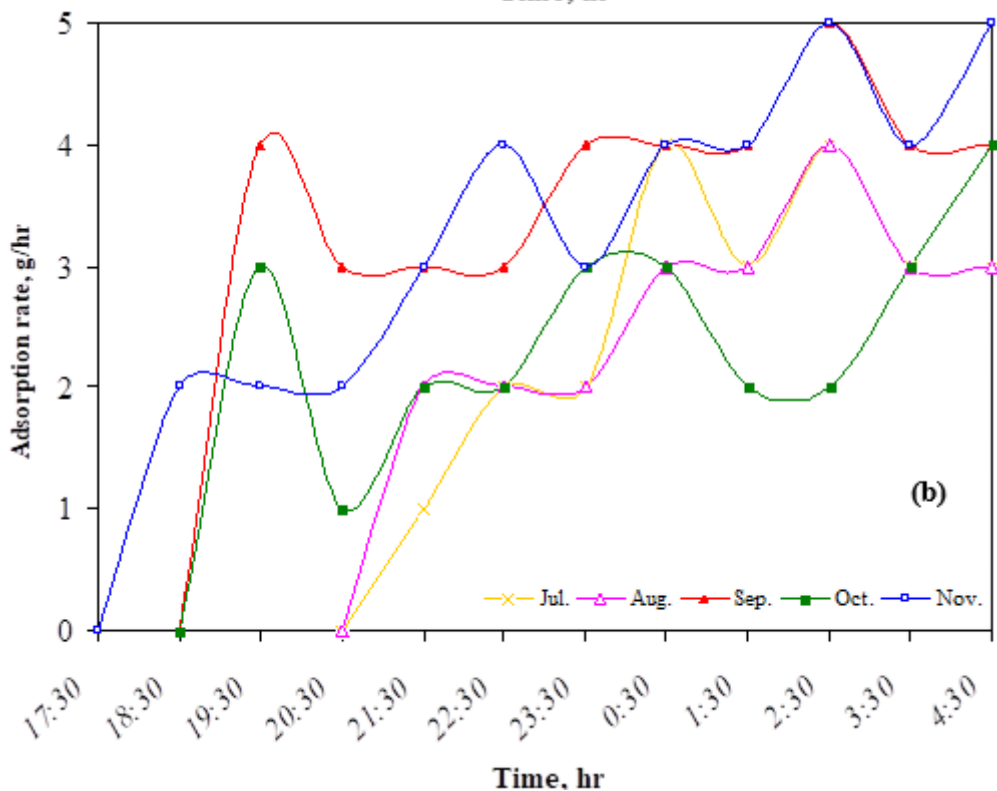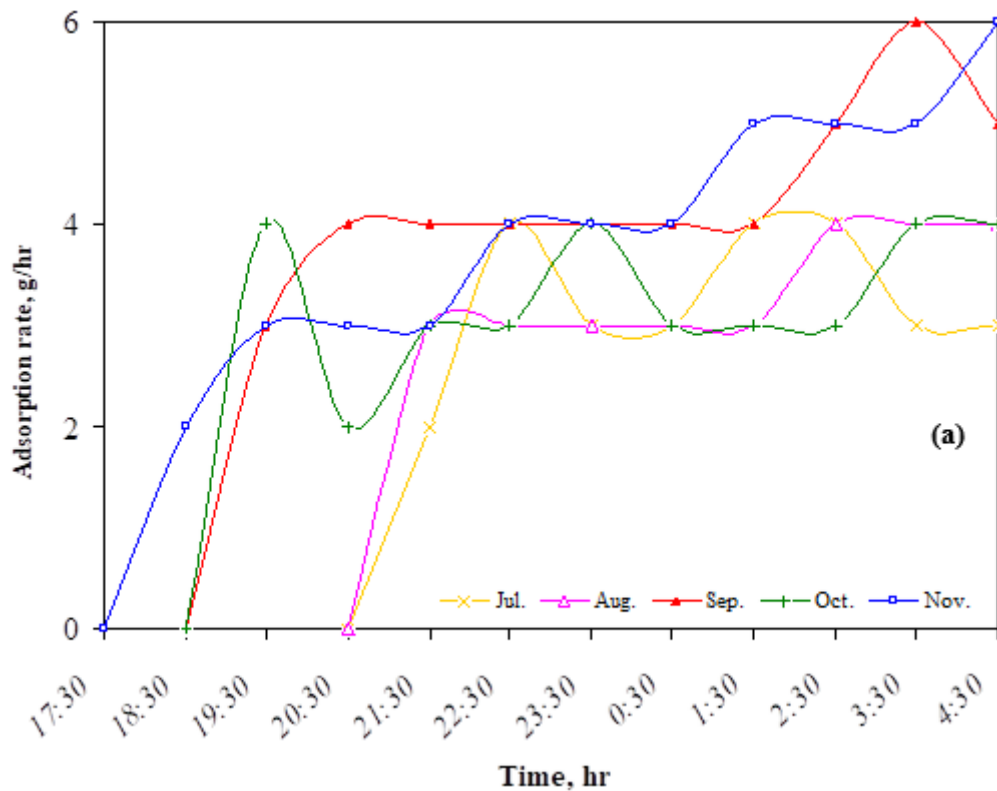
Figure 4.12. Adsorption rate for (a) Silica gel, (b) Composite material

Figure 4.13. presents a comparison between the adsorption rate of Silica gel and composite material. The adsorption rate for both desiccants fluctuates throughout the nighttime since it depends on the variation of various variables like relative humidity. The adsorption rate of Silica gel was higher than that of composite material since the Silica gel's ability to adsorb

moisture in our experiment was higher than that of Calcium chloride, which filled the Silica gel's pores in the composite material and led to a reduction in its performance as compared with that of pure Silica gel. The change in the average mass transfer coefficient of Silica gel and composite material for various months is shown in Figure 4.14. The mass transfer coefficient of all months fluctuates from one hour to another since it depends on several variables, like partial water pressure on both desiccant surface and ambient air. The mass transfer coefficient value in all months is close to each other, except in November, which is considerably higher than the rest.
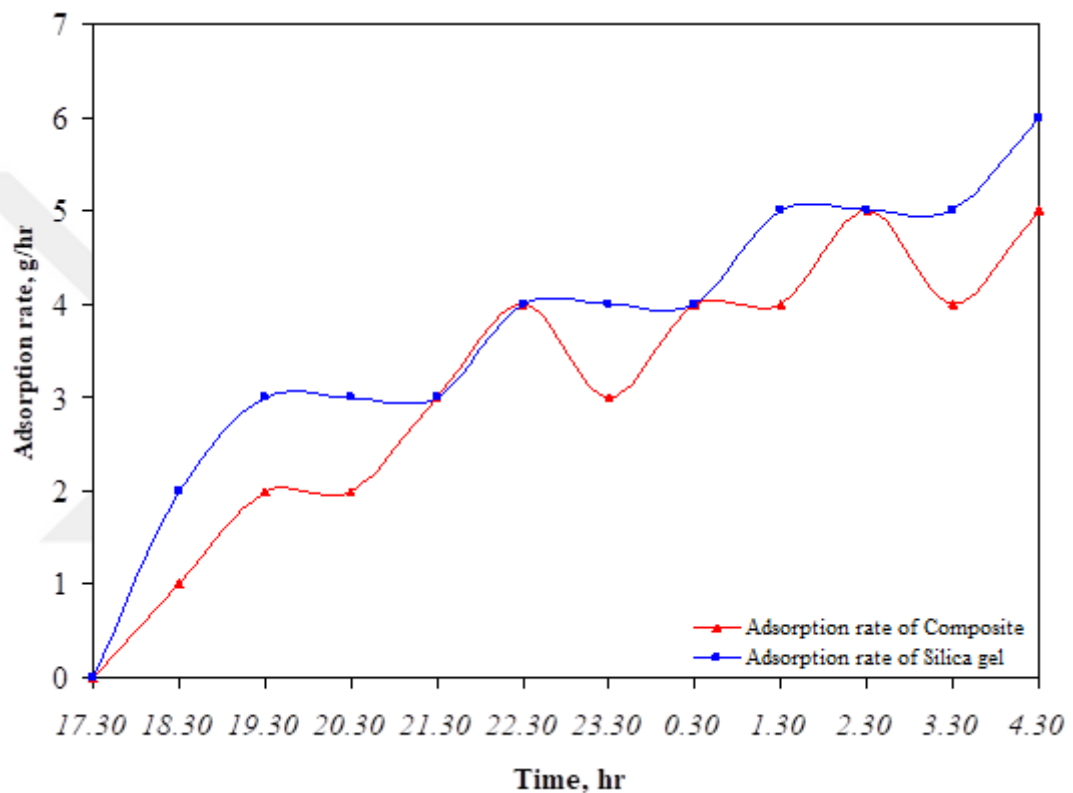
Figure 4.13. Comparison between the adsorption rates of Silica gel and composite material for November

A comparison between the mass transfer coefficient of Silica gel and composite material is shown in Figure 4.15. The mass transfer coefficient of both desiccants fluctuates since it depends on several variables, like adsorbed moisture quantity and the difference in partial pressures of the water. Due to Silica gel's greater adsorption rate than the composite material, its mass transfer coefficient is significantly higher than the latter's. Figure 4.16. displays the alteration in average accumulated water productivity for several months. There was no productivity in July since the adsorbed moisture was tiny, and the temperature inside the device was so high that it vaporised the little condensed moisture before the collection in the bottle. The water generation in November was much higher than that in August, and this is

due to the lesser solar radiation and higher amount of adsorbed moisture in November than in August.
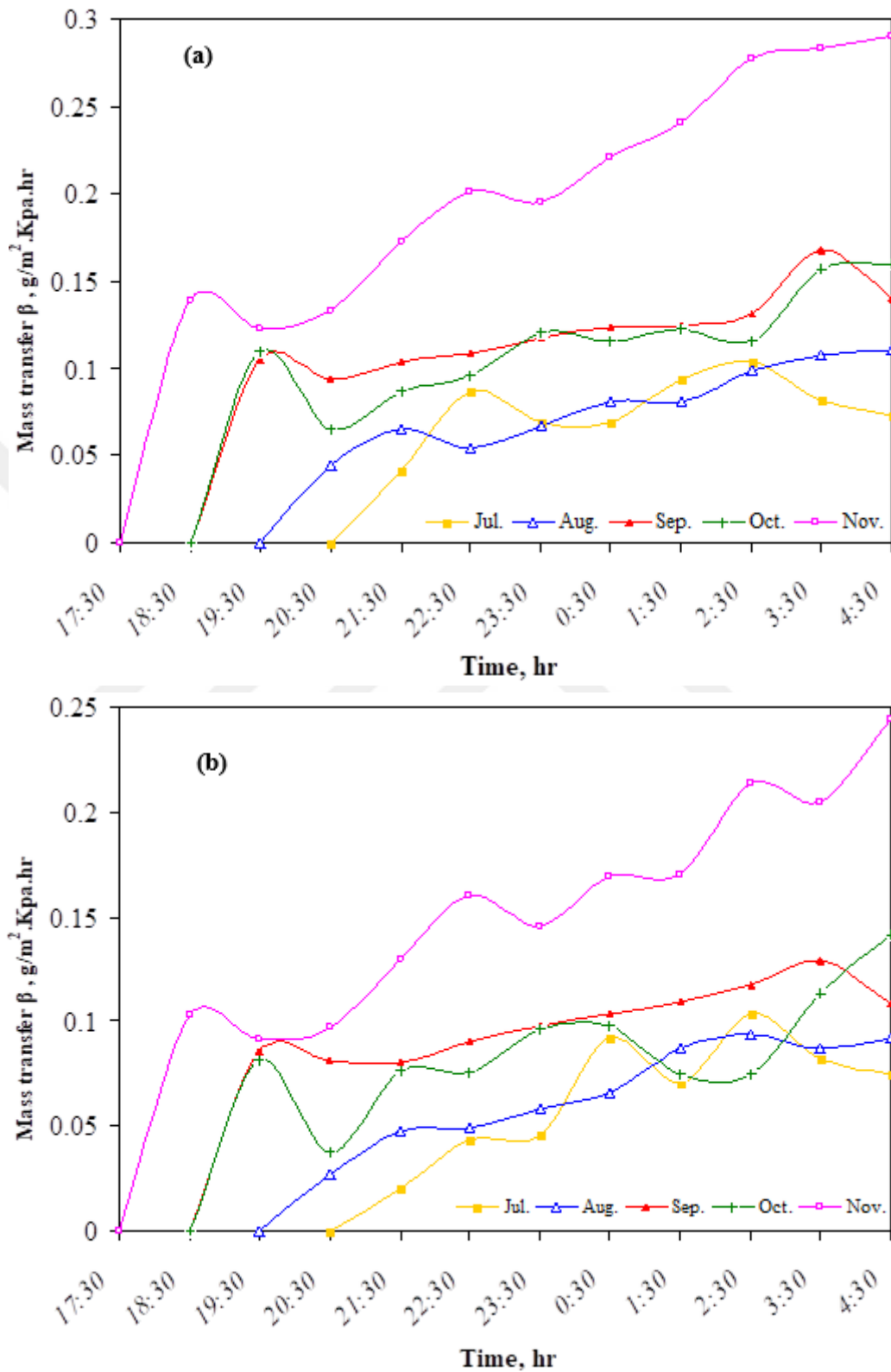
Figure 4.14. Mass transfer coefficient for: (a) Silica gel, (b) Composite material
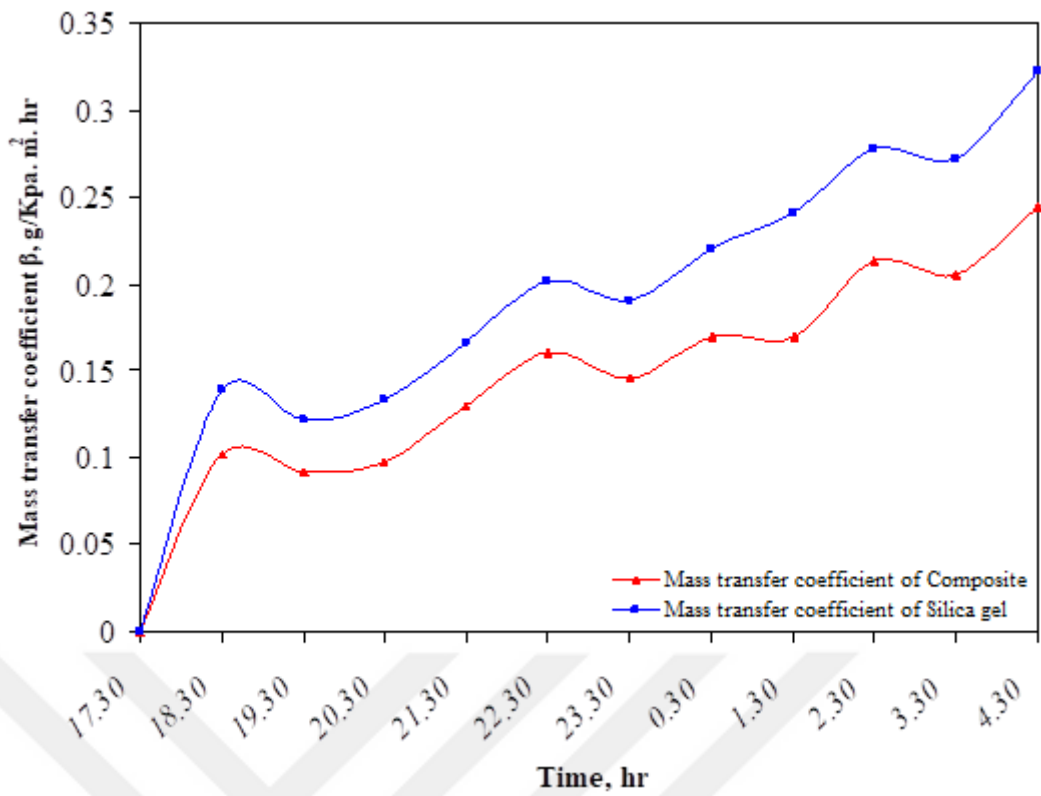
Figure 4.15. Comparison between the mass transfer coefficients of Silica gel and composite material for November
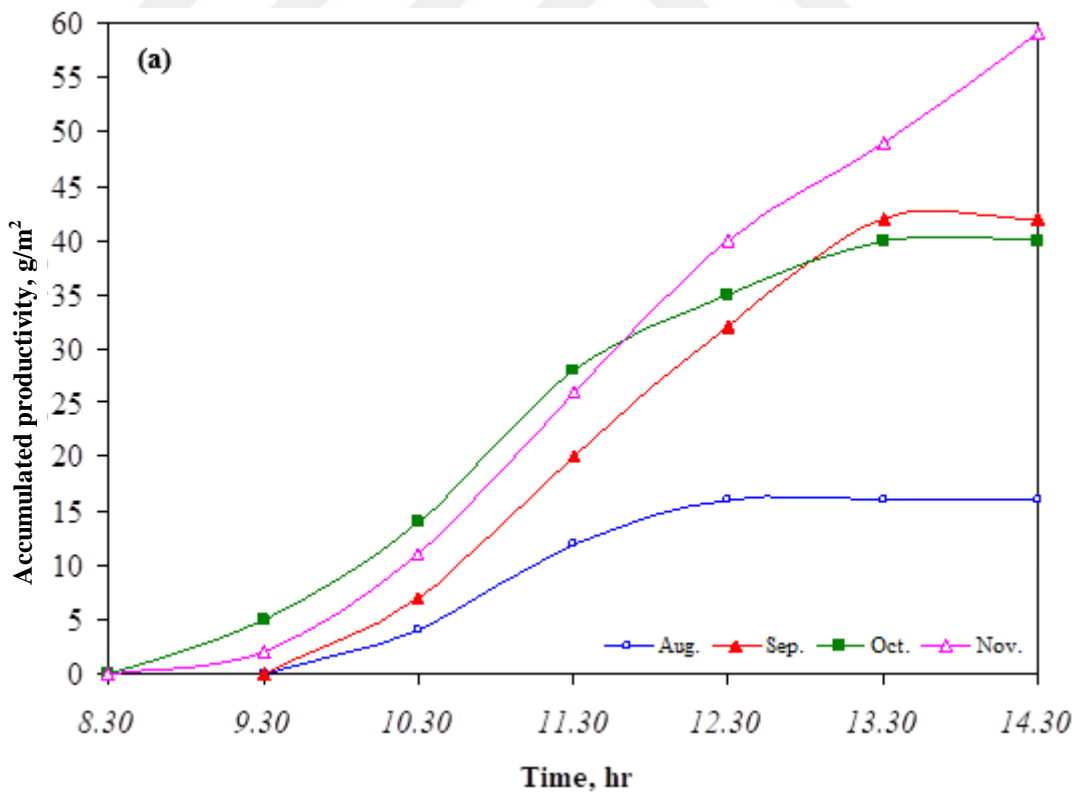
Figure 4.16. The accumulated productivity of (a) Silica gel, (b) Composite material

62
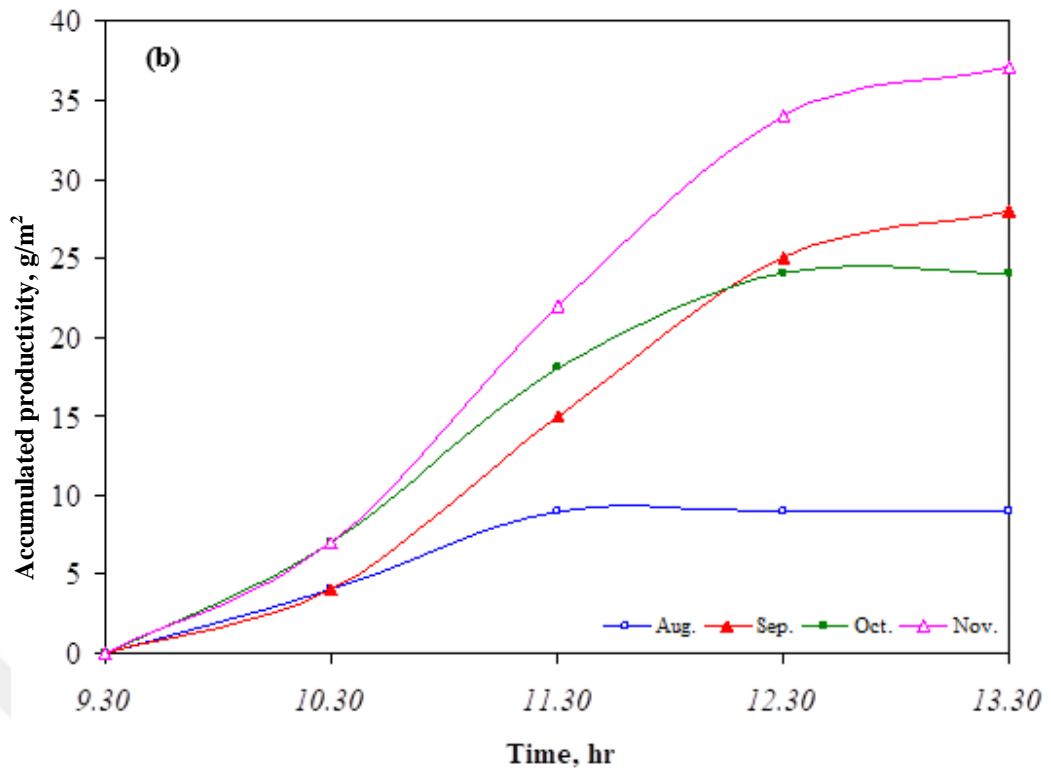
Figure 4.16. (Continue)

Figure 4.17. displays a comparison between the accumulated productivity of Silica gel and composite material. The total amount of accumulated productivity of Silica gel was 59 g/m^2, whereas it was 37 g/m^2 for the composite material.
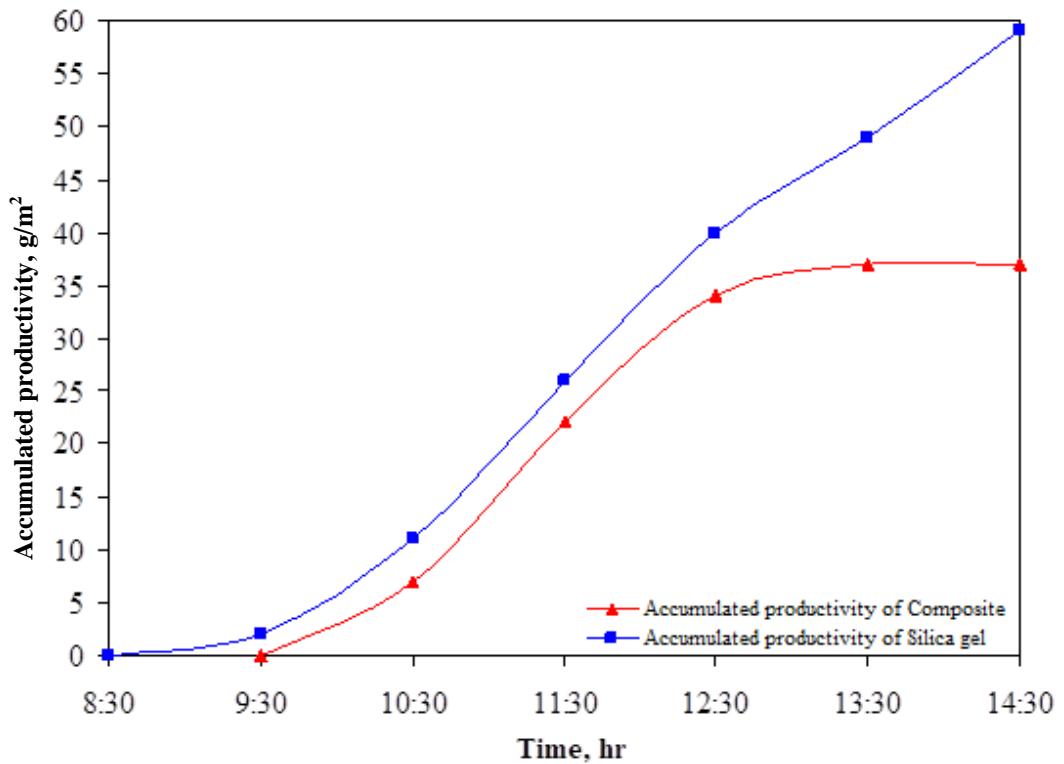
Figure 4.17. Comparison between the accumulated productivities of Silica gel and composite material for November

This difference is because the amount of adsorbed moisture by the Silica gel is higher than that of the composite material due to the higher moisture absorptivity of Silica gel than the composite material. Figure 4.18. shows theoretical and experimental calculations of the variation in the overall quantity of cumulative water output over several days. The quantity of the vapour that leaked in the regeneration process and the amount of generated water droplets that did not collect were not considered in the theoretical calculation. Therefore, the theoretical productivity is substantially significantly higher than the real one.
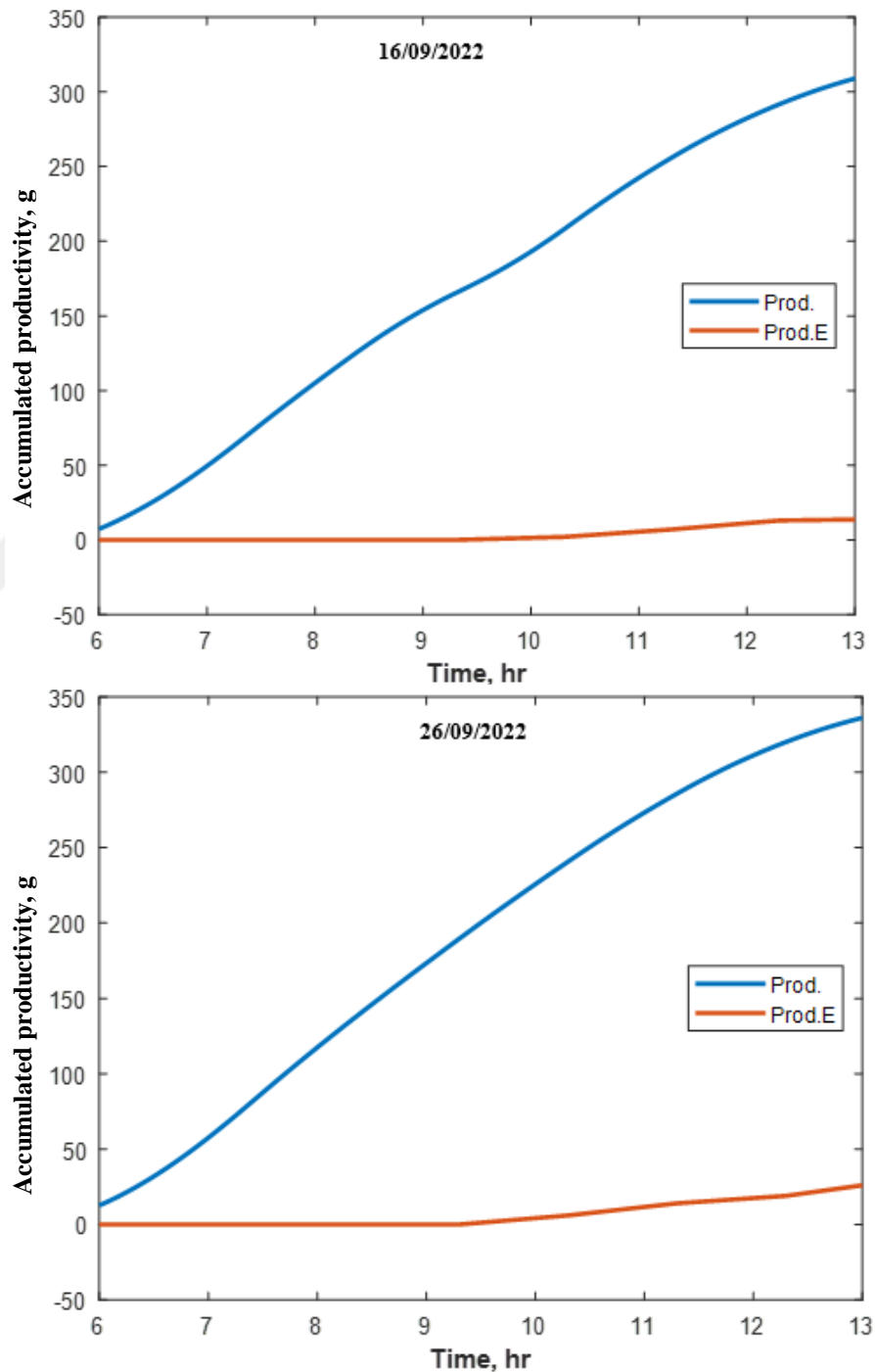
Figure 4.18. Comparison between the theoretical and experimental productivity for two days

The variation in the average thermal efficiency of both Silica gel and composite material for several months is presented in Figure 4.19. Since the thermal efficiency depends mainly on the amount of the produced water, the efficiency in November is much higher than in August. The efficiency of both desiccants in July is zero because neither Silica gel nor composite material produced any water in July.
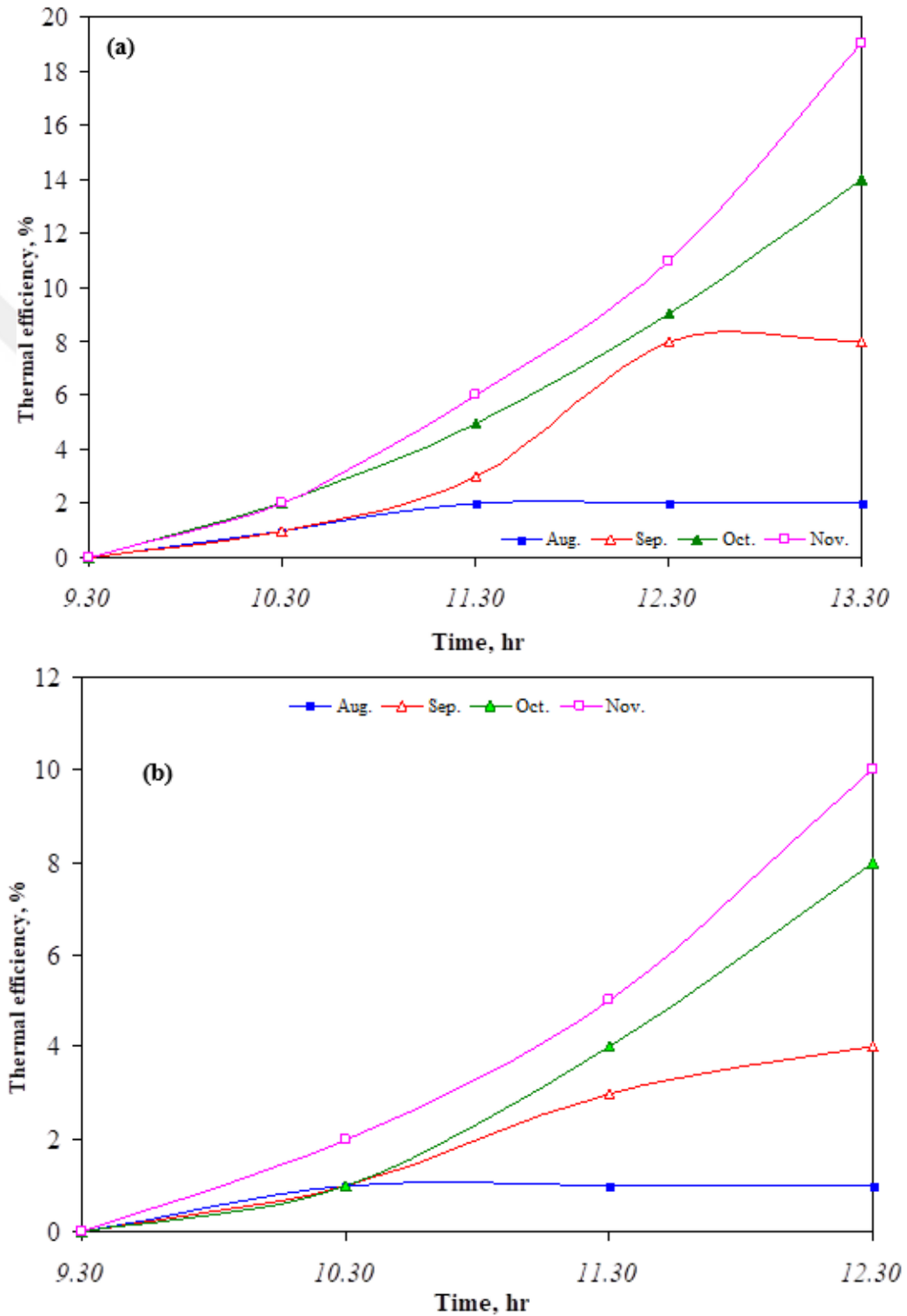
Figure 4.19. Thermal efficiency of (a) Silica gel, (b) Composite material

65

A comparison between the thermal efficiencies of Silica gel and composite material is depicted in Figure 4.20. At the end of the daytime process, the efficiency of Silica gel was 19 %, while the composite material's efficiency was 10 %. The significant difference between the efficiencies of the two desiccants is that the amount of water produced by Silica gel is much higher than that of composite material.
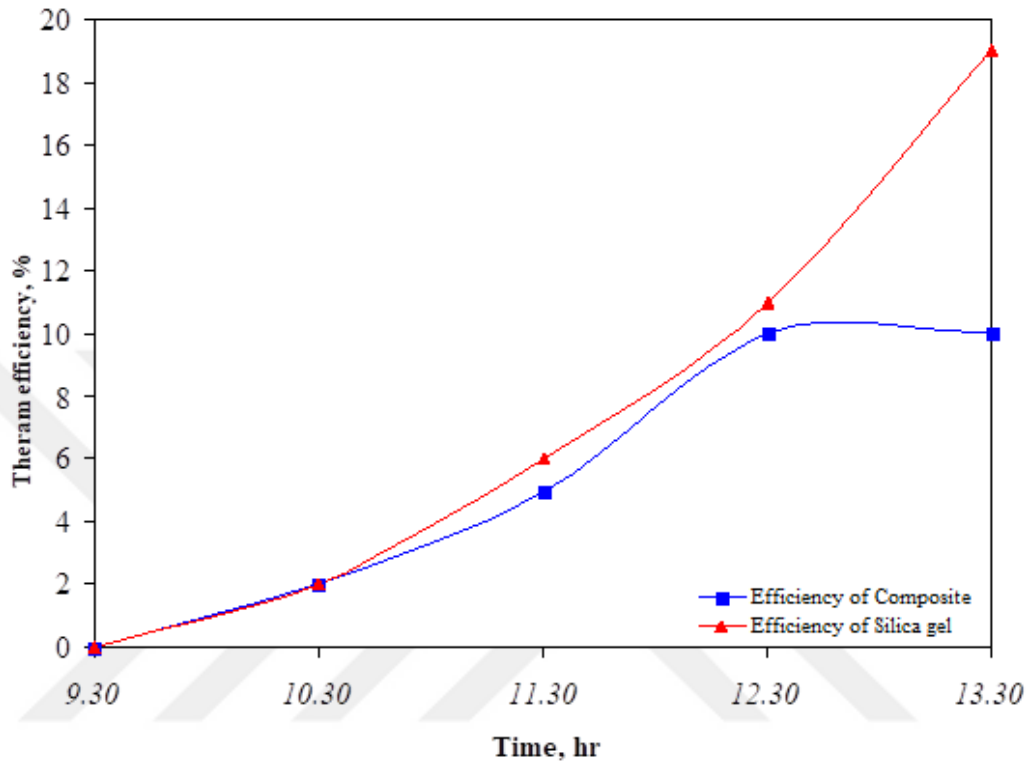
Figure 4.20. Comparison between the thermal efficiencies of both desiccants for November
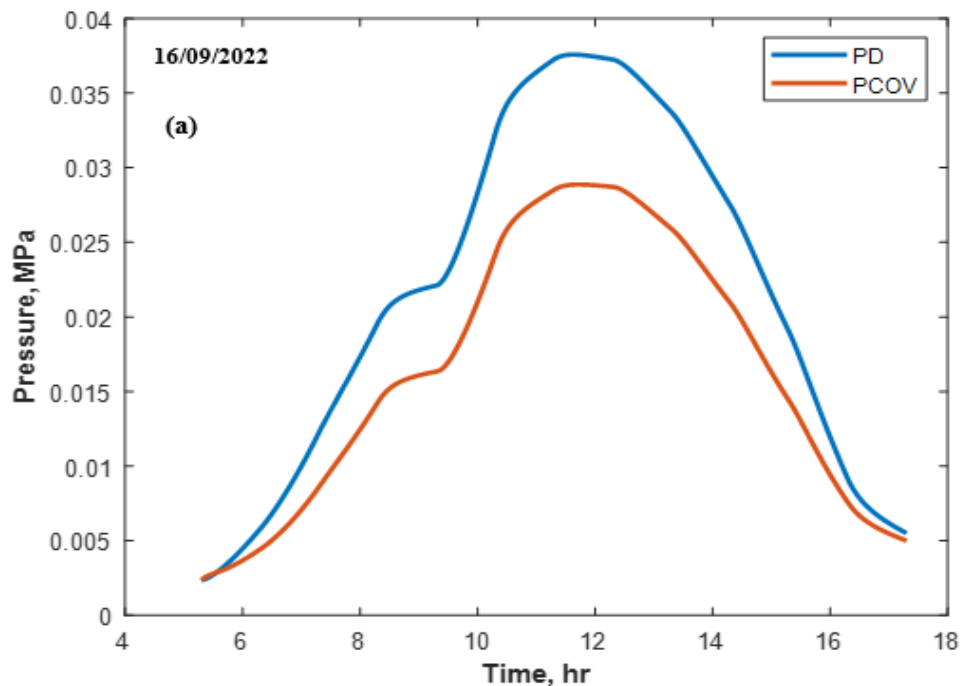
Figure 4.21. Partial water vapour pressure of desiccant and the cover for various days
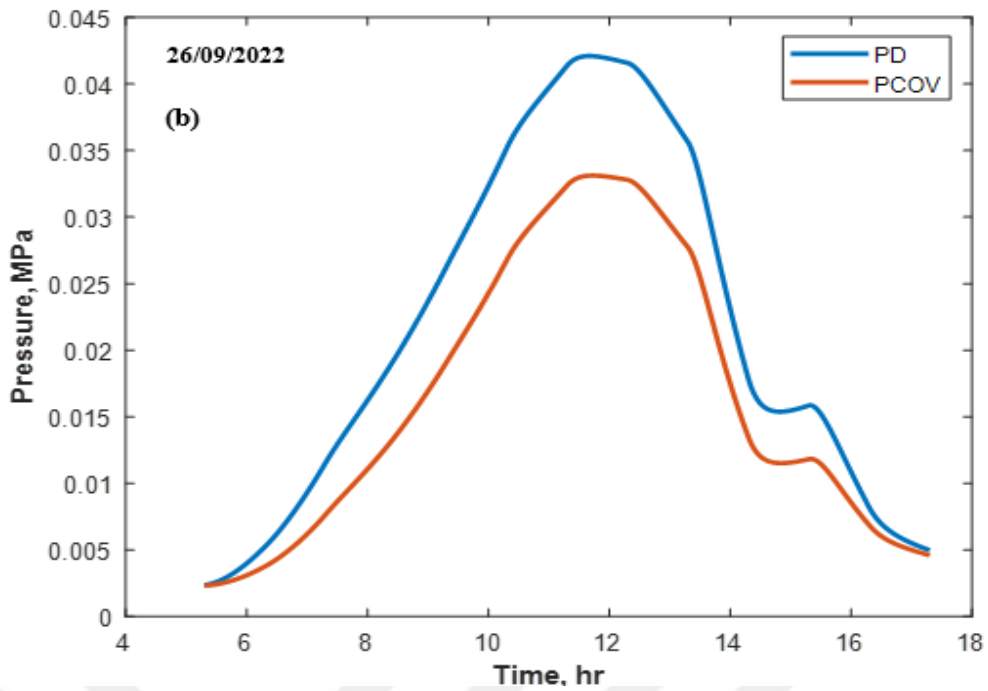
Figure 4.21. (Continue)

Figure 4.21 shows a partial water vapour pressure for the desiccant and the cover during a desorption operation over a few days. The variance between the partial pressure at the Silica gel surface and the interior surface of the cover is more significant during the day, peeking around noon. As a consequence of the difference, as the desiccant releases water vapour, it is transferred to the cover, where it condenses. This process continues until the pressure difference becomes zero. The plots for three additional days are presented in Appendix I.

4.4. Change of Different Variables with Others for Both Desiccants

The Variation in the adsorption rate of Silica gel and composite material with relative humidity is illustrated in Figure 4.22. The adsorption rate in both desiccant materials increases with the increment in relative humidity because the relative humidity is the most significant influencer on the amount of adsorbed moisture. For the whole adsorption process, the adsorption rate of Silica gel is higher than that of composite material because Silica gel's moisture adsorption capability is higher than composite material's. The variation in the average mass transfer coefficient of Silica gel and composite material with relative humidity is presented in Figure 4.23. The mass transfer coefficient increases with the increment in relative humidity since the mass transfer coefficient depends proportionally on the adsorption rate that depends on the relative humidity. It can be noticed that the mass transfer coefficient of Silica gel is higher than that of composite material, and this is because the amount of adsorbed moisture by Silica gel is higher than that of composite material.
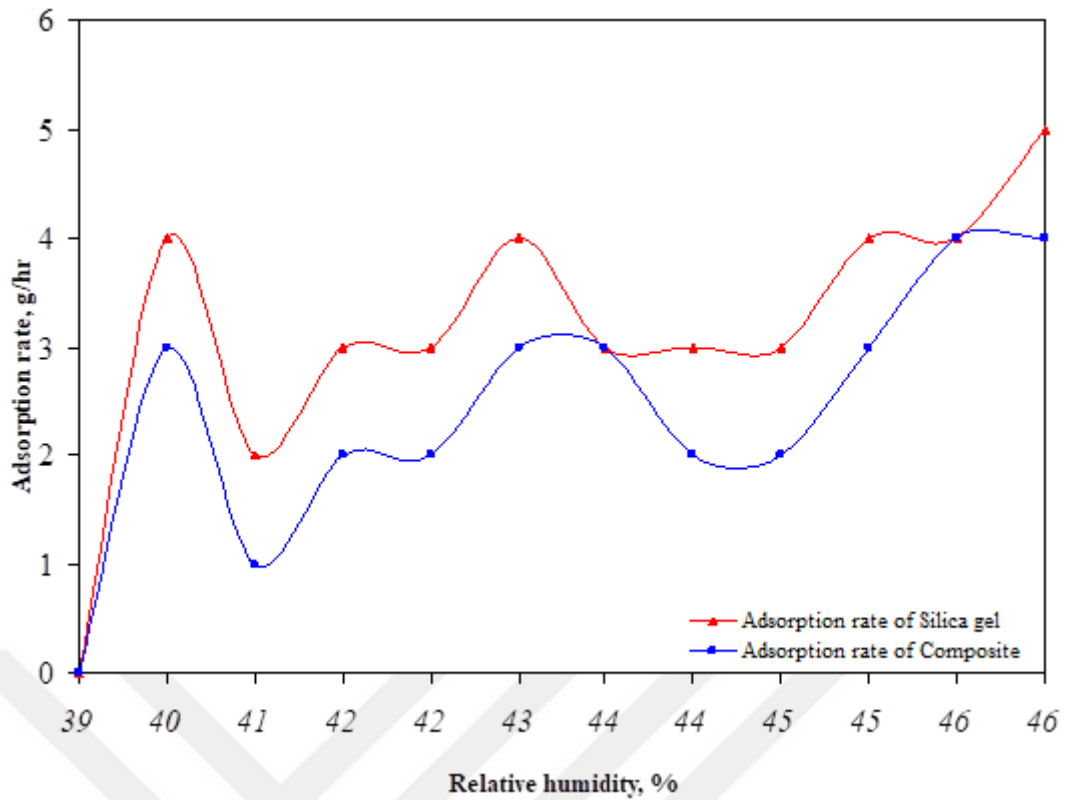
Figure 4.22. Change of adsorption rates of Silica gel and composite material with relative humidity for October
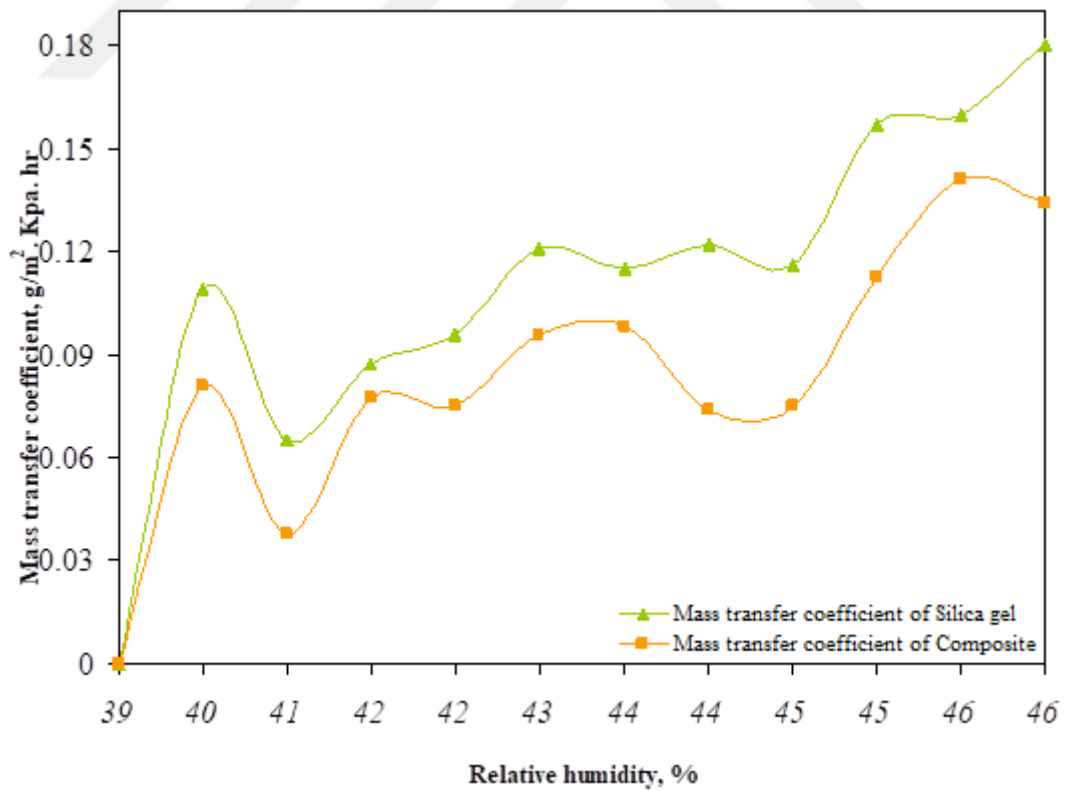
Figure 4.23. Variation of mass transfer coefficients of Silica gel and composite material with relative humidity for October

Figure 4.24. depicts the variation of Silica gel's water productivity with its temperature. The water production started as the Silica gel temperature reached 62 $^{\circ}$C. The productivity increased and decreased in the same manner as the Silica gel temperature, and this is because it mainly depends on the desiccant temperature needed to vaporise the moisture from the desiccant.

Figure 4.24. Change of Silica gel temperature with its productivity for October

The water productivity change of the composite material with its temperature is illustrated in Figure 4.25. The water production started when the composite material's temperature reached 69 $^{\circ}$C, enough to vaporise the adsorbed moisture from the desiccant. The productivity reached 21 g/m^2 as the desiccant temperature reached 71 $^{\circ}$C and then decreased until it ended at 41 $^{\circ}$C. Figure 4.26. presents the change in the water productivities of Silica gel and composite material with solar radiation. The water generation of both desiccants depends on solar radiation since the latter is used as the heating source that raises the desiccant temperature needed for adsorbed moisture vaporisation. As solar radiation reached 222 W/m^2, the productivity of both materials started and reached their maximum value at 295 W/m^2 and then decreased gradually. The productivity of Silica gel is significantly higher than the composite material's, and this is because the amount of adsorbed moisture by Silica gel is considerably higher than that of the composite material.
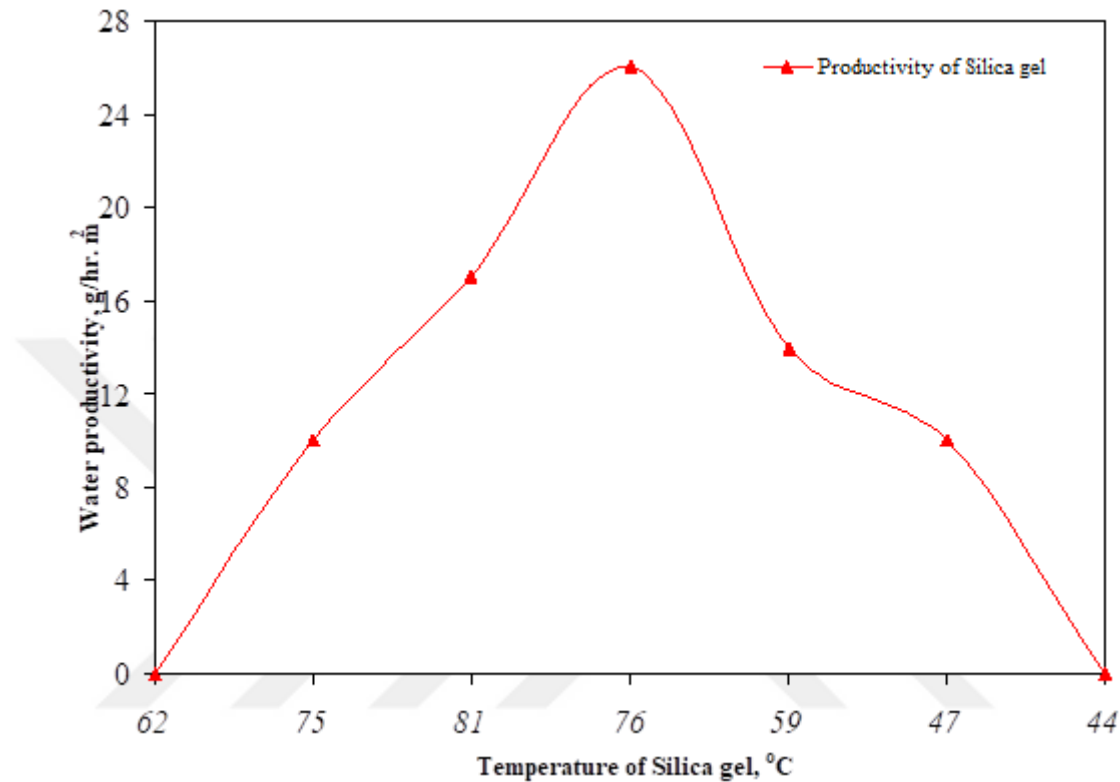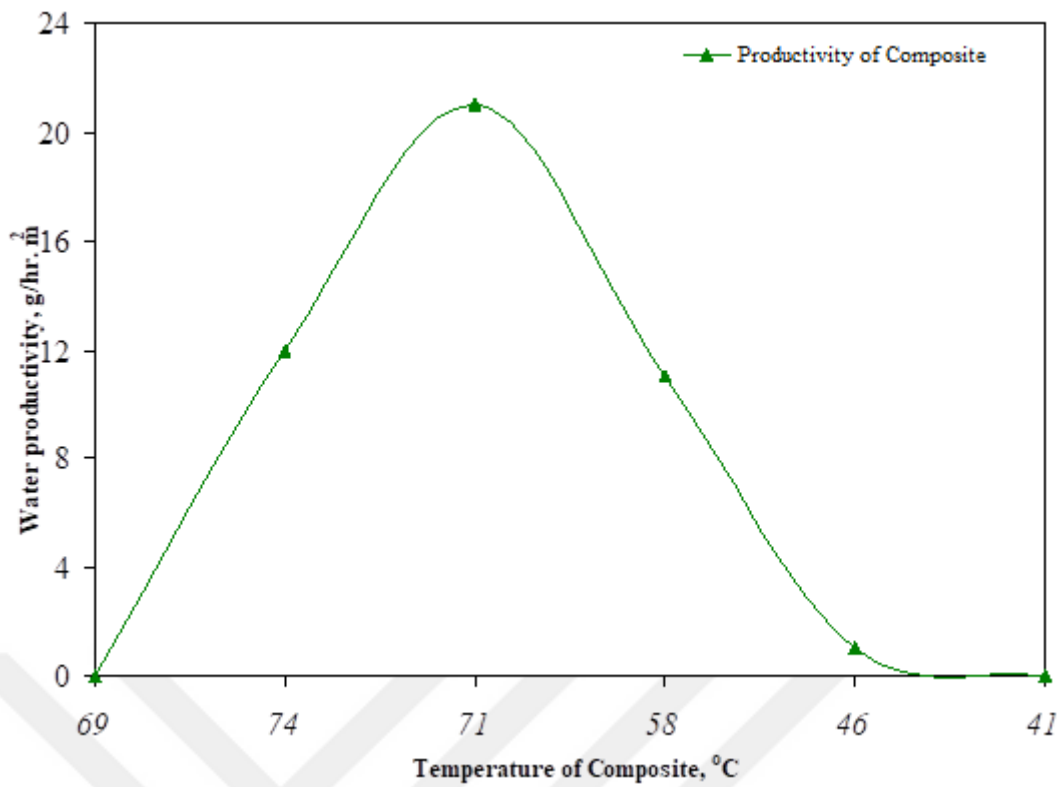
Figure 4.25. Change of composite temperature with its productivity for October
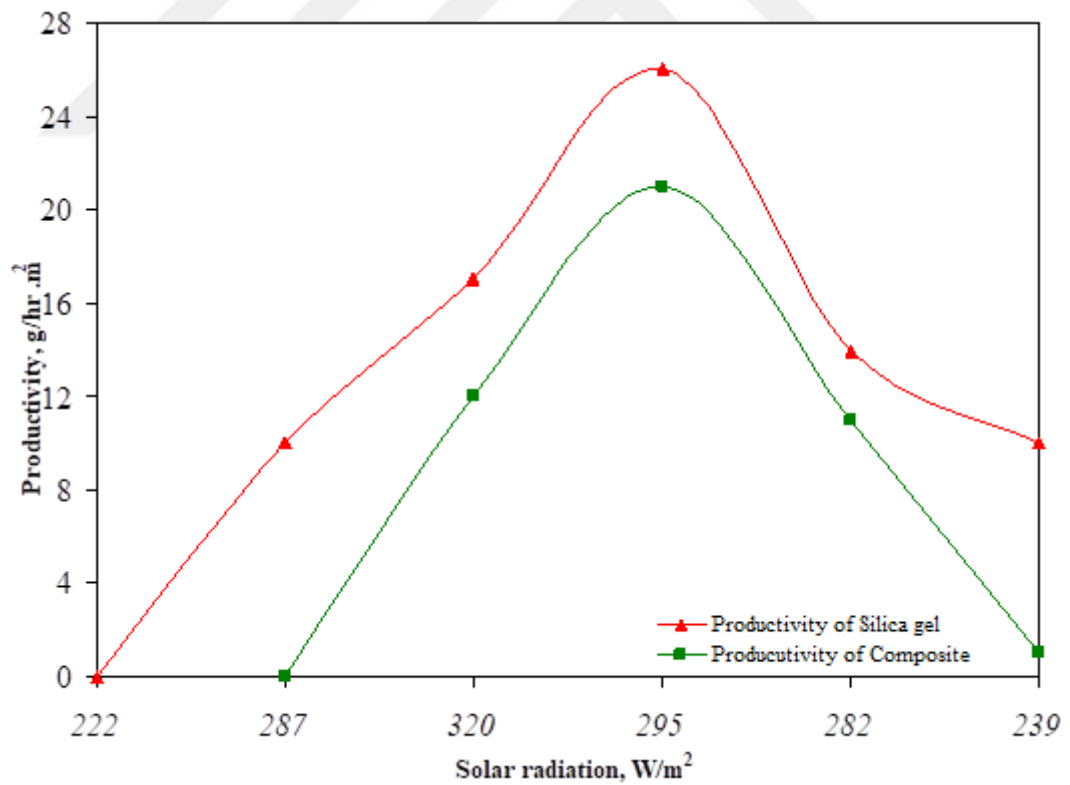
Figure 4.26. Change of solar radiation with water productivities of Silica gel and composite material for October

5. CONCLUSION AND RECOMMENDATIONS

In this study, a theoretical and experimental investigation was conducted for moisture harvesting from atmospheric air in the climatic conditions of Kirkuk City, Iraq. Blue Silica gel and composite material were used as desiccant materials in a rotatable single-slope apparatus with two identical sections of 56 x 68 x 82.5 cm^3 each. The experiments were conducted for several days over five months, and a theoretical calculation for the Silica gel was performed using the fourth-order Rung-Kutta method in the MATLAB program. A comparison was made among the average results of the five months for both desiccants, between the findings of Silica gel and composite material, between the theoretical results with the experimental one for Silica gel, and the change of different variables with others for both desiccants. The results revealed that:

- The highest water productivity for both desiccants occurs in the fall, where the relative humidity increases as months pass from July to November. Therefore, the amount of adsorbed moisture also increased.

- The highest accumulated productivity was 160 g/m^2 and 83 g/m^2, with a system thermal efficiency of 19 % and 10 % for Silica gel and composite material, respectively, and the annual cost of water production was nearly \$2.54.

- The comparison between the results of the two desiccants revealed that the performance of Silica gel in water generation is better than the composite material since the Silica gel's ability to adsorb moisture in our experiment was higher than that of Calcium chloride, which filled the Silica gel's pores in the composite material and led to a reduction in its performance as compared with that of pure Silica gel.

- According to the findings, the theoretical results of the water productivity were higher than the experimental one since the leakage and the lost water droplets were not considered in the theoretical calculations.

- More significant water generation levels may be achieved if this procedure is applied in a different environment with high relative humidity.

Using Peltier as a condensing surface to increase the amount of condensed vapour and preparation of new composite materials to be used as moisture adsorbers are recommended.

6. REFERENCES

Abualhamayel, H., & Gandhidasan, P. (1997, November). A method of obtaining fresh water from the humid atmosphere. *Desalination*, *113*(1), 51–63. https://doi.org/10.1016/s0011-9164(97)00114-8

Ackerman, E. B. (1968). Production of water from the atmosphere, United States Patent.

Alahmer, A., Al-Dabbas, M., Alsaqoor, S., & Al-Sarayreh, A. (2018, March). Utilizing of Solar Energy for Extracting Freshwater from Atmospheric Air. *Applied Solar Energy*, *54*(2), 110–118. https://doi.org/10.3103/s0003701x18020044

Alayli, Y., Hadji, N., & Leblond, J. (1987, December). A new process for the extraction of water from air. *Desalination*, *67*, 227–229. https://doi.org/10.1016/0011-9164(87)90246-3

Amarakoon, S. & Navaratne, S. (2017). Evaluation of the Effectiveness of Silica Gel Desiccant in Improving the Keeping Quality of Rice Crackers. *International Journal of Science and Research (IJSR)*, *6*(1), 2163-2168. https://doi.org/10.21275/ART2017538

Aristov, Y. I. (2007, June). New family of solid sorbents for adsorptive cooling: Material scientist approach. *Journal of Engineering Thermophysics*, *16*(2), 63–72. https://doi.org/10.1134/s1810232807020026

Aristov, Y. I., Tokarev, M. M., Cacciola, G., & Restuccia, G. (1996, November). Selective water sorbents for multiple applications, 1. $CaCl_2$ confined in mesopores of Silica gel: Sorption properties. *Reaction Kinetics & Catalysis Letters*, *59*(2), 325–333. https://doi.org/10.1007/bf02068130

Aristov, Y., Tokarev, M., Gordeeva, L., Snytnikov, V., & Parmon, V. (1999, June). New composite sorbents for solar-driven technology of fresh water production from the atmosphere. *Solar Energy*, *66*(2), 165–168. https://doi.org/10.1016/s0038-092x(98)00110-8

Arunkumar, T., Jayaprakash, R., Denkenberger, D., Ahsan, A., Okundamiya, M., kumar, S., Tanaka, H., & Aybar, H. (2012, February). An experimental study on a hemispherical solar still. *Desalination*, *286*, 342–348. https://doi.org/10.1016/j.desal.2011.11.047

Badrakia, H. C. (2015). Performance Review of Aqueous Calcium Chloride Liquid Desiccant Based Air Dehumidifier for HVAC Applications: A Review. *International Journal of Advance Research in Engineering, Science & Technology(IJAREST)*, *2*(12), 38-50.

Bardi, U. (2008, March). Fresh water production by means of solar concentration: the AQUASOLIS project. *Desalination*, *220*(1–3), 588–591. https://doi.org/10.1016/j.desal.2007.04.059

Calcium chloride. (2022, September 7). In *Wikipedia.* https://en.wikipedia.org/wiki/Calcium_chloride#/media/File:Calcium_chloride_CaCl₂.jpg

Cengel, Y. A., & Boles, M. A. (2014, January 7). *Thermodynamics: an Engineering Approach.*

Cohen, A. P. (2003). Desiccants. *Kirk-Othmer Encyclopedia of Chemical Technology.*

Çengel, Y. A., & Ghajar, A. J. (2015). *Heat and Mass Transfer: Fundamental & Applications* (5th ed.).

Danışmaz, M., & Alhurmuzi, M. (2022, January 3). A Literature Review on Extraction of Potable Water from Atmospheric Air Using Solar Stills: Recent Developments. *European Journal of Science and Technology*, (32), 991-999. https://doi.org/10.31590/ejosat.1039866

Daou, K., Wang, R., & Xıa, Z. (2006, April). Desiccant cooling air conditioning: a review. *Renewable and Sustainable Energy Reviews*, *10*(2), 55–77. https://doi.org/10.1016/j.rser.2004.09.010

Das, A., Sharma, R., Thirunavukkarasu, V., & Cheralathan, M. (2021, February 25). Desiccant-based water production from humid air using concentrated solar energy. *Journal of Thermal Analysis and Calorimetry*, *147*(3), 2641–2651. https://doi.org/10.1007/s10973-021-10558-z

District, M. & Ratchasima, N. (2010). Physical Model Simulations of Solar Thermal Energy Storage in Basaltic Rock Fills. Research and development journal, *21*(3), 11-24.

Duffie, J. A., & Beckman, W. A. (2006, July 28). *Solar Engineering of Thermal Processes.* https://doi.org/10.1604/9780471698678

Dunkak, E. B. (1949). solar Activated Dehumidifier, United States Patent.

Elashmawy, M. (2020, March). Experimental study on water extraction from atmospheric air using tubular solar still. *Journal of Cleaner Production*, *249*, 119322. https://doi.org/10.1016/j.jclepro.2019.119322

Elashmawy, M., & Alshammari, F. (2020, May). Atmospheric water harvesting from low humid regions using tubular solar still powered by a parabolic concentrator system. *Journal of Cleaner Production*, *256*, 120329. https://doi.org/10.1016/j.jclepro.2020.120329

Entezari, A., Ejeian, M., & Wang, R. (2019a, October). Modifying water sorption properties with polymer additives for atmospheric water harvesting applications. *Applied Thermal Engineering*, *161*, 114109. https://doi.org/10.1016/j.applthermaleng.2019.114109

Entezari, A., Ejeian, M., & Wang, R. (2019b, September). Extraordinary air water harvesting performance with three phase sorption. *Materials Today Energy*, *13*, 362–373. https://doi.org/10.1016/j.mtener.2019.07.001

Ertas, A., Anderson, E., & Kiris, I. (1992, September). Properties of a new liquid desiccant solution—Lithium chloride and Calcium chloride mixture. *Solar Energy*, *49*(3), 205–212. https://doi.org/10.1016/0038-092x(92)90073-j

Essa, F., Elsheikh, A. H., Sathyamurthy, R., Muthu Manokar, A., Kandeal, A., Shanmugan, S., Kabeel, A., Sharshir, S. W., Panchal, H., & Younes, M. (2020, June). Extracting water content from the ambient air in a double-slope half-cylindrical basin solar still using Silica gel under Egyptian conditions. *Sustainable Energy Technologies and Assessments*, *39*, 100712. https://doi.org/10.1016/j.seta.2020.100712

Fathieh, F., Kalmutzki, M. J., Kapustin, E. A., Waller, P. J., Yang, J., & Yaghi, O. M. (2018, June). Practical water production from desert air. *Science Advances*, *4*(6). https://doi.org/10.1126/sciadv.aat3198

Fathy, M. H., Awad, M. M., Zeidan, E. S. B., & Hamed, A. M. (2020, December). Solar powered foldable apparatus for extracting water from atmospheric air. *Renewable Energy*, *162*, 1462–1489. https://doi.org/10.1016/j.renene.2020.07.020

Faizal, M., Saidur, R., Mekhilef, S., Hepbasli, A., & Mahbubul, I. M. (2014, November 5). Energy, economic, and environmental analysis of a flat-plate solar collector operated with SiO_2 nanofluid. *Clean Technologies and Environmental Policy*, *17*(6), 1457–1473. https://doi.org/10.1007/s10098-014-0870-0

Gad, H., Hamed, A., & El-Sharkawy, I. (2001, April). Application of a solar desiccant/collector system for water recovery from atmospheric air. *Renewable Energy*, *22*(4), 541–556. https://doi.org/10.1016/s0960-1481(00)00112-9

Gandhidasan, P., & Abualhamayel, H. (1996, September). Water recovery from the atmosphere. *Renewable Energy*, *9*(1–4), 745–748. https://doi.org/10.1016/0960-1481(96)88391-1

Gandhidasan, P., & Abualhamayel, H. I. (2009, August 20). Investigation of humidity harvest as an alternative water source in the Kingdom of Saudi Arabia. *Water and Environment Journal*, *24*(4), 282–292. https://doi.org/10.1111/j.1747-6593.2009.00189.x

Gordeeva, L. G., & Aristov, Y. I. (2012, June 22). Composites 'salt inside porous matrix' for adsorption heat transformation: a current state-of-the-art and new trends. *International Journal of Low-Carbon Technologies*, *7*(4), 288–302. https://doi.org/10.1093/ijlct/cts050

Gordeeva, L. G., Solovyeva, M. V., Sapienza, A., & Aristov, Y. I. (2020, April). Potable water extraction from the atmosphere: Potential of MOFs. *Renewable Energy*, *148*, 72–80. https://doi.org/10.1016/j.renene.2019.12.003

Guangul, F. M., & Chala, G. T. (2019). Solar energy as renewable energy source: SWOT analysis. *2019 4th MEC international conference on big data and smart city (ICBDSC)*, IEEE.

Hamed, A. (2003, August). Experimental investigation on the natural absorption on the surface of sandy layer impregnated with liquid desiccant. *Renewable Energy*, *28*(10), 1587–1596. https://doi.org/10.1016/s0960-1481(03)00005-3

Hamed, A. M., & Sultan, A. A. (2002, September). Mass transfer in vertical cloth layers impregnated with Calcium chloride for recovery of water from air. *Renewable Energy*, *27*(1), 13–25. https://doi.org/10.1016/s0960-1481(01)00176-8

Hamed, A. M., Aly, A. A., & Zeidan, E. S. B. (2011). Application of Solar Energy for Recovery of Water from Atmospheric Air in Climatic Zones of Saudi Arabia. *Natural Resources*, *02*(01), 8–17. https://doi.org/10.4236/nr.2011.21002

Hamed, A. M., Kabeel, A. E., E-shafei, B. Z. & Aly, A. A. (2010). A Technical Review On The Extraction Of Water From Atmospheric Air In Arid Zones. *JP Journal of Heat and Mass Transfer*, *4*(3), 213-228. https://doi.org/10.1155/2012/285533435

Hussmann, P. (1982). Method and apparatus for recovery of water from the atmosphere, United States Patent.

Inbar, O., Gozlan, I., Ratner, S., Aviv, Y., Sirota, R., & Avisar, D. (2020, October 21). Producing Safe Drinking Water Using an Atmospheric Water Generator (AWG) in an Urban Environment. *Water*, *12*(10), 2940. https://doi.org/10.3390/w12102940

Jerman, M., Orbanic, H., Etxeberria, I., Suarez, A., Junkar, M. & Lebar, A. (2011). Measuring the water temperature changes throughout the abrasive water jet cutting system. *2011 WJTA American waterjet conference*.

Ji, J., Wang, R., & Li, L. (2007, June). New composite adsorbent for solar-driven fresh water production from the atmosphere. *Desalination*, *212*(1–3), 176–182. https://doi.org/10.1016/j.desal.2006.10.008

Kabeel, A. (2007, January). Water production from air using multi-shelves solar glass pyramid system. *Renewable Energy*, *32*(1), 157–172. https://doi.org/10.1016/j.renene.2006.01.015

Kabeel, A. E. (2006). Application of sandy bed solar collector system for water extraction from air. *International Journal of Energy Research*, *30*(6), 381–394. https://doi.org/10.1002/er.1155

Kabeel, A., Abdulaziz, M., & El-Said, E. M. (2014, February 24). Solar-based atmospheric water generator utilisation of a fresh water recovery: A numerical study. *International Journal of Ambient Energy*, *37*(1), 68–75. https://doi.org/10.1080/01430750.2014.882864

Kabeel, A., Harby, K., Abdelgaied, M., & Eisa, A. (2020, February). A comprehensive review of tubular solar still designs, performance, and economic analysis. *Journal of Cleaner Production*, *246*, 119030. https://doi.org/10.1016/j.jclepro.2019.119030

Kabir, E., Kumar, P., Kumar, S., Adelodun, A. A., & Kim, K. (2018). Solar energy: Potential and future prospects. *Renewable and Sustainable Energy Reviews, 82*, 894-900.

Kallenberger, P. A., & Fröba, M. (2018, May 17). Water harvesting from air with a hygroscopic salt in a hydrogel–derived matrix. *Communications Chemistry*, *1*(1). https://doi.org/10.1038/s42004-018-0028-9

Kalogirou, S. A. (2013, October 25). *Solar Energy Engineering: Processes and Systems*. Academic Press. https://doi.org/10.1016/B978-0-12-374501-9.00001-X

Kanae, S. (2009). Global Warming and the Water Crisis. *Journal of Health Science*, *55*(6), 860–864. https://doi.org/10.1248/jhs.55.860

Kannan, N., & Vakeesan, D. (2016, September). Solar energy for future world: - A review. *Renewable and Sustainable Energy Reviews*, *62*, 1092–1105. https://doi.org/10.1016/j.rser.2016.05.022

Karimi Estahbanati, M., Ahsan, A., Feilizadeh, M., Jafarpur, K., Ashrafmansouri, S. S., & Feilizadeh, M. (2016, March). Theoretical and experimental investigation on internal reflectors in a single-slope solar still. *Applied Energy*, *165*, 537–547. https://doi.org/10.1016/j.apenergy.2015.12.047

Karpov, D., Dyudina, O., & Pavlov, M. (2021). A review on modern heat-insulating materials for improving the energy efficiency of buildings and life-support utilities. *E3S Web of Conferences*, *288*, 01099. https://doi.org/10.1051/e3sconf/202128801099

Kim, H., Rao, S. R., Kapustin, E. A., Zhao, L., Yang, S., Yaghi, O. M., & Wang, E. N. (2018, March 22). Adsorption-based atmospheric water harvesting device for arid climates. *Nature Communications*, *9*(1). https://doi.org/10.1038/s41467-018-03162-7

Kim, H., Yang, S., Rao, S. R., Naryanan, S., Kapustin, E. A., Furukawa, H., Umans, A. S., Yaghi, O. M. & Wang, E. N. (2017). Water harvesting from air with metal-organic frameworks powered by natural sunlight. Science, *356*(6336), 430-434. https://doi.org/10.1126/science.aam8743

Krumsvik, P. K. (1998). Method and Device for Recovering Water from a Humid Atmosphere, United States Patent.

Kumar, M., & Yadav, A. (2015a, July 26). Solar-driven technology for freshwater production from atmospheric air by using the composite desiccant material "CaCl$_2$/floral foam." *Environment, Development and Sustainability*, *18*(4), 1151–1165. https://doi.org/10.1007/s10668-015-9693-3

Kumar, M., & Yadav, A. (2015b, July). Experimental investigation of solar powered water production from atmospheric air by using composite desiccant material "CaCl$_2$ /saw wood." *Desalination*, *367*, 216–222. https://doi.org/10.1016/j.desal.2015.04.009

Kumar, M., & Yadav, A. (2015c, May). Experimental investigation of design parameters of solar glass desiccant box type system for water production from atmospheric air. *Journal of Renewable and Sustainable Energy*, *7*(3), 033122. https://doi.org/10.1063/1.4922142

Kumar, M., & Yadav, A. (2016, April 1). Composite desiccant material "CaCl$_2$/Vermiculite/Saw wood": a new material for fresh water production from atmospheric air. *Applied Water Science*, *7*(5), 2103–2111. https://doi.org/10.1007/s13201-016-0406-3

Kumar, M., Yadav, A., & Mehla, N. (2017, November 13). Water generation from atmospheric air by using different composite desiccant materials. *International Journal of Ambient Energy*, *40*(4), 343–349. https://doi.org/10.1080/01430750.2017.1392350

Kumar, P. M., Arunthathi, S., Jeevan Prasanth, S., Aswin, T., Anish Antony, A., Daniel, D., Mohankumar, D., & Nikhil Babu, P. (2021). Investigation on a desiccant based solar water recuperator for generating water from atmospheric air. *Materials Today: Proceedings*, *45*, 7881–7884. https://doi.org/10.1016/j.matpr.2020.12.506

Kumar, S., & Kurmaji, K. T. (2013, May 28). Carbon credit earned by some designs of solar stills. *Desalination and Water Treatment*, *51*(22–24), 4699–4708. https://doi.org/10.1080/19443994.2013.770269

Li, R., Shi, Y., Alsaedi, M., Wu, M., Shi, L., & Wang, P. (2018a, September 7). Hybrid Hydrogel with High Water Vapor Harvesting Capacity for Deployable Solar-Driven Atmospheric Water Generator. *Environmental Science & Technology*, *52*(19), 11367–11377. https://doi.org/10.1021/acs.est.8b02852

Li, R., Shi, Y., Shi, L., Alsaedi, M., & Wang, P. (2018b, April 2). Harvesting Water from Air: Using Anhydrous Salt with Sunlight. *Environmental Science & Technology*, *52*(9), 5398–5406. https://doi.org/10.1021/acs.est.7b06373

Li, R., Shi, Y., Wu, M., Hong, S., & Wang, P. (2020, January). Improving atmospheric water production yield: Enabling multiple water harvesting cycles with nano sorbent. *Nano Energy*, *67*, 104255. https://doi.org/10.1016/j.nanoen.2019.104255

Meng, Q., Zhao, Z., Zhang, T., van Es, J., Pauw, A., Zhang, H., & Yan, Y. (2020, October). Experimental study on the transient behaviors of mechanically pumped two-phase loop with a novel accumulator for thermal control of space camera payload. *Applied Thermal Engineering*, *179*, 115714. https://doi.org/10.1016/j.applthermaleng.2020.115714

Misha, S., Mat, S., Ruslan, M., & Sopian, K. (2012, September). Review of solid/liquid desiccant in the drying applications and its regeneration methods. *Renewable and Sustainable Energy Reviews*, *16*(7), 4686–4707. https://doi.org/10.1016/j.rser.2012.04.041

Modi, K. V., & Modi, J. G. (2019, February). Performance of single-slope double-basin solar stills with small pile of wick materials. *Applied Thermal Engineering*, *149*, 723–730. https://doi.org/10.1016/j.applthermaleng.2018.12.071

Mohamed, M., William, G., & Fatouh, M. (2017, May). Solar energy utilization in water production from humid air. *Solar Energy*, *148*, 98–109. https://doi.org/10.1016/j.solener.2017.03.066

Mousavi Maleki, S., Hizam, H., & Gomes, C. (2017, January 22). Estimation of Hourly, Daily and Monthly Global Solar Radiation on Inclined Surfaces: Models Re-Visited. *Energies*, *10*(1), 134. https://doi.org/10.3390/en10010134

Mulchandani, A., Malinda, S., Edberg, J., & Westerhoff, P. (2020). Sunlight-driven atmospheric water capture capacity is enhanced by nano-enabled photothermal desiccants. *Environmental Science: Nano*, *7*(9), 2584–2594. https://doi.org/10.1039/d0en00463d

Nandakumar, D. K., Zhang, Y., Ravi, S. K., Guo, N., Zhang, C., & Tan, S. C. (2019, January 13). Solar Energy Triggered Clean Water Harvesting from Humid Air Existing above Sea Surface Enabled by a Hydrogel with Ultrahigh Hygroscopicity. *Advanced Materials*, *31*(10), 1806730. https://doi.org/10.1002/adma.201806730

Nascutiu, L., Giurgea, C., Damian, M., Bode, F., Budiu, O., & Andercou, O. (2016, January). Considerations Regarding the Optically Transparent Rigid Model for PIV Investigations. A Case Study. Part1: Model Manufacturing. *Energy Procedia*, *85*, 358–365. https://doi.org/10.1016/j.egypro.2015.12.262

Nayak, J. P., & Bera, J. (2011, December). Preparation of an efficient humidity indicating Silica gel from rice husk ash. *Bulletin of Materials Science*, *34*(7), 1683–1687. https://doi.org/10.1007/s12034-011-0377-9

Omara, Z., Hamed, M. H., & Kabeel, A. (2011, August). Performance of finned and corrugated absorbers solar stills under Egyptian conditions. *Desalination*, *277*(1–3), 281–287. https://doi.org/10.1016/j.desal.2011.04.042

Qi, H., Wei, T., Zhao, W., Zhu, B., Liu, G., Wang, P., Lin, Z., Wang, X., Li, X., Zhang, X., & Zhu, J. (2019, September 15). An Interfacial Solar-Driven Atmospheric Water Generator Based on a Liquid Sorbent with Simultaneous Adsorption–Desorption. *Advanced Materials*, *31*(43), 1903378. https://doi.org/10.1002/adma.201903378

Rajamani, M., & Maliyekkal, S. M. (2018, August). Chitosan reinforced boehmite nanocomposite desiccant: A promising alternative to Silica gel. *Carbohydrate Polymers*, *194*, 245–251. https://doi.org/10.1016/j.carbpol.2018.04.051

Ramli, M. S. A., Misha, S., Haminudin, N. F., Rosli, M. A. M., Yusof, A. A., Md Basar, M. F., Sopian, K., Ibrahim, A., & Abdullah, A. F. (2021, October 31). Review of Desiccant in the Drying and Air-Conditioning Application. *International Journal of Heat and Technology*, *39*(5), 1475–1482. https://doi.org/10.18280/ijht.390509

Rose, B. R. (2019). Experimental investigation of maximum stress concentrations in a femur bone by photoelastic approach. *Kuwait Journal of Science*, *46*(4), 66-74.

Salehi, A. A., Ghannadi-Maragheh, M., Torab-Mostaedi, M., Torkaman, R., & Asadollahzadeh, M. (2020, March). A review on the water-energy nexus for drinking water production from humid air. *Renewable and Sustainable Energy Reviews*, *120*, 109627. https://doi.org/10.1016/j.rser.2019.109627

Scrivani, A., El Asmar, T., & Bardi, U. (2007, February). Solar trough concentration for fresh water production and waste water treatment. *Desalination*, *206*(1–3), 485–493. https://doi.org/10.1016/j.desal.2006.02.075

Silica gel. (2022, September 7).

In *Wikipedia*. https://en.wikipedia.org/wiki/Silica_gel#/media/File:Silica_gel_bag_open_with_beads.jpg

Simonova, I. A., Freni, A., Restuccia, G., & Aristov, Y. I. (2009, June). Water sorption on composite "Silica modified by Calcium nitrate." *Microporous and Mesoporous Materials*, *122*(1–3), 223–228. https://doi.org/10.1016/j.micromeso.2009.02.034

Singh, R. P., Mishra, V. K., & Das, R. K. (2018, September 28). Desiccant materials for air conditioning applications - A review. *IOP Conference Series: Materials Science and Engineering*, *404*, 012005. https://doi.org/10.1088/1757-899x/404/1/012005

Sleiti, A. K., Al-Khawaja, H., Al-Khawaja, H., & Al-Ali, M. (2021, February). Harvesting water from air using adsorption material – Prototype and experimental results. *Separation and Purification Technology*, *257*, 117921. https://doi.org/10.1016/j.seppur.2020.117921

Srivastava, N., & Eames, I. (1998, September). A review of adsorbents and adsorbates in solid–vapour adsorption heat pump systems. *Applied Thermal Engineering*, *18*(9–10), 707–714. https://doi.org/10.1016/s1359-4311(97)00106-3

Srivastava, S., & Yadav, A. (2018a, July). Water generation from atmospheric air by using composite desiccant material through fixed focus concentrating solar thermal power. *Solar Energy*, *169*, 302–315. https://doi.org/10.1016/j.solener.2018.03.089

Srivastava, S., & Yadav, A. (2018b, September 13). Extraction of water particles from atmospheric air through a Scheffler reflector using different solid desiccants. *International Journal of Ambient Energy*, *41*(12), 1357–1369. https://doi.org/10.1080/01430750.2018.1517667

Tahseen, T. A. (2014). Optimal Geometric Arrangement of Unfinned and Finned Flat Tube Heat Exchangers Under Laminar Forced Convection

Talaat, M., Awad, M., Zeidan, E., & Hamed, A. (2018, April). Solar-powered portable apparatus for extracting water from air using desiccant solution. *Renewable Energy*, *119*, 662–674. https://doi.org/10.1016/j.renene.2017.12.050

Tu, Y., Wang, R., Zhang, Y., & Wang, J. (2018, August). Progress and Expectation of Atmospheric Water Harvesting. *Joule*, *2*(8), 1452–1475. https://doi.org/10.1016/j.joule.2018.07.015

Velmurugan, V., & Srithar, K. (2007, October). Solar stills integrated with a mini solar pond — analytical simulation and experimental validation. *Desalination*, *216*(1–3), 232–241. https://doi.org/10.1016/j.desal.2006.12.012

Wang, J., Liu, J., Wang, R., & Wang, L. (2017a, December). Experimental investigation on two solar-driven sorption based devices to extract fresh water from atmosphere. *Applied Thermal Engineering*, *127*, 1608–1616. https://doi.org/10.1016/j.applthermaleng.2017.09.063

Wang, J., Wang, R., & Wang, L. (2016, May). Water vapor sorption performance of ACF-CaCl$_2$ and Silica gel-CaCl$_2$ composite adsorbents. *Applied Thermal Engineering*, *100*, 893–901. https://doi.org/10.1016/j.applthermaleng.2016.02.100

Wang, J., Wang, R., Tu, Y., & Wang, L. (2018, December). Universal scalable sorption-based atmosphere water harvesting. *Energy*, *165*, 387–395. https://doi.org/10.1016/j.energy.2018.09.106

Wang, J., Wang, R., Wang, L., & Liu, J. (2017b, November). A high efficient semi-open system for fresh water production from atmosphere. *Energy*, *138*, 542–551. https://doi.org/10.1016/j.energy.2017.07.106

Wang, Y., Danook, S. H., AL-bonsrulah, H. A., Veeman, D., & Wang, F. (2022, January 7). A Recent and Systematic Review on Water Extraction from the Atmosphere for Arid Zones. *Energies*, *15*(2), 421. https://doi.org/10.3390/en15020421

William, G., Mohamed, M., & Fatouh, M. (2015, October). Desiccant system for water production from humid air using solar energy. *Energy*, *90*, 1707–1720. https://doi.org/10.1016/j.energy.2015.06.125

Yousef, M. S., & Hassan, H. (2019, February). An experimental work on the performance of single slope solar still incorporated with latent heat storage system in hot climate conditions. *Journal of Cleaner Production*, *209*, 1396–1410. https://doi.org/10.1016/j.jclepro.2018.11.120

Yousef, M. S., Hassan, H., & Sekiguchi, H. (2019, March). Energy, exergy, economic and enviroeconomic (4E) analyses of solar distillation system using different absorbing materials. *Applied Thermal Engineering*, *150*, 30–41. https://doi.org/10.1016/j.applthermaleng.2019.01.005

Yu, N., Wang, R., Lu, Z., & Wang, L. (2014, May). Development and characterization of Silica gel–LiCl composite sorbents for thermal energy storage. *Chemical Engineering Science*, *111*, 73–84. https://doi.org/10.1016/j.ces.2014.02.012

Yuce, I., Canoglu, S., Yukseloglu, S. M., Li Voti, R., Cesarini, G., Sibilia, C., & Larciprete, M. C. (2022, May 22). Titanium and Silicon Dioxide-Coated Fabrics for Management and Tuning of Infrared Radiation. *Sensors*, *22*(10), 3918. https://doi.org/10.3390/s22103918

Zhao, F., Zhou, X., Liu, Y., Shi, Y., Dai, Y., & Yu, G. (2019, January 11). Super Moisture-Absorbent Gels for All-Weather Atmospheric Water Harvesting. *Advanced Materials*, *31*(10), 1806446. https://doi.org/10.1002/adma.201806446

Zheng, L., Zhou, F., Zhou, Z., Song, X., Dong, G., Wang, M., & Diao, X. (2015, May). Angular solar absorptance and thermal stability of Mo–SiO$_2$ double cermet solar selective absorber coating. *Solar Energy*, *115*, 341–346. https://doi.org/10.1016/j.solener.2015.02.013

Zheng, X., Ge, T., Wang, R., & Hu, L. (2014, December). Performance study of composite Silica gels with different pore sizes and different impregnating hygroscopic salts. *Chemical Engineering Science*, *120*, 1–9. https://doi.org/10.1016/j.ces.2014.08.047

APPENDIX A

Table A.1. Properties of the Silica gel[a].

Item		Blue gel indicator	Discoloring Silica gel	Blue Silica gel	Typical value
Adsorption capacity %	RH=20%	8.0	--	--	8.5
	RH=35%	13.0	--	--	13.6
	RH=50%	20.0	20.0	18.0	22.5
	RH=90%	--	--	28.0	31.4
Rattler loss %		10.0	10.0	10.0	0.5
Qualified size ratio		96	9.0	9.0	97
Loss on heating		5.0	5.0	5.0	0.9
Colour	RH=20%	Blue or light blue	--	--	*
	RH=35%	Purple or purplish red	--	--	*
	RH=50%	Light red	Lightered light	Purple or light red	*

[a] Qingdao Double Dragon Industry Co., Ltd. provides these characteristics.

Table A.2. Day number of the year

Month	Day Number	Hour of the Month	Average Day of the Month		
			Date	N	δ (degrees)
January	i	k	17	17	−20.92
February	$31 + i$	$744 + k$	16	47	−12.95
March	$59 + i$	$1416 + k$	16	75	−2.42
April	$90 + i$	$2160 + k$	15	105	9.41
May	$120 + i$	$2880 + k$	15	135	18.79
June	$151 + i$	$3624 + k$	11	162	23.09
July	$181 + i$	$4344 + k$	17	198	21.18
August	$212 + i$	$5088 + k$	16	228	13.45
September	$243 + i$	$5832 + k$	15	258	2.22
October	$273 + i$	$6552 + k$	15	288	−9.60
November	$304 + i$	$7296 + k$	14	318	−18.91
December	$334 + i$	$8016 + k$	10	344	−23.05

Table A.3. Estimated values of A, E, and D from the ASHARE model

	Jan.	Feb.	Mar.	Apr.	May	Jun.	Jul.	Aug.	Sept.	Oct.	Nov.	Dec.
A	1230	1215	1186	1136	1104	1088	1085	1107	1152	1193	1221	1234
E	0.142	0.144	0.156	0.180	0.196	0.205	0.207	0.201	0.177	0.160	0.149	0.142
D	0.058	0.060	0.071	0.097	0.121	0.134	0.136	0.122	0.092	0.073	0.063	0.057

Table A.4. Mc Adams relation coefficient

Parameter	a	b	n
Smooth	5.61	1.09	1
Rough	6.18	1.19	1

APPENDIX B

1- Material type test

    I.   Friday (13/05/2022):

Time (hr)		8.00	10.00	12.00	14.00	16.00	18.00
Received Solar radiation (W/m²)	Without Glass	955	958	812	950	971	547
	Regular Glass (3mm)	843	840	818	827	848	473
	Plastic Glass (3mm)	884	888	833	886	893	482
	Acrylic sheet (2.4mm)	894	902	831	910	910	505

    II.   Friday (20/05/2022):

Time (hr)		8.00	10.00	12.00	14.00	16.00 *	18.00*
Received Solar radiation (W/m²)	Without Glass	842	897	760	843	235	67
	Regular Glass (3mm)	738	762	768	758	197.7	60.3
	Plastic Glass (3mm)	778	823	789	839	212	63.5
	Acrylic sheet (2.4mm)	796	846	781	866	218	64.3

* Dusty weather with sunlight absence.

    III.   Tuesday (28/06/2022):

Time (hr)		8.00	10.00	12.00	14.00	16.00	18.00
Received Solar radiation (W/m²)	Without Glass	917	897	734	948	998	712
	Regular Glass (3mm)	809	768	745	813	878	622
	Plastic Glass (3mm)	852	819	765	871	920	654
	Acrylic sheet (2.4mm)	867	836	760	892	941	665

2- Material thickness test

    I.   Friday (13/05/2022)

Time (hr)	9.00	11.00	13.00	15.00	17.00
Regular Glass (3mm)	893	870	817	893	735

84

Received Solar radiation (W/m²)	Regular Glass (4mm)	785	717	556	786	646
	Plastic Glass (3mm)	939	865	796	938	780
	Plastic Glass (4mm)	935	722	662	931	766

II.   Thursday (19/05/2022):

Time (hr)		**9.00**	**11.00**	**13.00**	**15.00**	**17.00**
Received Solar radiation (W/m²)	Regular Glass (3mm)	816	794	749	798	503
	Regular Glass (4mm)	723	769	531	705	445
	Plastic Glass (3mm)	857	804	721	835	522
	Plastic Glass (4mm)	861	750	617	829	527

III.   Saturday (21.05.2022):

Time (hr)		**9.00**	**11.00**	**13.00**	**15.00**	**17.00**
Received Solar radiation (W/m²)	Regular Glass (3mm)	893	866	855	863	655
	Regular Glass (4mm)	799	779	693	765	575
	Plastic Glass (3mm)	957	873	863	912	678
	Plastic Glass (4mm)	945	739	706	909	663

APPENXID C

Solar intensity model:

The theoretical model of solar intensity calculation for 6.30 a.m. on 16 September can be done using the following equations:

Declination angle:

$$\delta = 23.45 \sin\left[\frac{360}{365}(284 + N)\right]$$

= 23.45 Sin [(360/365) * (284+ 259) = 1.81°

Where: N for 16 September is equal to 259.

Equation of time:

$$G = \frac{360(N - 81)}{365}$$

= (360/365) * (259-81) = 175.56

$$ET = 9.87 \sin 2G - 7.53 \cos G - 1.5 \sin G$$

= 9.87 *[Sin (2*175.56)] – [7.53 * Cos (175.56)] – [1.5 * Sin (175.56)] = 5.87 min

Apparent solar time:

$$AST = LST + \frac{ET}{60} + \frac{4}{60}[SL - LL]$$

= 6.30 + (5.87/60) + [(4/60) * (45-44.38)] = 6.43 hr

Where: LST = 6.30, which is the time that regeneration operation starts; SL= 45°, LL= 44.38
°

Hour angle:

$$h = (AST - 12)15$$

= (5.44-12) * 15 = - 83.41°

Altitude angle:

$$sin(\Theta) = sin(L)sin(\delta) + cos(L)cos(\delta)cos(h)$$

$$= [\text{Sin} (35.47) * \text{Sin} (1.81)] + [\text{Cos} (35.47) * \text{Cos} (1.81) * \text{Cos} (-83.41)] = 0.11\,^o$$

Normal beam radiation:

$$H_{bN} = A. exp \left[\frac{-E}{Sin\,\Theta}\right]$$

$$= 1152 * \text{exp} (-0.177/ 0.11) = 236.39$$

A and B are constants equal to 1152 and -0.177, respectively.

Direct beam radiation:

$$H_b = H_{bN}\, sin\,\Theta$$

$$= 236.39 * 0.11 = 26.42 \text{ W/m}^2$$

Diffused radiation:

$$H_d = DH_{bn}F_{ss}$$

$$= 0.092 * 236.39 * 1 = 21.75 \text{ W/m}^2$$

Where D is constant and equals 0.092, and Fss can be calculated from the following equation:

$$F_{ss} = 0.5(1 + cos\,\gamma)$$

Where: $\gamma = 0^o$, since the absorption surface is horizontal.

Global solar radiation:

$$H = H_b + H_d$$

$$= 26.42 * 21.75 = 48.17 \text{ W/m}^2$$

Values of global solar radiation in the daytime hours for 16 September are listed below:

LST	AST	h	Sin (θ)	H_{bn}	H_b	H_d	H
6.30	6.439145	-83.4128	0.111757	236.3863	26.41793	21.74754	48.16547
7.30	7.439145	-68.4128	0.317875	660.127	209.8379	60.73169	270.5696
8.30	8.439145	-53.4128	0.503582	810.5986	408.203	74.57507	482.7781
9.30	9.439145	-38.4128	0.656223	879.6548	577.2499	80.92824	658.1781
10.30	10.43915	-23.4128	0.765396	914.1567	699.6918	84.10241	783.7942
11.30	11.43915	-8.41282	0.82366	929.2338	765.373	85.48951	850.8625
12.30	12.43915	6.587178	0.827046	930.0516	769.1953	85.56475	854.76
13.30	13.43915	21.58718	0.775322	916.8671	710.8669	84.35177	795.2187
14.30	14.43915	36.58718	0.672013	885.2473	594.8975	81.44275	676.3403
15.30	15.43915	51.58718	0.52416	821.8611	430.7864	75.61122	506.3976
16.30	16.43915	66.58718	0.341838	686.4035	234.6387	63.14912	297.7879
17.30	17.43915	81.58718	0.137473	317.8969	43.70217	29.24652	72.94868

APPENDIX D

The theoretical model of mass transfer coefficient calculation in adsorption process for 19.30 at 15 September as an example can be done using the following equations:

$$P_{sat@T_a} = 6.11 \times 10^{\frac{7.5 \times T_a}{237.3 + T_a}}$$

$$= 6.11 * 10\text{^} (7.5*34/237.3+34) = 53.27 \text{ mbar}$$

$$P_\infty = \emptyset P_{sat@T_a}$$

$$= 41 * 53.27 = 215717.3 \text{ Pa}$$

$$log_{10} P_d = -3.21254 + 3.13619 \times 10^{-2} T_{dE} - 1.22512 \times 10^{-4} T_{dE}^2 + 3.63841$$
$$\times 10^{-7} T_{dE}^3 - 5.67607 \times 10^{-10} T_{dE}^4$$
$$= -3.21254 + 3.13619 \times 10^{-2} * 33 - 1.22512 \times 10^{-4} (33)^2 + 3.63841$$
$$\times 10^{-7} (33)^3 - 5.67607 \times 10^{-10} (33)^4 = 5051.503 \text{ Pa}$$

$$\Delta p = p_\infty - p_d$$

$$= (215717.3 - 5051.503) * 1000 = 212.8 \text{ KPa}$$

$$\beta = \frac{\dot{m}}{A\Delta p}$$

$$= 3/0.2505*212.8 = 0.069 \text{ g/m}^2. \text{ hr. KPa}$$

Where A is the adsorption area., representing the tray's area that holds the desiccant material. A= 0.2052, m^2, $\dot{m}$: is mass of adsorbed moisture from atmospheric air, g/hr.

Values of mass transfer coefficient in the nighttime hours for 15 September are listed below:

Date	$\dot{m}$ (g/hr)	RH (%)	Ta (ºC)	TdE (ºC)	Psat (mbar)	Pam (Pa)	logP$_d$ (MPa)	P$_d$ (Pa)	Δp (KPa)	β (g/m².hr. KPa)
18.30	0	39	35	35	57.24	221301.96	-2.26	5535.33	215.77	0
19.30	3	41	34	33	53.27	217854.73	-2.30	5051.50	212.80	0.069
20.30	4	43	33	32	50.34	215717.26	-2.33	4701.59	211.02	0.092
21.30	4	43	32	31	48.26	205214.62	-2.36	4398.01	200.82	0.097
22.30	5	43	32	31	46.97	202636.37	-2.36	4376.28	198.26	0.123
23.30	4	43	31	30	45.84	195831.18	-2.37	4278.00	191.55	0.102
0.30	6	46	30	29	43.43	200189.73	-2.40	4004.63	196.19	0.149
1.30	5	46	30	28	41.82	191515.87	-2.41	3860.64	187.66	0.130
2.30	5	46	29	28	40.83	186349.80	-2.42	3789.79	182.56	0.133
3.30	7	47	29	27	40.02	187598.15	-2.44	3662.20	183.94	0.185
4.30	6	47	29	27	39.26	182655.83	-2.44	3618.86	179.04	0.163

APPENDIX E

The codes written in MATLAB program using the Fourth-Order-Rung-Kutta method to solve the regeneration equations are listed below:

```
clear
clc

%% constants
gamma   =   35;
Ka      =   0.02881;
Dy      =   56.5/100;
cd      =   765;
cw      =   4180;
cc      =   900;
Ab      =   0.2052;
md      =   1;
mw      =   37/1000;
mc      =   0.365;
alphad  =   0.95;
taucover=   0.92;
ccov    =   1470;
mcov    =   1.13;
Acov    =   0.3565;
sigma   =   5.67*10^-8;
a       =   5.61;
b       =   1.09;
n       =   1;
epsoncov=   0.86;
epsond  =   0.85;


Cb          =(cd*md+cw*mw+cc*mc)/Ab;
Ccov        =(ccov*mcov)/Acov;
Fpcovsky    =0.5*(1+cos(gamma*pi/180));
Fcovsky     =1/(((1-epsoncov)/epsoncov)+(1/Fpcovsky));
Fdcov       =1/((1/epsond)+(1/epsoncov)-(1));




%% data from an experimental device

% 30 September
time = [5.30, 6.30, 7.30, 8.30, 9.30, 10.30, 11.30, 12.30, 13.30, 14.30,
15.30, 16.30, 17.30]*60*60;
H = [3, 77, 191, 283, 365, 416, 424, 401, 352, 124, 129, 21, 2];
v = [0.01, 0, 0, 0, 0, 0, 0, 0, 0, 0, 0, 0, 0];
Ta = [25, 27, 30, 34, 36, 39, 41, 41, 41, 40, 39, 37, 35];


%DATE   Solar w/m2  Wind Speed m/sec    RH% Ta  Tcover  Td accum.prod.
exper=[
5.30    3   0.01    44  25  22  23  0
6.30    77  0       43  27  33  31  0
7.30    191 0       38  30  51  58  0
8.30    283 0       33  34  59  79  0
9.30    365 0       32  36  65  91  0
10.30   416 0       30  39  71  101 2
11.30   424 0       29  41  72  104 7
12.30   401 0       29  41  70  103 13
```

90

```
13.30   352 0        28  41  60  78  0
14.30   124 0        29  40  59  72  0
15.30   129 0        30  39  53  61  0
16.30   21  0        32  37  37  42  0
17.30   2   0        35  35  32  35  0
];


%% functions (time)

Ht      = @(t) interp1(time, H, t, 'linear', 'extrap');
vt      = @(t) interp1(time, v, t, 'linear', 'extrap');
Tat     = @(t) interp1(time, Ta, t, 'linear', 'extrap');


hcovat  = @(t) a+b*vt(t)^n;
Tskyt   = @(t) Tat(t)-10;
qcovat  = @(t,Td,Tcov) hcovat(t)*(Tcov-Tat(t))+ Fcovsky * sigma * (
(Tcov+273)^4 - (Tskyt(t)+273)^4);
qc      = @(t,Td,Tcov) Ka * (Td - Tcov)/Dy ;
hfg      = @(t,Td,Tcov) (2501.67-2.389*Td)*10^3;
pcov    = @(t,Td,Tcov) (6.11*10^((7.5*Tcov)/(237.3+Tcov)))*0.0001;
pd      = @(t,Td,Tcov) 10^(-3.21254+3.13619*10^(-2) * Td-1.22512*10^(-4)
* Td^2+3.63841*10^(-7) * Td^3-5.67607*10^(-10) *  Td^4);
qe      = @(t,Td,Tcov) 0.0061* ( (Td-Tcov)+((pd(t,Td,Tcov)-
pcov(t,Td,Tcov))/(0.265-pd(t,Td,Tcov))) * (Td+273) )^(1/3) *
(pd(t,Td,Tcov)-pcov(t,Td,Tcov)) * hfg(t,Td,Tcov);
qr      = @(t,Td,Tcov) Fdcov * sigma * ( (Td+273)^4 - (Tcov+273)^4);

%% main ode
dTd_dt  = @(t,Td,Tcov) (taucover*alphad*Ht(t)-
(qe(t,Td,Tcov)+qc(t,Td,Tcov)+qr(t,Td,Tcov)))/Cb;

dTcov_dt = @(t,Td,Tcov)
((qe(t,Td,Tcov)+qc(t,Td,Tcov)+qr(t,Td,Tcov)+Ht(t))-
(taucover*Ht(t)+qcovat(t,Td,Tcov)))/Ccov;

dydt = @(t,y) [dTd_dt(t,y(1),y(2)); dTcov_dt(t,y(1),y(2))];

initial_conditions=[20 ; 20]; %% need to change
tspan = [time(1) time(end)];

options = odeset('MaxStep', 10);
[t, y] = ode45(dydt, tspan, initial_conditions,options);

th=t/3600;
y=real(y);



%% output
figure;
plot(t/3600, y(:,1),'-r', t/3600, y(:,2),'-b','linewidth',2);
hold on
plot(exper(:,1), exper(:,7),'ro',exper(:,1), exper(:,6),'bs',exper(:,1),
exper(:,5),'gx');


legend('T_d', 'T_{cov}','T_d_E',
'T_{cov}_E','T_a','location','northwest');
xlabel('Time, hr','FontWeight', 'bold');
```

91

```matlab
ylabel('Temperature, \circC','FontWeight', 'bold');

%% productivity
count=0;
sqe=0;
shfg=0;
sht=0;
for i=1:length(t)
    count=count+1;
    QE(count)=qe(t(count),y(count,1),y(count,2));
    sqe=sqe+QE(count);
    HFG(count)=hfg(t(count),y(count,1),y(count,2));
    shfg=shfg+HFG(count);
    PD(count)=pd(t(count),y(count,1),y(count,2));
    PCOV(count)=pcov(t(count),y(count,1),y(count,2));
    HT(count)=Ht(t(count));
    sht=sht+HT(count);
    SQE(count)=real(sqe);
    SHFG(count)=real(shfg);
    SHT(count)=real(sht);
    P(count)=SQE(count)./SHFG(count);
    EF(count)=SQE(count)./SHT(count);
end

figure (2);
plot(t/3600,P*1000*3600,'linewidth',2);
hold on
plot(exper(:,1), exper(:,8),'ro');
legend('Prod.', 'Prod.E','location','northwest');
xlabel('Time, hr','FontWeight', 'bold');
ylabel('Accumulated productivity, g/hr','FontWeight', 'bold');
xlim([6 13]);

figure (3);
plot(t/3600,EF*100)
xlabel('Time (hr)','FontWeight', 'bold');
ylabel('EF (%)','FontWeight', 'bold');
xlim([7 14]);

figure(4);
plot(t/3600, PD,'-','linewidth',2)
hold on
plot(t/3600, PCOV,'-','linewidth',2)
legend('PD', 'PCOV')
xlabel('Time, hr','FontWeight', 'bold')
ylabel('Pressure, MPa','FontWeight', 'bold');
```

APPENDIX F

The uncertainty calculations are detailed below:

I. Uncertainty for independent variables:

1- Solar intensity: The solar intensity is measured using a Data logging solar power meter with a resolution of 0.1 and accuracy equal to ± 10 W/m². The relative uncertainty was calculated as follows:

$$B_{H_E} = \pm \left[\left(\frac{1}{2}0.1\right)^2 + (10)^2\right]^{1/2} = \pm 10.0001 \text{ W/m}^2$$

$$\overline{H_E} = \frac{1}{30}\sum_{i=1}^{30} H_{Ei} = 855.77$$

$$\sigma_{H_E} = \left[\frac{1}{30-1}\sum_{i=1}^{30}(H_{Ei} - \overline{H_E})^2\right]^{1/2} = 1.48$$

$$\sigma_{\overline{H_E}} = \frac{\sigma_{H_E}}{\sqrt{30}} = 0.27$$

$$Ps_H = t_{(30-1),95\%} * \sigma_{\overline{H_E}} = 0.552 \text{ W/m}^2$$

$$U_{H_E} = \pm[B^2 + Ps^2]^{1/2} = \pm 10.015 \text{ W}/_{m^2}$$

$$\frac{U_{H_E}}{H_E}\% = \left(\frac{U_{H_E}}{H_E}\right) * 100 = \pm 1.17\%$$

2- Wind speed: The wind speed is recorded using an RS-FSJT-V05 type anemometer having a resolution of 0.1 and accuracy of ± 0.15:

$$B_v = \pm \left[\left(\frac{1}{2}0.1\right)^2 + (0.15)^2\right]^{1/2} = \pm 0.158114 \text{ m/s}$$

$$\overline{v} = \frac{1}{30}\sum_{i=1}^{30} v_i = 0.258333$$

$$\sigma_v = [\frac{1}{30-1}\sum_{i=1}^{30}(v_i - \overline{v})^2]^{1/2} = 0.31577$$

$$\sigma_{\overline{v}} = \frac{\sigma_v}{\sqrt{30}} = 0.057652$$

$$Ps_v = t_{(30-1),95\%} * \sigma_{\overline{v}} = 0.117897 \ ^m/_s$$

$$U_v = \pm[B^2 + Ps^2]^{1/2} = \pm0.1972 \ ^m/_s$$

$$\frac{U_v}{v}\% = \left(\frac{U_v}{v}\right) * 100 = \pm3.3\%$$

3- Relative humidity: An AM2302 (wired DHT22) sensor was used to measure relative humidity. The sensor has a resolution of 0.1 and an accuracy of $\pm$ 2%.

$$B_{RH} = \pm\left[\left(\frac{1}{2}0.1\right)^2 + (2)^2\right]^{1/2} = \pm0.000625$$

$$\overline{RH} = \frac{1}{30}\sum_{i=1}^{30}RH_i = 38.4$$

$$\sigma_{RH} = [\frac{1}{30-1}\sum_{i=1}^{30}(RH_i - \overline{RH})^2]^{1/2} = 0.471242$$

$$\sigma_{\overline{RH}} = \frac{\sigma_{RH}}{\sqrt{30}} = 0.086037$$

$$Ps_{RH} = t_{(30-1),95\%} * \sigma_{\overline{RH}} = 0.175945$$

$$U_{RH} = \pm[B^2 + Ps^2]^{1/2} = \pm2.008347 \ \%$$

$$\frac{U_{RH}}{RH}\% = \left(\frac{U_{RH}}{RH}\right) * 100 = \pm5.23\%$$

4- Temperature: A K-type thermocouples were used to measure the temperature at various points. The thermocouple has a resolution of 0.5 and an accuracy of 0.25. The uncertainty in temperature measurement was calculated as follows:

$$U_{Temp} = \pm \left[(U_{Std})^2 + (U_{Fitting\text{-}curve})^2 \right]^{0.5}$$

Where: U_{std} is the uncertainty of the standard instrument.

$$B_T = \pm \left[\left(\frac{1}{2} 0.5 \right)^2 + (0.25)^2 \right]^{1/2} = \pm 0.353553 \, °C$$

The precision error for the ambient, desiccant, and cover temperature were calculated as follows:

$$Ps_{T_a} = t_{(30-1),95\%} * \sigma_{\overline{T_a}} = 0.16793 \, °C$$

$$Ps_{T_{dE}} = t_{(30-1),95\%} * \sigma_{\overline{T_{dE}}} = 0.159653 \, °C$$

$$Ps_{T_{covE}} = t_{(30-1),95\%} * \sigma_{\overline{T_{covE}}} = 0.109406 \, °C$$

So, the uncertainty of the standard instrument for the ambient, desiccant, and cover temperature is equal to:

$$U_{T_a} = \pm [B_T{}^2 + Ps_{T_a}{}^2]^{1/2} = 0.391409 \, °C$$

$$U_{T_{dE}} = \pm [B_T{}^2 + Ps_{T_{dE}}{}^2]^{1/2} = 0.387929 \, °C$$

$$U_{T_{covE}} = \pm [B_T{}^2 + Ps_{T_{covE}}{}^2]^{1/2} = 0.370094 \, °C$$

The uncertainty of the fitting curve ($U_{fitting\text{-}curve}$) was calculated as follows:

$$U_{Fitting\text{-}curve} = \sigma_{\overline{T}} \times t_{(30-1),95\%}$$

Where $B_{fitting\text{-}curve} = 0$

First, we calculated the corrected temperature using the following equation:

$$T_{corr.} = 0.000006 T_{exp.}^2 + 0.9966 T_{exp.} + 0.1924$$

And then:

$$U_{Fitting\text{-}curve} = 0.081862 * 2.045 = 0.167408$$

Then:

$$U_{T_a} = \pm[(0.391409)^2 + (0.167408)^2]^{0.5} = \pm0.426\ ℃$$

$$U_{T_{dE}} = \pm[(0.387429)^2 + (0.167408)^2]^{0.5} = \pm0.423\ ℃$$

$$U_{T_{covE}} = \pm[(0.370094)^2 + (0.167408)^2]^{0.5} = \pm0.406\ ℃$$

$$\frac{U_{T_a}}{T_a}\% = \left(\frac{U_{T_a}}{T_a}\right) * 100 = \pm1.77\%$$

$$\frac{U_{T_{dE}}}{T_{dE}}\% = \left(\frac{U_{T_{dE}}}{T_{dE}}\right) * 100 = \pm1.46\%$$

$$\frac{U_{T_{covE}}}{T_{covE}}\% = \left(\frac{U_{T_{covE}}}{T_{covE}}\right) * 100 = \pm1.61\%$$

II.   Uncertainty for dependent variables:

1- Uncertainty of saturated water pressure at desiccant temperature P_d:

$$P_{dE} = 10^{-3.21254+3.13619\times10^{-2}\ T_{dE}-1.22512\times10^{-4}\ T_{dE}^2+3.63841\times10^{-7}\ T_{dE}^3-5.67607\times10^{-10}\ T_{dE}^4}$$

$$\frac{U_{P_d}}{P_d} = [\left(\frac{U_{T_{dE}}}{T_{dE}}\right)^2]^{0.5} * 100 = [(0.0146)^2]^{0.5} * 100 = \pm1.46\%$$

2- Uncertainty of saturated water pressure on cover temperature P_{cov}:

$$P_{cov} = 6.11 * 10^{\frac{7.5*T_{covE}}{237.3+T_{covE}}}$$

$$\frac{U_{P_{cov}}}{P_{cov}} = [\left(\frac{U_{T_{covE}}}{T_{covE}}\right)^2]^{0.5} * 100 = [(0.0161)^2]^{0.5} * 100 = \pm1.61\%$$

3- Uncertainty of the latent heat h_{fg}:

$$h_{fg} = (2501.67 - 2.389 T_{dE}) 10^3$$

$$\frac{U_{h_{fg}}}{h_{fg}} = [\left(\frac{U_{T_{dE}}}{T_{dE}}\right)^2]^{0.5} * 100 = [(0.0146)^2]^{0.5} * 100 = \pm 1.46\%$$

4- Uncertainty of heat transfer by evaporation q_e:

$$q_e = 0.0061 \left[(T_{dE} - T_{covE}) + \left(\frac{p_d - p_{cov}}{0.265 - p_d}\right)(T_{dE} + 273) \right]^{1/3} (p_d - p_{cov}) h_{fg}$$

$$\frac{U_{q_e}}{q_e} = \left[\left(\frac{U_{h_{fg}}}{h_{fg}}\right)^2 + \left(\frac{U_{T_{dE}}}{T_{dE}}\right)^2 + \left(\frac{U_{T_{covE}}}{T_{covE}}\right)^2 + \left(\frac{U_{Ps_d}}{Ps_d}\right)^2 + \left(\frac{U_{Ps_{cov}}}{Ps_{cov}}\right)^2 \right]^{0.5} * 100$$

$$= [(0.0146)^2 + (0.0146)^2 + (0.0161)^2 + (0.0146)^2 + (0.0161)^2]^{0.5}$$

$$* 100 = \pm 3.4\%$$

5- Uncertainty of the water productivity P:

$$P = \frac{q_e}{h_{Ffg}}$$

$$\frac{U_P}{P} = [\left(\frac{U_{q_e}}{q_e}\right)^2 + \left(\frac{U_{h_{fg}}}{h_{fg}}\right)^2]^{0.5} * 100 = [(0.034)^2 + (0.0146)^2]^{0.5} * 100 = \pm 3.7\%$$

6- Uncertainty of the system efficiency η:

$$\eta = \frac{\Sigma q_e}{\Sigma H_E}$$

$$\frac{U_\eta}{\eta} = [\left(\frac{U_{qe}}{q_e}\right)^2 + \left(\frac{U_{H_E}}{H_E}\right)^2]^{0.5} * 100 = [(0.034069)^2 + (0.011703)^2]^{0.5} * 100 = \pm 3.6\%$$

Table F1. T table of confidence level

t Table

cum. prob	$t_{.50}$	$t_{.75}$	$t_{.80}$	$t_{.85}$	$t_{.90}$	$t_{.95}$	$t_{.975}$	$t_{.99}$	$t_{.995}$	$t_{.999}$	$t_{.9995}$
one-tail	0.50	0.25	0.20	0.15	0.10	0.05	0.025	0.01	0.005	0.001	0.0005
two-tails	1.00	0.50	0.40	0.30	0.20	0.10	0.05	0.02	0.01	0.002	0.001
df											
1	0.000	1.000	1.376	1.963	3.078	6.314	12.71	31.82	63.66	318.31	636.62
2	0.000	0.816	1.061	1.386	1.886	2.920	4.303	6.965	9.925	22.327	31.599
3	0.000	0.765	0.978	1.250	1.638	2.353	3.182	4.541	5.841	10.215	12.924
4	0.000	0.741	0.941	1.190	1.533	2.132	2.776	3.747	4.604	7.173	8.610
5	0.000	0.727	0.920	1.156	1.476	2.015	2.571	3.365	4.032	5.893	6.869
6	0.000	0.718	0.906	1.134	1.440	1.943	2.447	3.143	3.707	5.208	5.959
7	0.000	0.711	0.896	1.119	1.415	1.895	2.365	2.998	3.499	4.785	5.408
8	0.000	0.706	0.889	1.108	1.397	1.860	2.306	2.896	3.355	4.501	5.041
9	0.000	0.703	0.883	1.100	1.383	1.833	2.262	2.821	3.250	4.297	4.781
10	0.000	0.700	0.879	1.093	1.372	1.812	2.228	2.764	3.169	4.144	4.587
11	0.000	0.697	0.876	1.088	1.363	1.796	2.201	2.718	3.106	4.025	4.437
12	0.000	0.695	0.873	1.083	1.356	1.782	2.179	2.681	3.055	3.930	4.318
13	0.000	0.694	0.870	1.079	1.350	1.771	2.160	2.650	3.012	3.852	4.221
14	0.000	0.692	0.868	1.076	1.345	1.761	2.145	2.624	2.977	3.787	4.140
15	0.000	0.691	0.866	1.074	1.341	1.753	2.131	2.602	2.947	3.733	4.073
16	0.000	0.690	0.865	1.071	1.337	1.746	2.120	2.583	2.921	3.686	4.015
17	0.000	0.689	0.863	1.069	1.333	1.740	2.110	2.567	2.898	3.646	3.965
18	0.000	0.688	0.862	1.067	1.330	1.734	2.101	2.552	2.878	3.610	3.922
19	0.000	0.688	0.861	1.066	1.328	1.729	2.093	2.539	2.861	3.579	3.883
20	0.000	0.687	0.860	1.064	1.325	1.725	2.086	2.528	2.845	3.552	3.850
21	0.000	0.686	0.859	1.063	1.323	1.721	2.080	2.518	2.831	3.527	3.819
22	0.000	0.686	0.858	1.061	1.321	1.717	2.074	2.508	2.819	3.505	3.792
23	0.000	0.685	0.858	1.060	1.319	1.714	2.069	2.500	2.807	3.485	3.768
24	0.000	0.685	0.857	1.059	1.318	1.711	2.064	2.492	2.797	3.467	3.745
25	0.000	0.684	0.856	1.058	1.316	1.708	2.060	2.485	2.787	3.450	3.725
26	0.000	0.684	0.856	1.058	1.315	1.706	2.056	2.479	2.779	3.435	3.707
27	0.000	0.684	0.855	1.057	1.314	1.703	2.052	2.473	2.771	3.421	3.690
28	0.000	0.683	0.855	1.056	1.313	1.701	2.048	2.467	2.763	3.408	3.674
29	0.000	0.683	0.854	1.055	1.311	1.699	2.045	2.462	2.756	3.396	3.659
30	0.000	0.683	0.854	1.055	1.310	1.697	2.042	2.457	2.750	3.385	3.646
40	0.000	0.681	0.851	1.050	1.303	1.684	2.021	2.423	2.704	3.307	3.551
60	0.000	0.679	0.848	1.045	1.296	1.671	2.000	2.390	2.660	3.232	3.460
80	0.000	0.678	0.846	1.043	1.292	1.664	1.990	2.374	2.639	3.195	3.416
100	0.000	0.677	0.845	1.042	1.290	1.660	1.984	2.364	2.626	3.174	3.390
1000	0.000	0.675	0.842	1.037	1.282	1.646	1.962	2.330	2.581	3.098	3.300
z	0.000	0.674	0.842	1.036	1.282	1.645	1.960	2.326	2.576	3.090	3.291
	0%	50%	60%	70%	80%	90%	95%	98%	99%	99.8%	99.9%
						Confidence Level					

APPENDIX G

The main calculation parameters used in the cost analysis are:

By assuming the number of life years, Y = 5 years, and interest per year, I = 10 %.

The present capital cost, PC = 205.18$

Capital Recovery Factor, CRF

$$CRF = \frac{I(I+1)^Y}{(I+1)^Y - 1} = 0.264$$

Fixed Annual Cost, FAC:

$$FAC = PC^*CRF = 54.13\$$$

Annual Maintenance Cost, AMC:

It is assumed as 15% of the fixed annual cost:

$$AMC = 0.15^*FAC = 8.12\$$$

Annual Salvage Value, ASV:

$$SFF = \frac{I}{(I+1)^Y - 1} = 0.16$$

$$S = 0.2 * PC = 41.04\$$$

$$ASV = SFF^*S = 6.72$$

Annual Cost, AC:

$$AC = FAC + AMC - ASV = 55.52$$

The total amount of produced water over the year, M:

$$M = amount\ of\ collected\ water * 365 = 21.9$$

Cost of Produced Kilogram of water, CPK:

$$CPK = \frac{AC}{M} = 2.54 \text{ \$/Kg}$$

I.   Variation of surrounding conditions
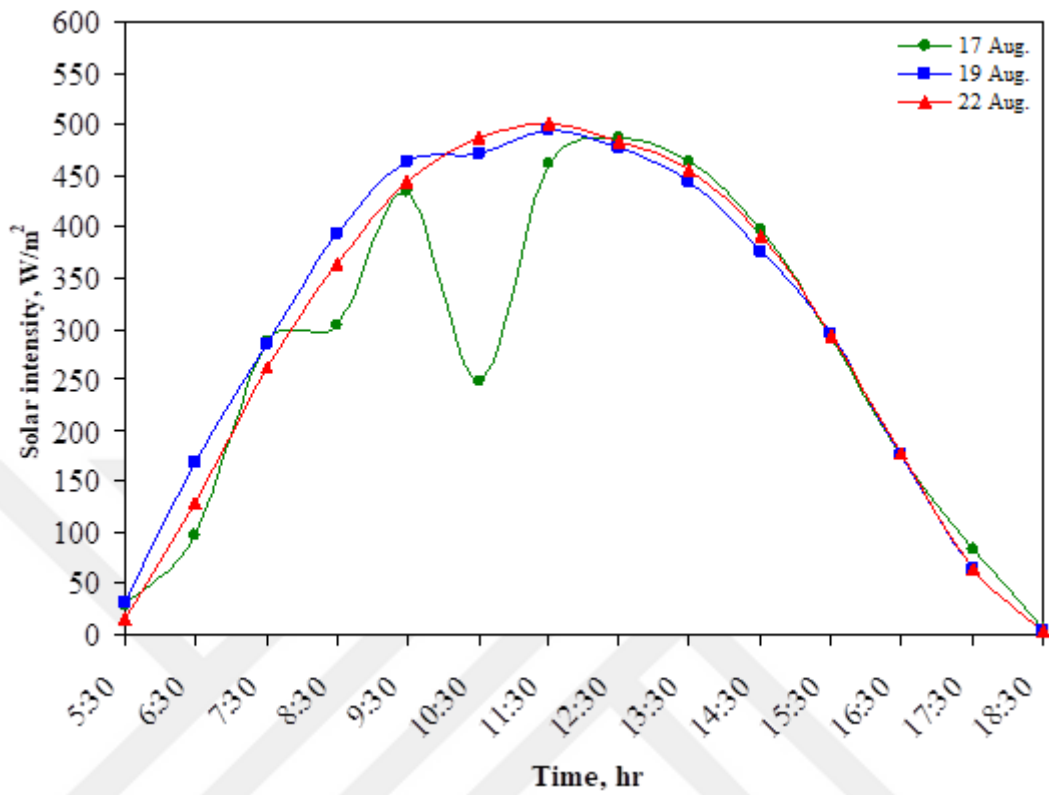
Figure H.1. Change in solar intensity with time for various days
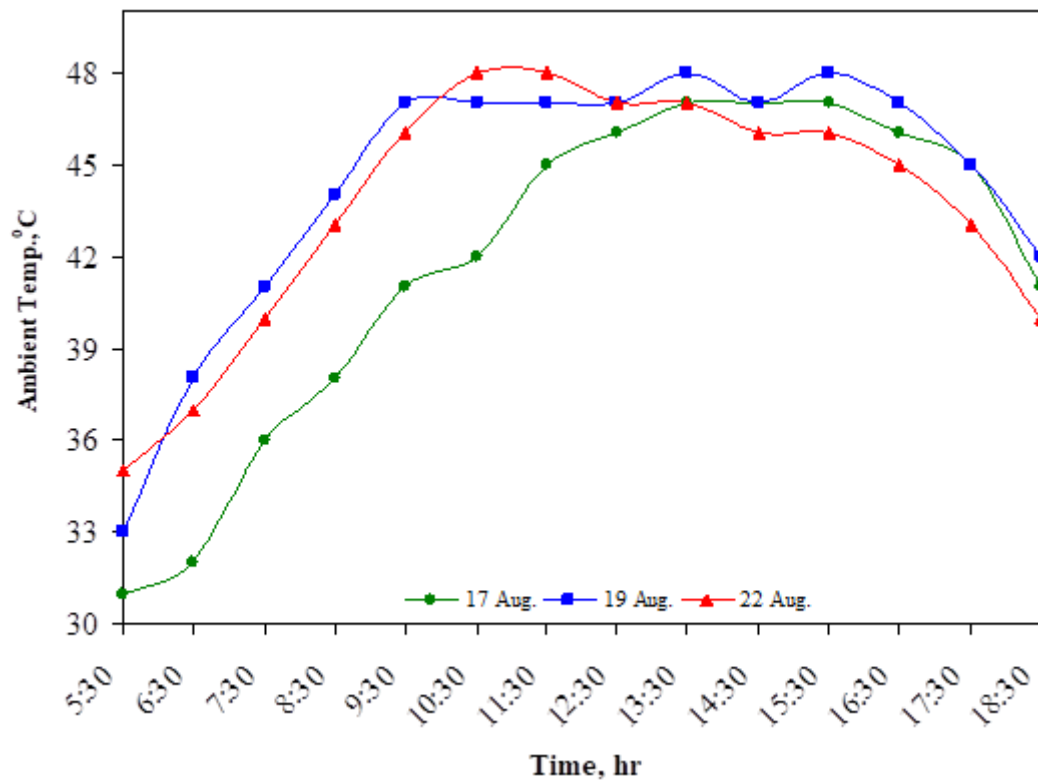
Figure H.2. Change in ambient temperature for various days
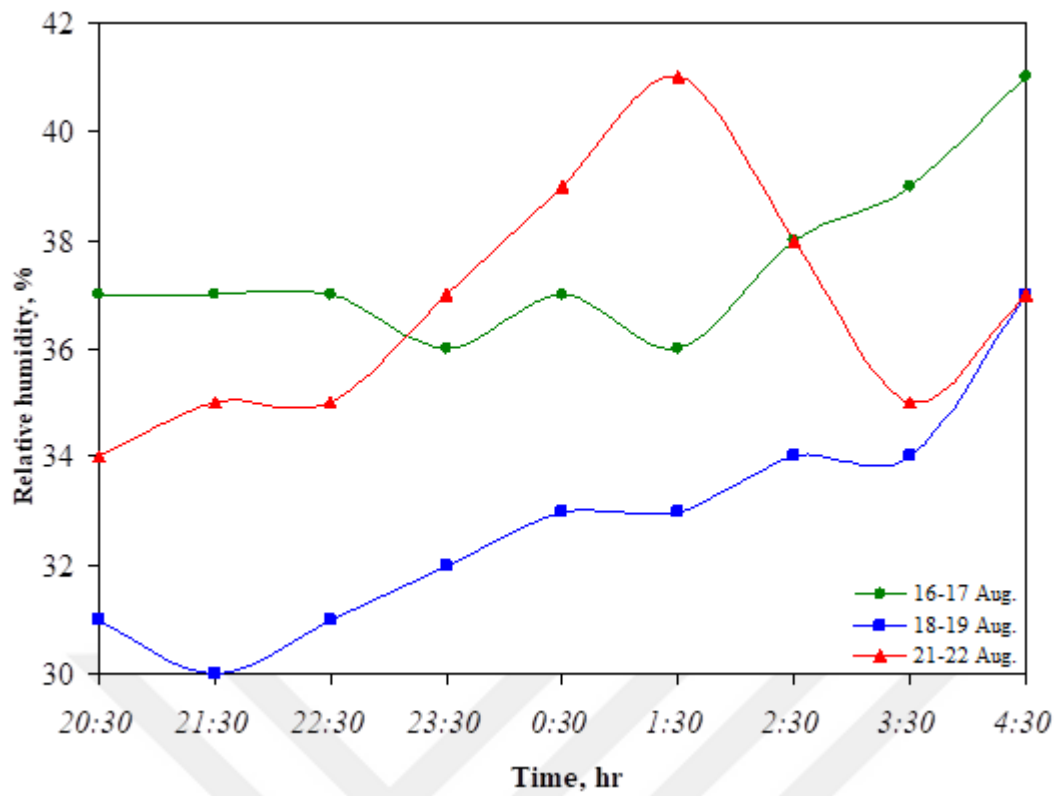
Figure H.3. Change in relative humidity for various days
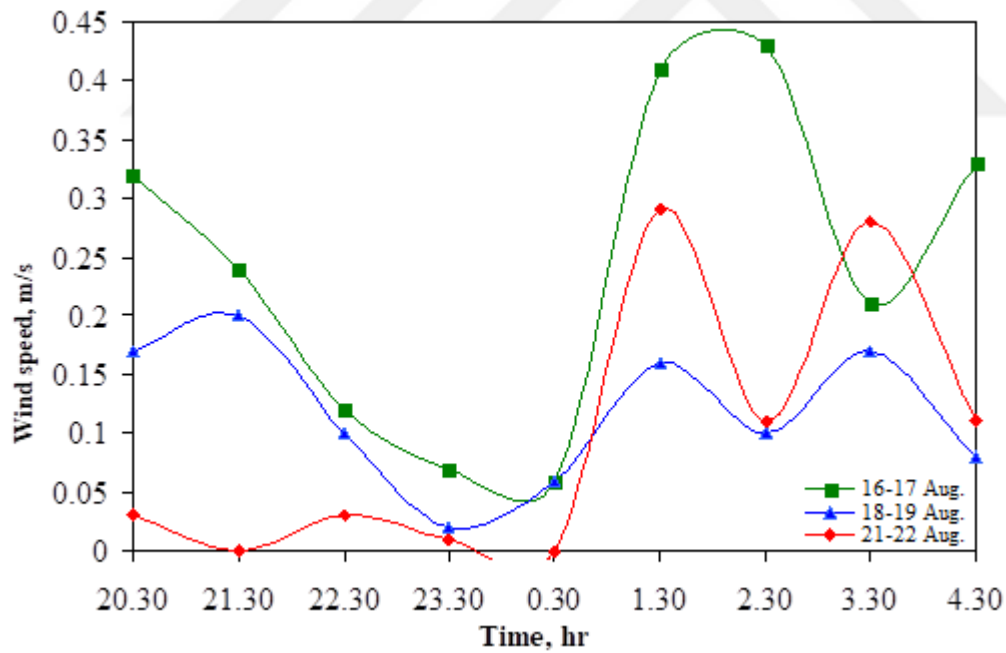
Figure H.4. Change in wind speed for various days

II.   Variation of setup's temperatures
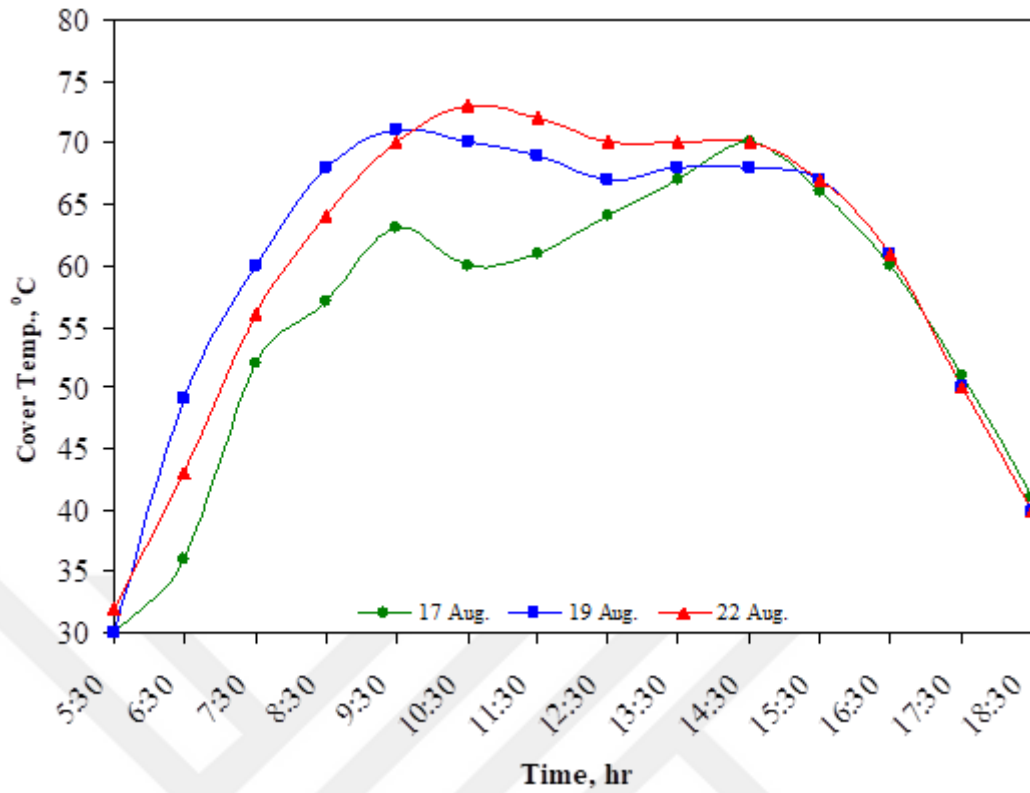
Figure H.5. Change in cover temperature of Silica gel for various days
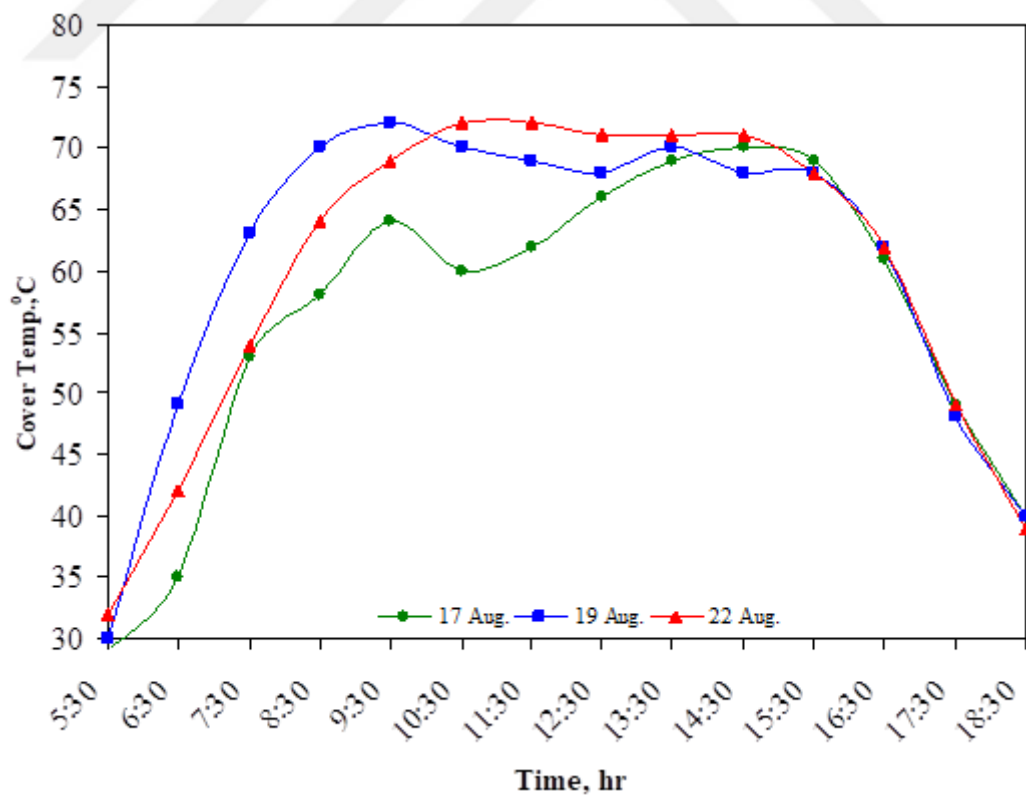
Figure H.6. Change in cover temperature of composite material for various days.
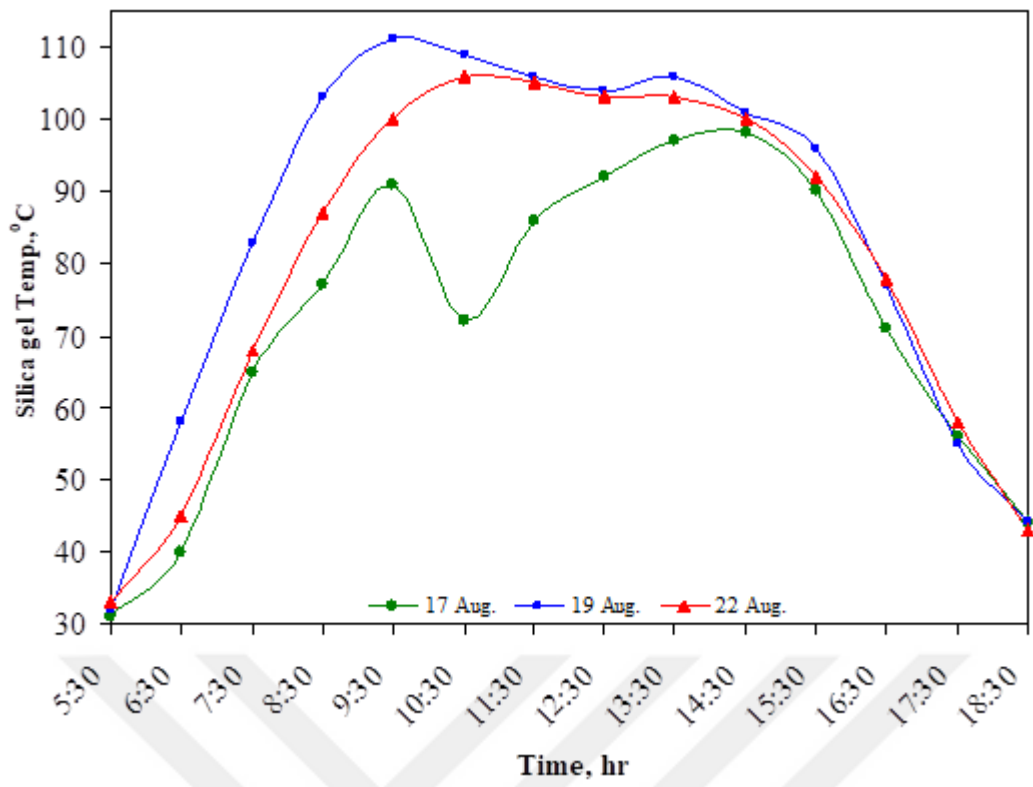
Figure H.7. Change of Silica gel temperature with time for various days
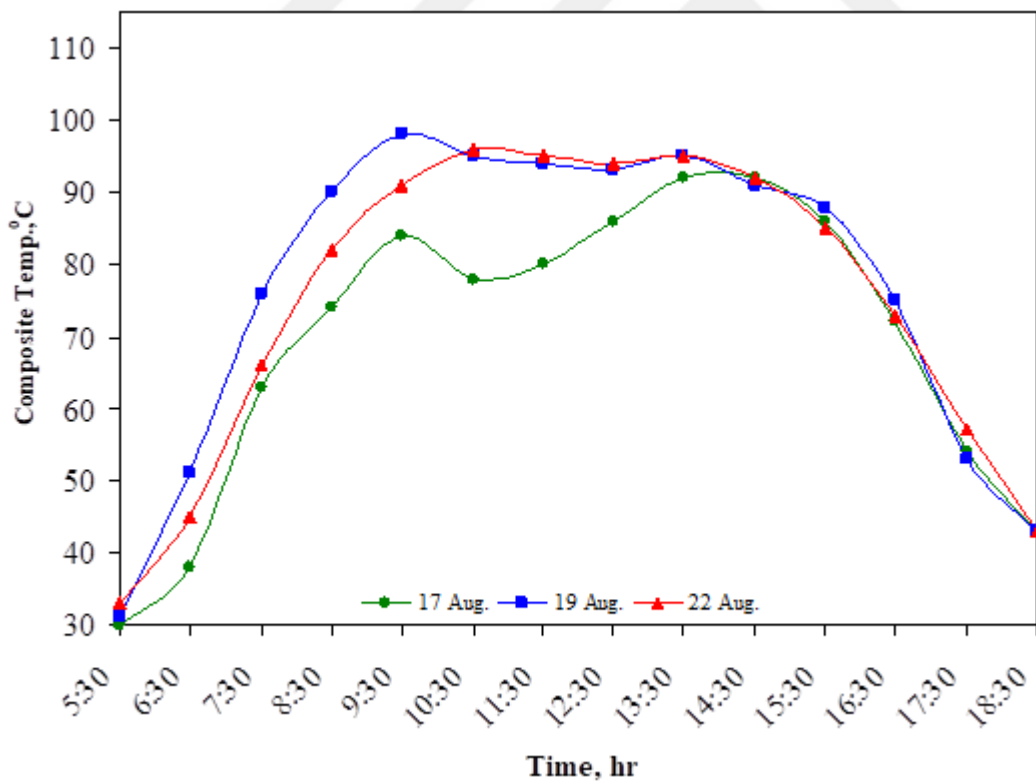
Figure H.8. Change of composite material temperature with time for various days

104
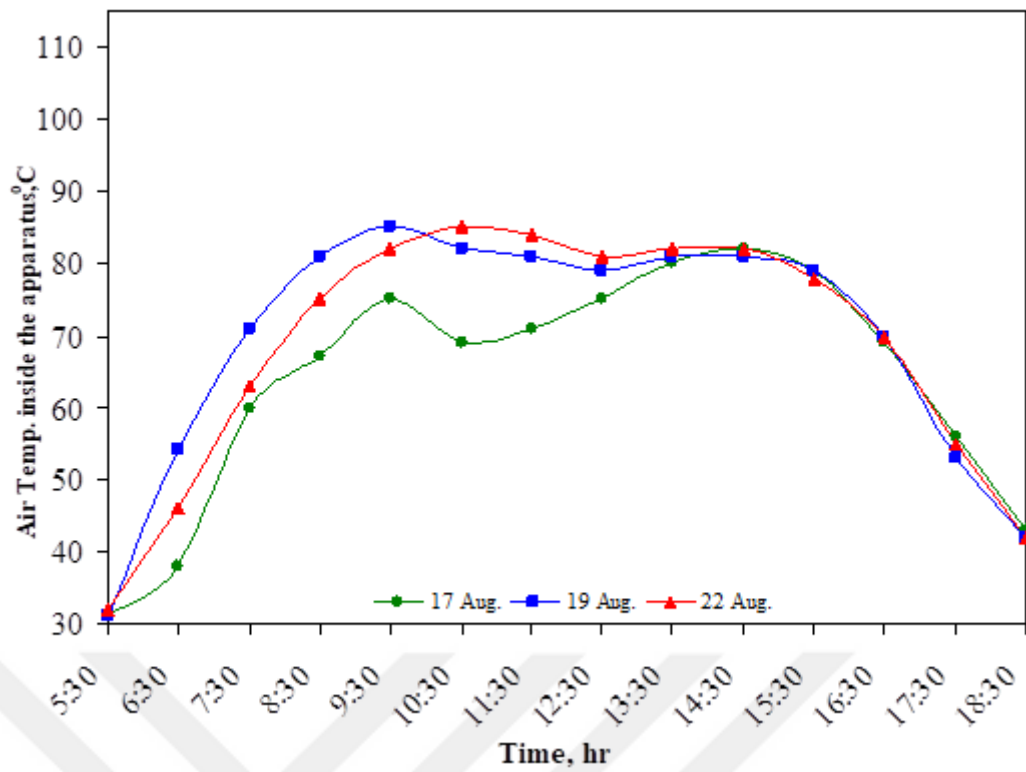
Figure H.9. Air temperature inside the apparatus for Silica gel for several days
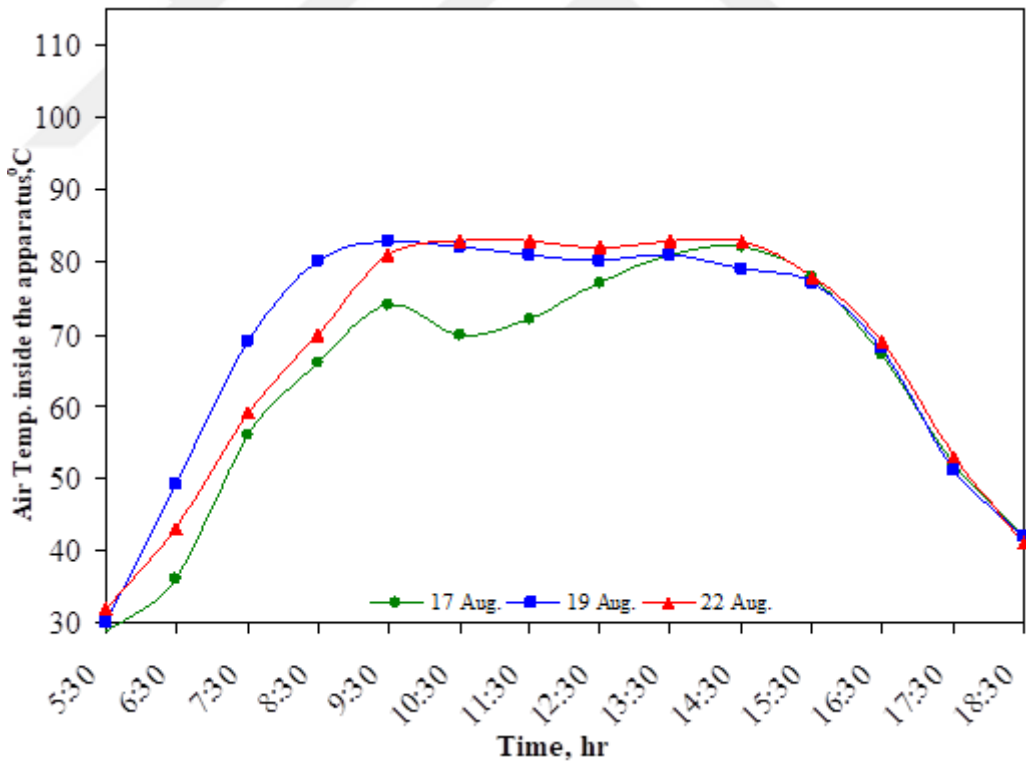
Figure H.10. Air temperature inside the apparatus for composite material for several days

III.   Variation of adsorption and desorption
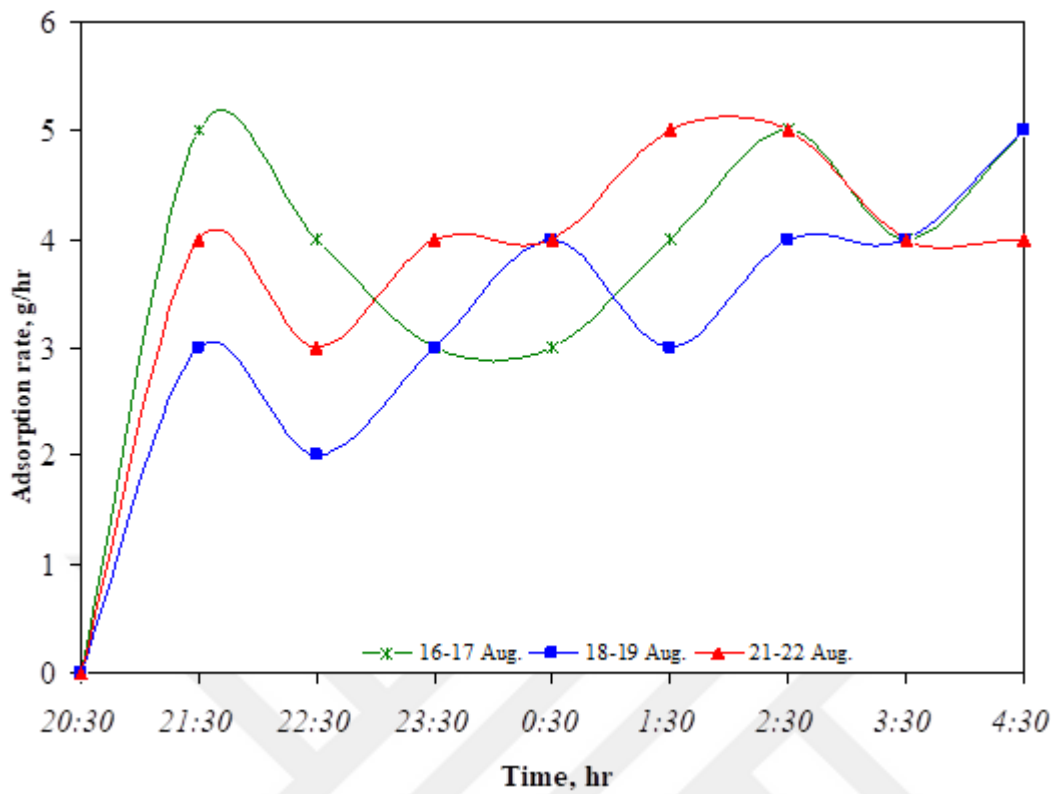
Figure H.11. Change of adsorption rate of Silica gel with time for various days
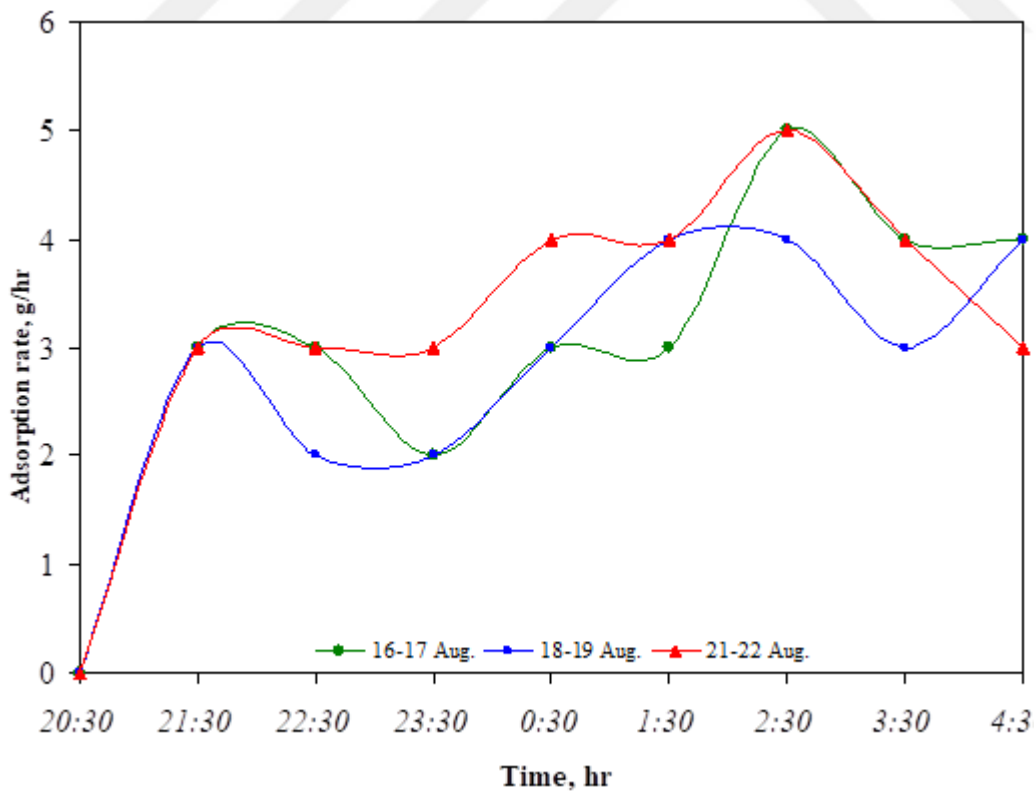
Figure H.12. Change of adsorption rate of composite material with time for various days
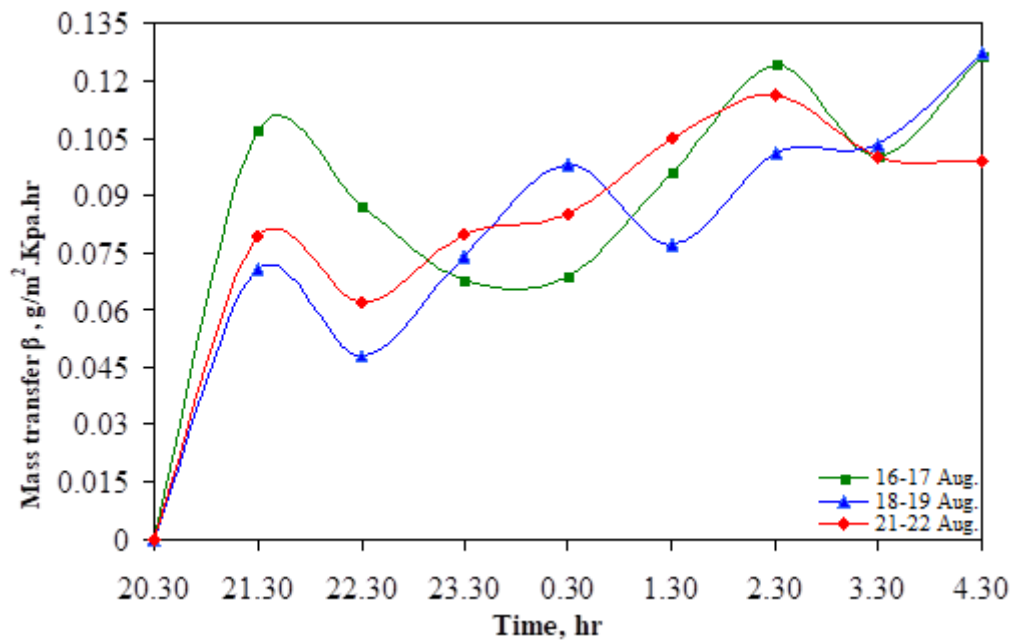
Figure H.13. Mass transfer coefficient of Silica gel for several days
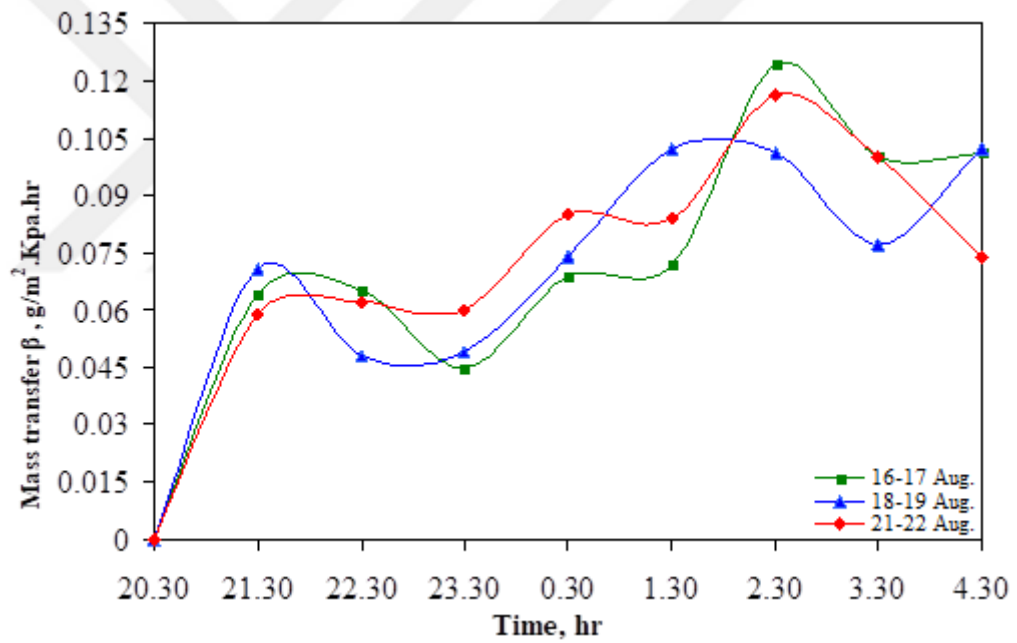
Figure H.14. Mass transfer coefficient of composite material for several days
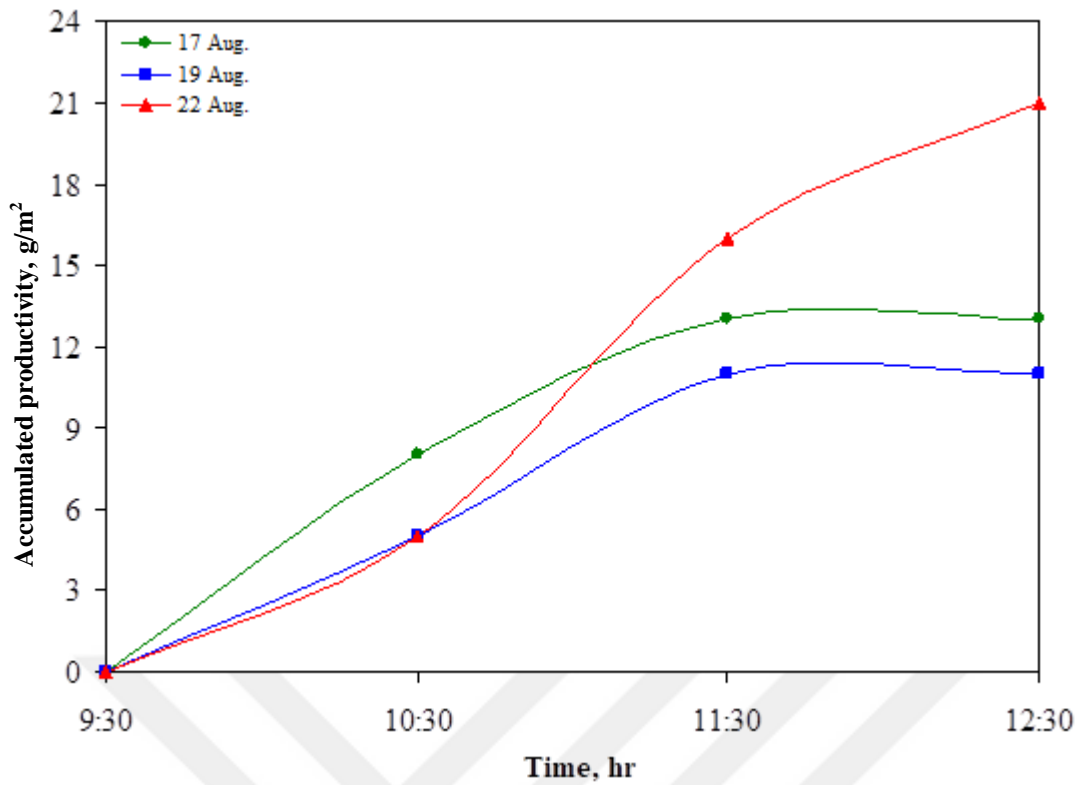
Figure H.15. Accumulated water productivity of Silica gel for several days
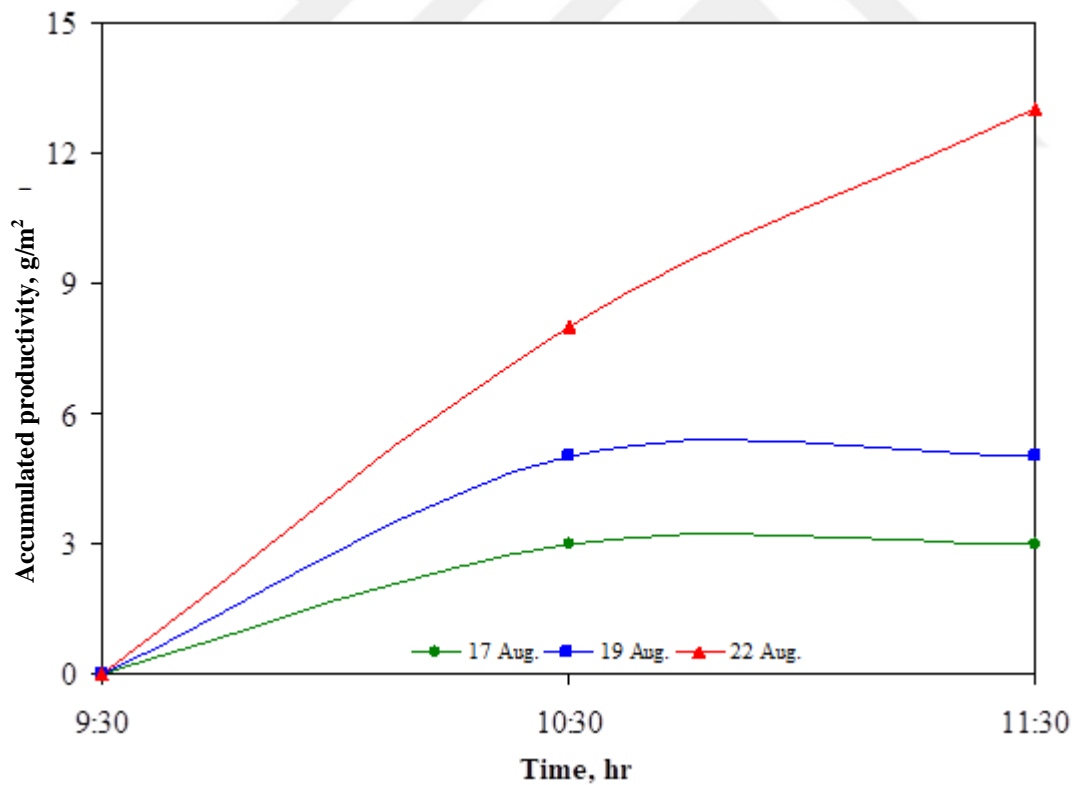
Figure H.16 Accumulated water productivity of composite material for several days
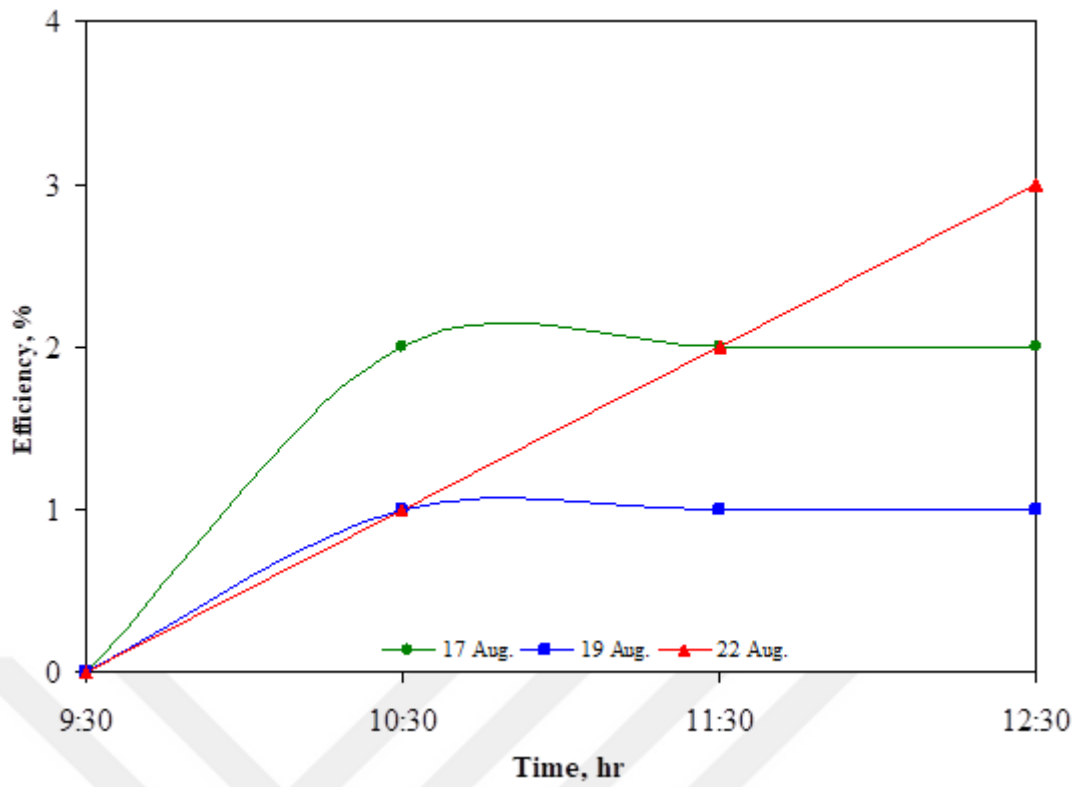
Figure H.17. System efficiency of Silica gel for several days
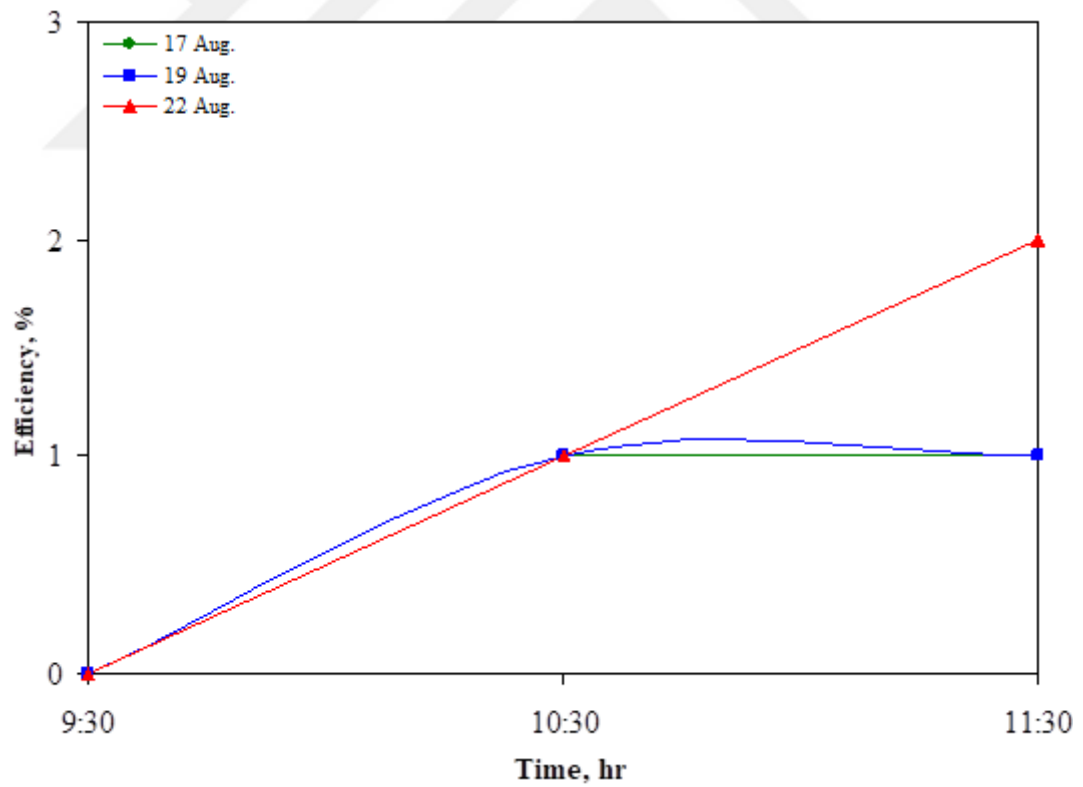
Figure H.18. System efficiency of composite material for several days

109
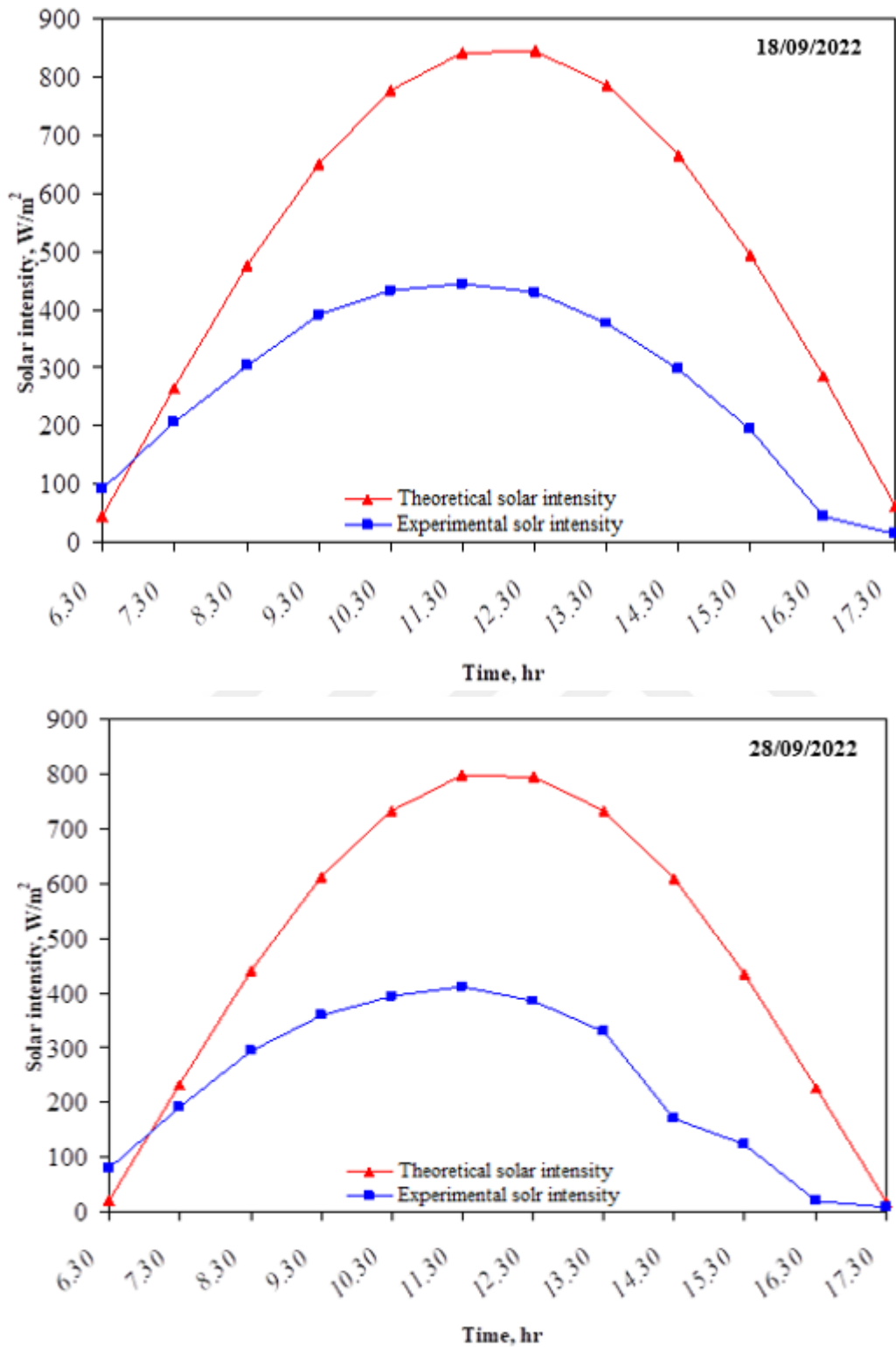
Figure I.1. Comparison between theoretical and experimental solar radiation for three different days
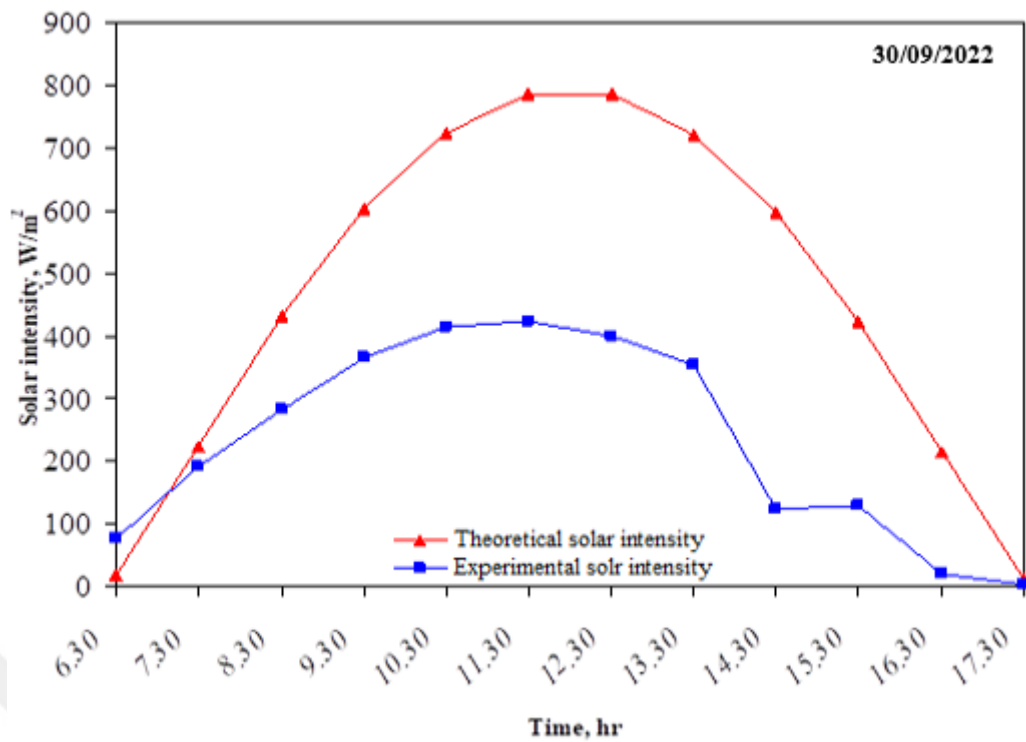
Figure I.1. (Continue)
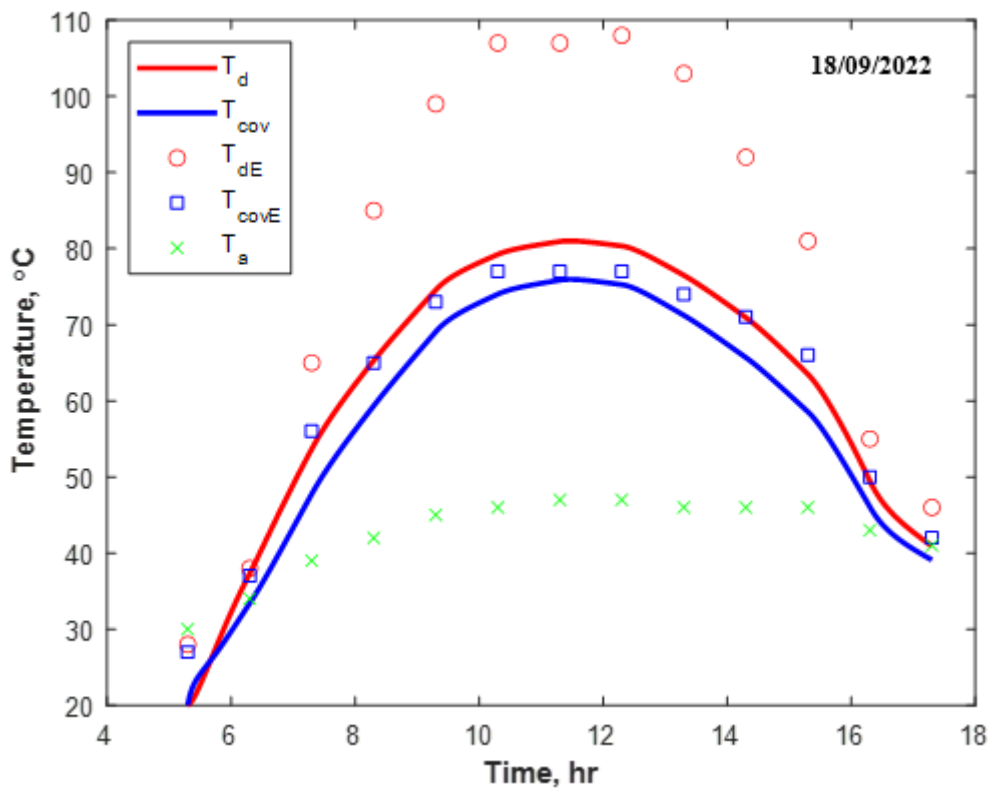
Figure I.2. Comparison between theoretical and experimental setup temperatures for various days
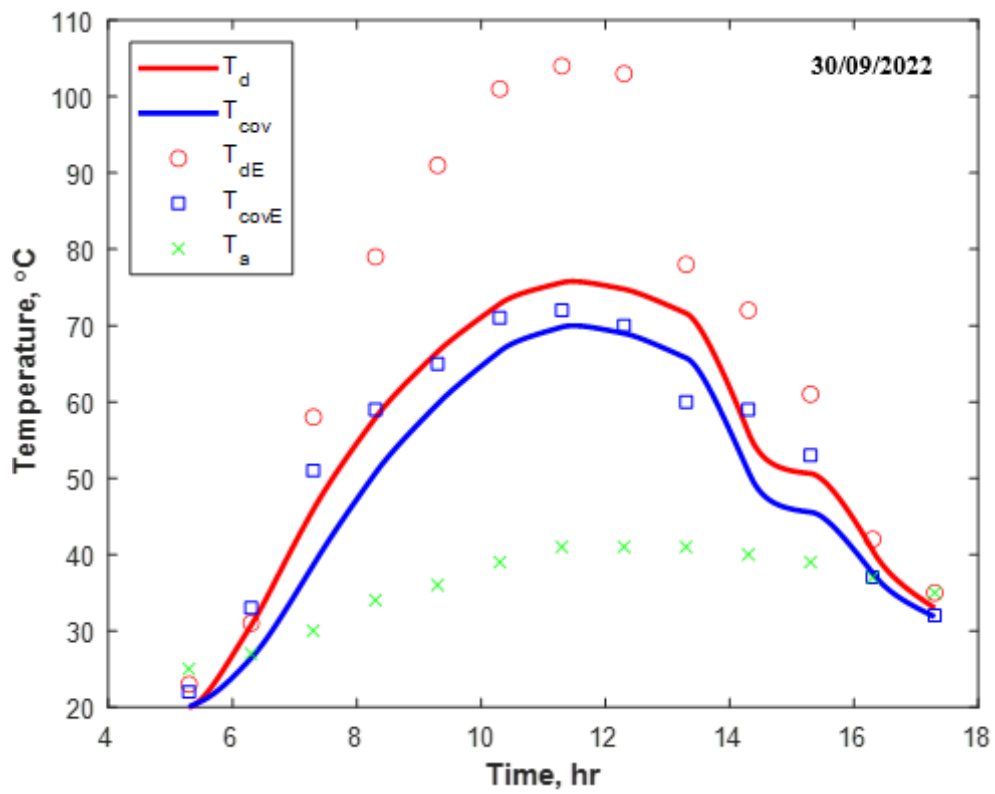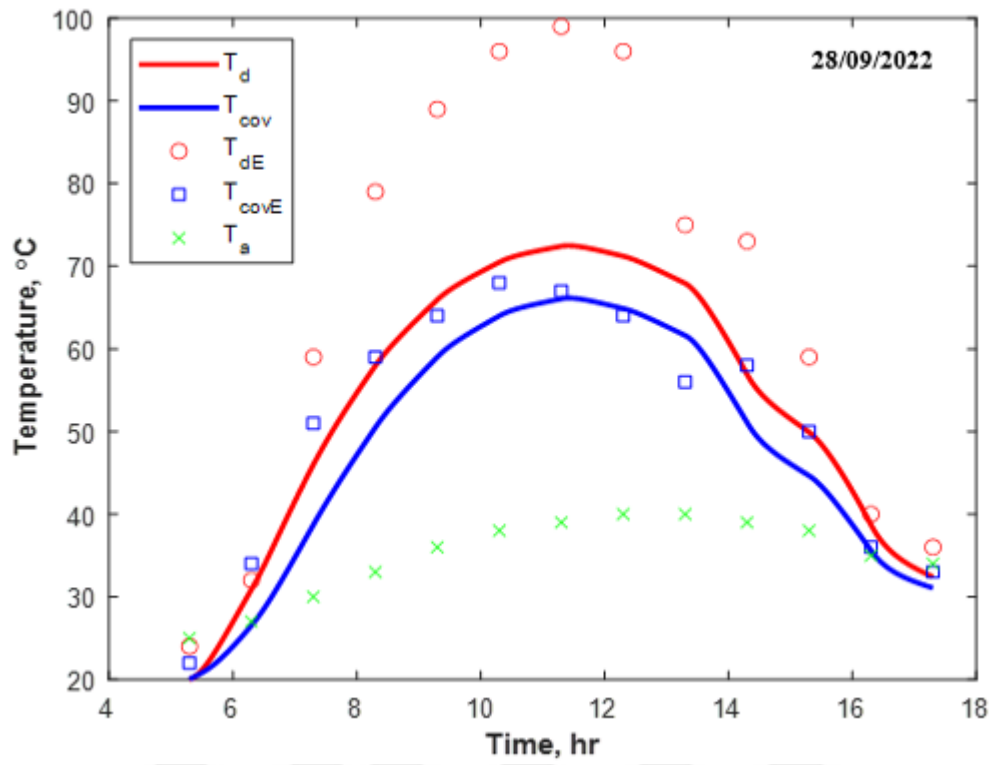
Figure I.2. (Continue)
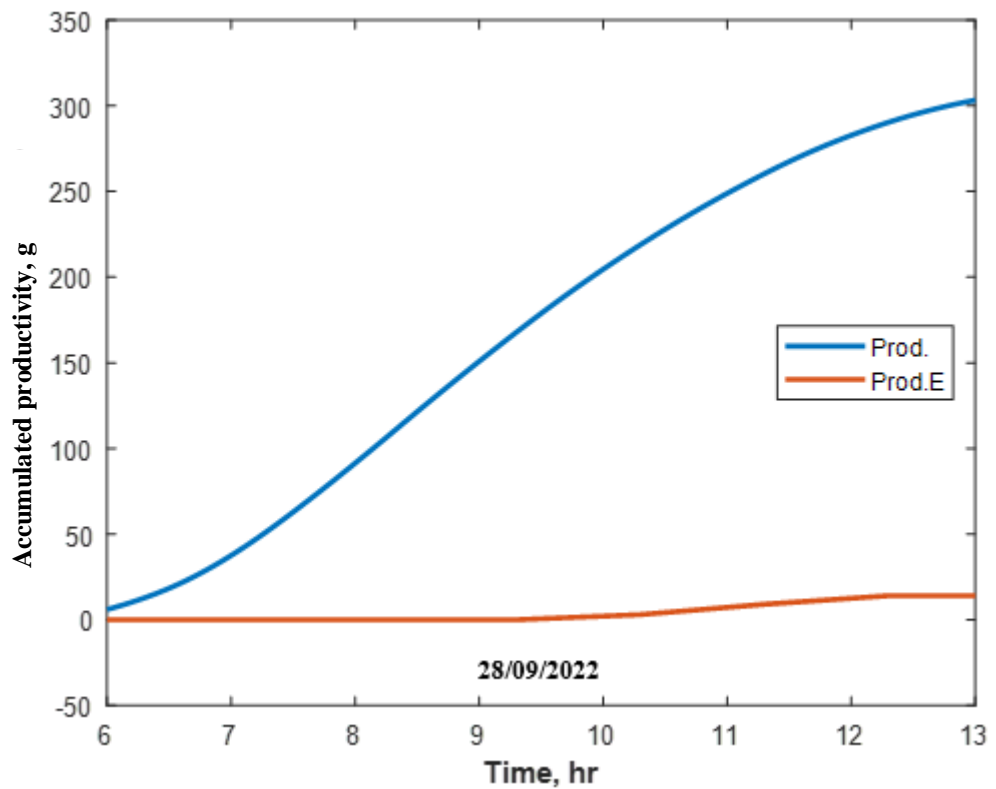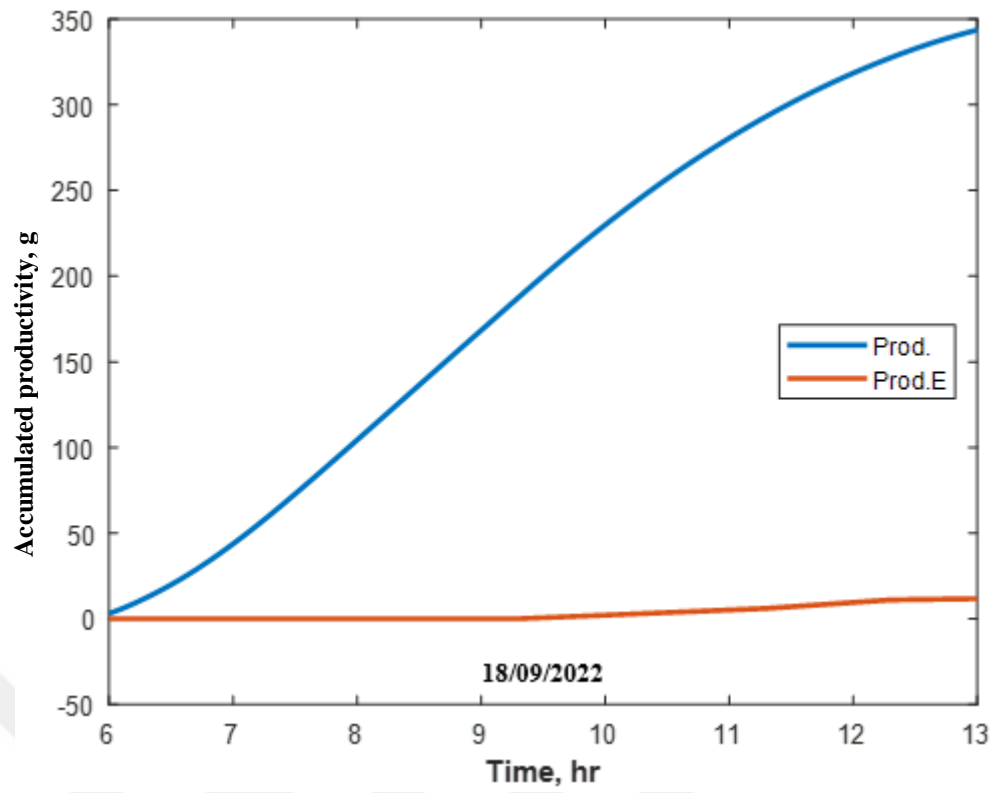
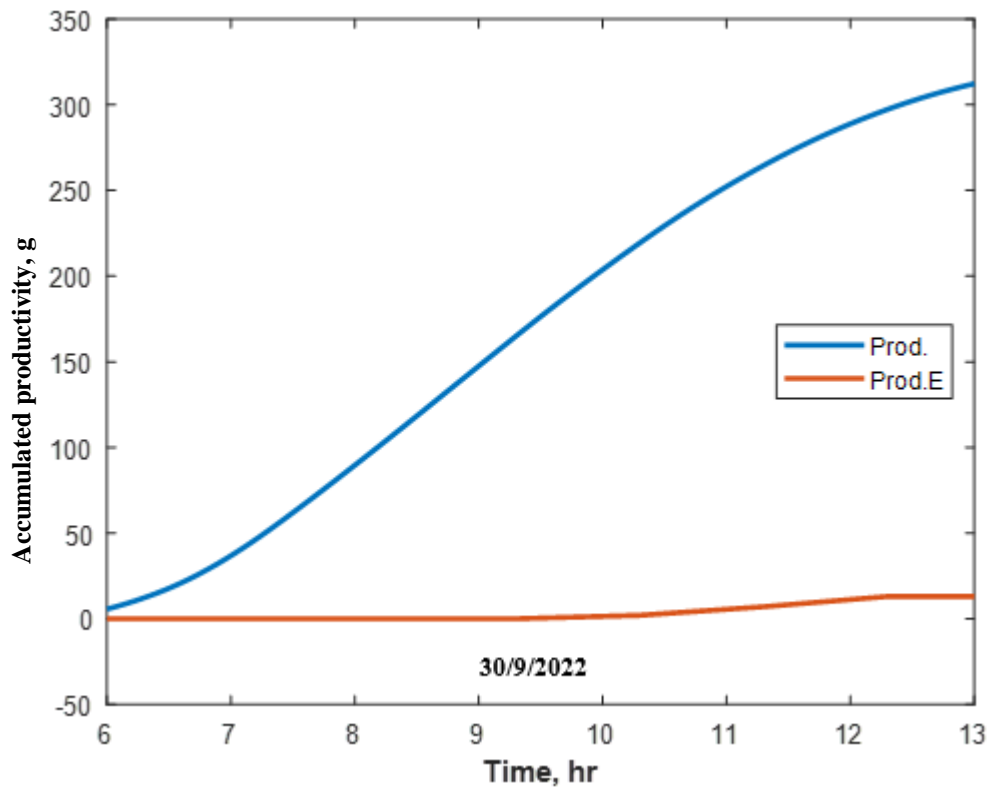**Figure I.3.** Comparison between theoretical and experimentally accumulated water productivity for different days
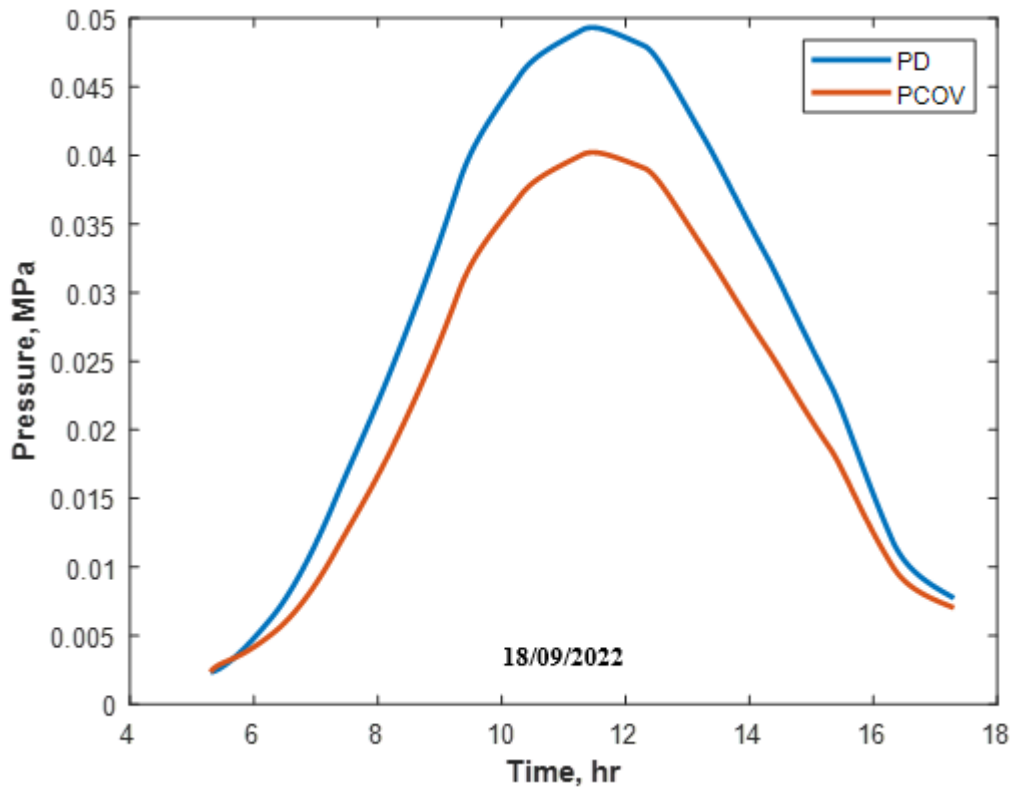
Figure I.3. (Continue)

Figure I.4. Difference between Partial water vapour pressure of desiccant and the cover
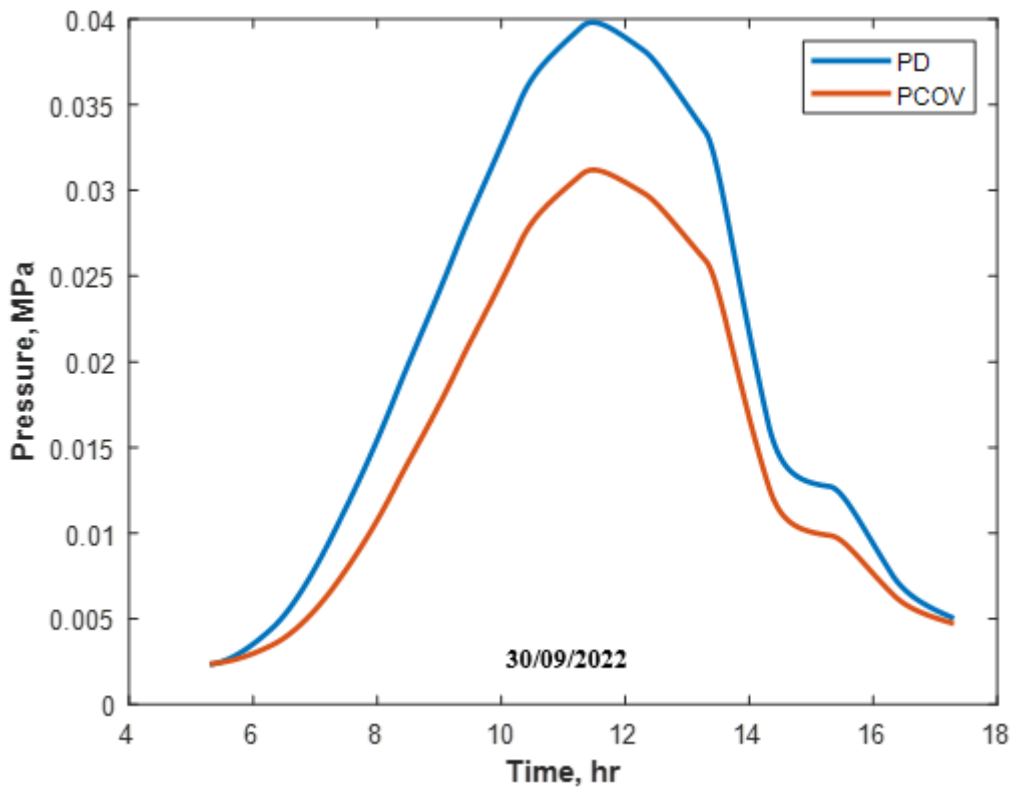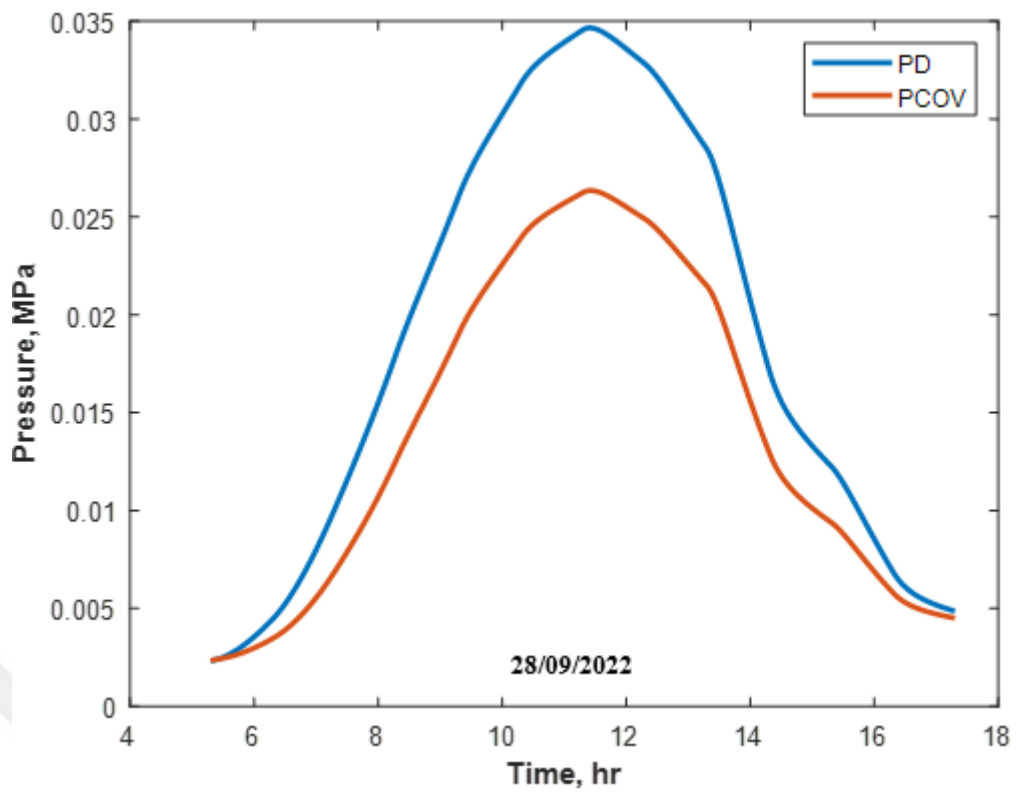
for various days

Figure I.4. (Continue)

RESUME

PERSONAL INFORMATION	
Name Surname:	Mohammed Oral Hashım AL-HURMUZI
Nationality:	Iraqi
Orcid Number:	0000-0002-7045-4628

EDUCATIONAL INFORMATION	
Bachelor	
University:	Kirkuk University
Faculty:	Faculty of Engineering
Department:	Mechanical Engineering
Graduation Year:	2015-2016
MSc	
University:	Kırşehir Ahi Evran University
Faculty:	Faculty of Engineering Architecture
Department:	Mechanical Engineering
Graduation Year:	2023

Articles and Papers
Articles in International Refereed Journals Alhurmuzi, M. O., Danışmaz, M., & Zainal, O. A. (2023). Investigation of Silica Gel Performance on Potable Water Harvesting from Ambient Air Using a Rotatable Apparatus with a Solar Tracking System. *Desalination and Water Treatment*. Danışmaz, M., & Alhurmuzi, M. (2022). A Literature Review on Extraction of Potable Water from Atmospheric Air Using Solar Stills: Recent Developments. *European Journal of Science and Technology*, (32), 991-999. https://doi.org/10.31590/ejosat.1039866   **International Conferences and Symposia** International Conference on Design, Research and Development (RDCONF)